HYDROLOGIC MODELLING OF NEW-ENGLAND RIVER BASINS USING RADAR RAINFALL DATA

by

JONATHAN DAVID WYSS

B.S., Earth, Atmospheric, and Planetary Sciences
Massachusetts Institute of Technology, 1986

Submitted to the Department of Earth, Atmospheric, and Planetary Sciences in partial fulfillment of the requirements for the Degree of Master of Science

at the

Massachusetts Institute of Technology

January 1988

Signature of Author _____
Dept. Earth, Atmospheric, and Planetary Sciences
January 15, 1988

Certified by _____
Earle R. Williams
Thesis Supervisor

Certified by _____
Rafael L. Bras
Thesis Supervisor

Accepted by _____
Chairman, Departmental Committee on Graduate Students

HYDROLOGIC MODELLING OF NEW-ENGLAND RIVER BASINS USING RADAR RAINFALL DATA

by

JONATHAN DAVID WYSS

Submitted to the Department of Earth, Atmospheric and Planetary Sciences on January 15, 1988 in partial fulfillment of the requirements for the Degree of Master of Science in Meteorology

ABSTRACT

Quantitative weather radar measurements of rainfall provide the input to a hydrologic forecast model designed to use the full spatial resolution of the radar data. The gridded model, which incorporates a detailed map of the stream network, is based on a simple kinematic representation of the river basin response. Only two parameters control the shape of the hydrograph: the velocity characteristic of subsurface flow to the nearest stream; and the streamflow velocity itself. Comparisons are made between model hydrograph forecasts and observed streamflow records for the Souhegan (440 km^2), and the Squannacook (160 km^2) river basins.

A linear scaling of the volume of the radar-derived storm rainfall produces reasonable agreement between the predicted and observed hydrographs. The volume scale factor, which varies from 20% or less in the summer to 100% in the spring, is consistent with the climatological mean monthly rainfall-runoff ratio. A single Z-R relation was used for all storms ($Z = 230R^{1.4}$), except for one case with strong convection ($Z = 400R^{1.3}$). In the two basins studied, for hydrograph peaks of moderate amplitude, overland flow and other quickflow components of the hydrograph are not generally observed. The hillslope response is modelled by a single characteristic subsurface flow velocity (2×10^3 ms^{-1}), with a characteristic streamflow velocity of 0.6 ms^{-1} in the Souhegan, (0.3 ms^{-1} in the Squannacook). These parameters do not vary significantly for the different storms considered here. Under such conditions, detailed modelling of the spatial character of the rainfall and basin characteristics is unnecessary for operational flood forecasting. Weather radar remains invaluable, however, for determining areal average rainfall rates over the watersheds in a manner which only an extremely dense network of raingauges could accomplish.

With a view to explaining some of the observed discrepancy between radar and raingauge rainrate measurements at a point, a statistical description of the rainfall field is derived. The probability distribution of rainfall rates is well described by a lognormal distribution, while the spectral density of the field is consistent with the power law which governs the inertial subrange of the turbulent wind field, ($S(k) \propto k^{-5/3}$). The relevance of potential sources of error in the radar rainfall measurement to hydrologic applications is considered.

Research related to the development of the gridded model and to other aspects of radar hydrology is included. A comprehensive analysis of the geomorphology of the two river basins provides the necessary background for the kinematic representation of the basin response. In particular, it is observed that the distribution of basin area as a function of distance to the nearest stream decreases approximately exponentially. This provides a possible explanation for the observed character of the hydrograph recession curve. Technical aspects of the radar hydrologic model are also discussed, including post-processing of the radar data for ground clutter rejection.

Thesis supervisors: Earle R.Williams
Professor of Meteorology
Dept. of Earth, Atmospheric and Planetary Sciences

Rafael L. Bras
Professor of Hydrology
Dept. of Civil Engineering

HYDROLOGIC MODELLING OF NEW-ENGLAND RIVER BASINS USING RADAR RAINFALL DATA

This thesis developed from a joint project involving the MIT Weather Radar Lab and the Parsons Lab, which was initiated by my advisors, Earle Williams and Rafael Bras. I am grateful to both for this opportunity to engage yet again in some form of inter-disciplinary research.

At the Radar Lab, I wish to thank Speed Geotis and Pauline Austin for sharing their experience and lively discussions; Oliver Newell and Ray Vieth, who finally succeeded in taming the computer; and Earle, whose unbounded curiosity for the natural world explains the hodgepodge of topics included in this thesis. Across the street, my thanks go to Rafael Bras for his time and patience in introducing me to the other side of the hydrologic cycle. Ignacio Rodríguez-Iturbe, when in town, always had an interesting comment on the current topic of research, and I am sure that his overflowing enthusiasm played a role in the success of the project.

From a practical standpoint, this project would not have been possible without the collaboration of the USGS and the Army Corps of Engineers who provided the stream gauge data. I would particularly like to thank Tim Buckelew for his assistance in obtaining the real-time data for the Souhegan.

I am of course most grateful to my parents and family for their love in so many guises; to Kerry, Heather, Earle and Rafael and yes, many others, teachers and friends, I have appreciated all of your words of encouragement and advice, concerning my studies and beyond; and my best friend Kelly, for your patience, humor and loving support of this and so many other adventures, I thank you.

Introduction

Since the development of meteorological radar, particularly with the advent of digital processing and longer wavelength Doppler systems, flood forecasting has been presented as one of the most useful applications of this technology. The potential of radar rainfall observations is obvious: measurements can be made with kilometer resolution over a region 10^5 km^2, from a central location. The density of a comparable raingauge network, with associated maintenance costs, would be staggering. Such a comparison however, assumes that the radar is capable of quantitative rainfall measurements with errors comparable to the raingauge. This capability has not yet been achieved. For hydrologic applications, the compromise lies in using the radar rainfall data, subject to possible quantitative errors, in order to benefit from the improved spatial resolution. Austin (1980) recognized this in writing:

> . . . for showery rain at least, the errors associated with using gauge data can be significantly greater than the errors in the radar technique. One particular storm is remembered which passed over the city of Ottawa causing significant flooding that did not pass over any of the gauges in the area. The streamflow model which could cope with this particular event needs to be quite ingenious!

The research presented here describes the development of a streamflow forecast model designed to operate using data from the 11 cm radar located at MIT. This study is neither the first of its kind, nor is it definitive. It parallels, in intention, similar research reported in the literature (e.g., Curry et al., 1970; Hudlow, 1972; Klatt and Schultz, 1983; Collier and Knowles, 1986; and Fortin et al., 1987). Interest in the problem has logically increased in anticipation of the NEXRAD radar network, which was designed to incorporate hydrological applications (c.f., Walton et al., 1985).

I should, at the outset, confess my complete lack of experience in hydrology prior to this research. When I was approached concerning this project, I naïvely assumed that state-of-the-art flood forecast models existed which, when coupled with the radar data, would provide a useful tool for verifying the quantitative accuracy of the radar. I imagined that in a flood situation all of the storm rainfall would make its way directly to the basin outlet, as a giant raingauge, or at least could be accounted for in the model. In reality, of course, this is not an accurate

description of the problem. For river basins in New England with permeable soils, a considerable fraction of the rainfall is retained by the soil; during the course of the year, nearly 50% of the rainfall is subsequently lost to the atmosphere through evapotranspiration.

For this project, rather than adapting an existing river basin model to the radar data, we decided to develop a new model, based simply on the travel times of water through the river basin system. In hydrology, where abandoned watershed models litter the journals, it has become customary to apologize for the introduction of yet another model, or at least to place the new model "into the perspective of the models that already exist," as we are admonished by Kundzewicz (1986). The primary intention of this model is to use the distributed nature of the radar data to best advantage. This is accomplished with a gridded spatial representation of the basin geometry. Most of the available basin models, developed for raingauge data with limited spatial resolution, consider only the "lumped" response of the river basin. Or, at the other extreme, complex finite element models have been developed which solve the dynamical equations numerically, for watersheds of a few square kilometers. Neither scheme is particularly well suited to the spatially distributed radar rainfall data over basins of several hundred km^2.

The extremely simple linear model of the basin response described here is based on the geomorphology of the river basin, i.e. on the spatial arrangement of the stream network. It characterizes the contribution of each "raindrop" to the storm hydrograph by a travel time. The model might well be the sort of experiment that the earliest hydrologists would have conducted, had they access to a digital computer. For research purposes, the simple model provides certain advantages over the multi-parameter models which are "tuned" to fit the observed data for forecast purposes. At the very least, it allows us to isolate the contribution of the river network to the basin response, and provides us with a reasonable approximation to the observed storm hydrograph for the purposes of assessing the accuracy of the radar rainfall measurement.

In a sense this thesis represents a journey upstream ("A Report on the Exploration of the River Sawheegan to whence it derives its flowe, . . ."): much of the material presented here considers topics only indirectly related to the modelling study (". . . and on the Nature of its tributarie streams"). Floating

back downstream, the main channel is clearer now, but I have included in the thesis, for the sake of interest and completeness, results from a variety of peripheral investigations.

Chapter 1 considers the nature of the radar rainfall measurement and possible sources of error, and includes results from a study of the small-scale structure of the rainfall field. The statistical description of the rainfall field described in this chapter might be used in a numerical model to investigate the differences between the radar and raingauge sampling. Chapter 2, which provides the necessary background to the development of the river basin model, includes data from a comprehensive "Horton analysis" of the Souhegan and Squannacook basins. These data are tabulated here for the benefit of further research on the topic of geomorphology. The final chapter, which includes comparisons between the model forecasts and the streamflow data, also describes several components of the model which were included in the design but subsequently abandoned.

CHAPTER 1: THE RADAR

Weather radar differs in many respects from the familiar raingauge of the hydrologist. In fact, the weather radar does not measure rainfall, but a functionally related quantity, and it performs this measurement over a region several orders of magnitude larger than the sample volume of a rain gauge. This first difference leads to an empirical function relating the radar reflectivity to the water flux at the earth's surface: the Z-R relationship. The second distinction is more subtle, but it is precisely this large difference between the sample volumes that allows the radar to map the rainfall field in space and time, over a vast area, in a manner which only a prohibitively dense network of raingauges could accomplish.

Much time has been devoted to both empirical and theoretical radar–raingauge comparisons. Some of this research will be considered here, but no attempt will be made to present either a complete or a particularly unified summary of previous studies. The emphasis will be on the application of radar measurements to hydrology, and on errors relevant to quantitative precipitation measurement. Post-processing of the radar data for input to the hydrologic model is discussed at the end of the chapter.

1.1 THE STRUCTURE OF RAINFALL

Even at intermediate ranges of 75 km, the pulse volume of a 1 degree radar beam is on the order of 1 km^3. Clearly, the radar reflectivity measurement is a spatially averaged estimator of the reflectivity, and hence of the rainfall rate. Without independent measurements of the small-scale structure of the rainfall field, it is not obvious to what extent the radar measurement might be biased by variability in the rainfall on scales smaller than the pulse volume. Knowledege of the amplitude and frequency structure of rainfall rates on small scales might permit a simulation of the rainfall field within the radar pulse volume, ultimately leading to a better understanding of the nature of the radar reflectivity measurement. Probability distributions and spectra of the rainfall rate are calculated here with a view to obtaining an empirical yet mathematically tractable description of the rainfall field. Analyses of both radar and raingauge data are presented, along with a summary of related studies.

In the following, stationarity of the rainfall process and linearity between spatial and temporal scales have been tacitly assumed. Raingauge data at a point are related to the spatial rainfall pattern through Taylor's hypothesis, (Taylor, 1938). Zawadzki (1973) has demonstrated the validity of this assumption for radar data over time scales less than about 40 minutes (i.e. comparable to the average lifetime of a convective cell). Transformation from the frequency domain of a time series to the wavenumber domain is thus accomplished by a scaling factor equal to the advective velocity of the rainfall.

a) The Distribution of Rainfall Rates

Recently, interest in the probability distribution of rainfall rates has been rekindled by speculation on the fractal character of the rainfall process. If rainfall is indeed a scaling process, argue various researchers (Lovejoy and Mandelbrot, 1985; Schertzer and Lovejoy, 1987), then the probability of occurrence of rainfall rates should follow a hyperbolic distribution. Lovejoy and Mandelbrot (1985) present radar data in support of this hypothesis, although objections to the techniques employed were raised by Zawadzki (1987).

It is worth noting that the proponents of this model argue only for fractal behavior at high rainfall rates. No evidence, including their own, indicates that a power-law dependence is a meaningful description over a wider range of rainfall rates. Data from both Austin (1971) and Zawadzki (1984) indicate that, in the mean for Boston and Montreal, 70% of the total rainfall depth results from rainfall at rates less than 8 $mmhr^{-1}$, although in thunderstorms this fraction is probably closer to 50%. Because of the meager data available for determining the functional form of the distribution tail, we will concentrate here on rainfall rates less than 100 $mmhr^{-1}$.

The lognormal distribution has been proposed as a convenient functional form for the occurrence of rainfall rates (c.f., Crane, 1985; Lin et al. 1980). This model appears to be valid for many radar and raingauge data sets, as we shall demonstrate in this section.

i) Raingauge Data

Archived records were analyzed from two raingauges operating at MIT. The tipping bucket mechanisms, labelled "coarse" and "fine", have resolutions of 0.09 mm and 0.018 mm respectively. Together, these gauges provide an

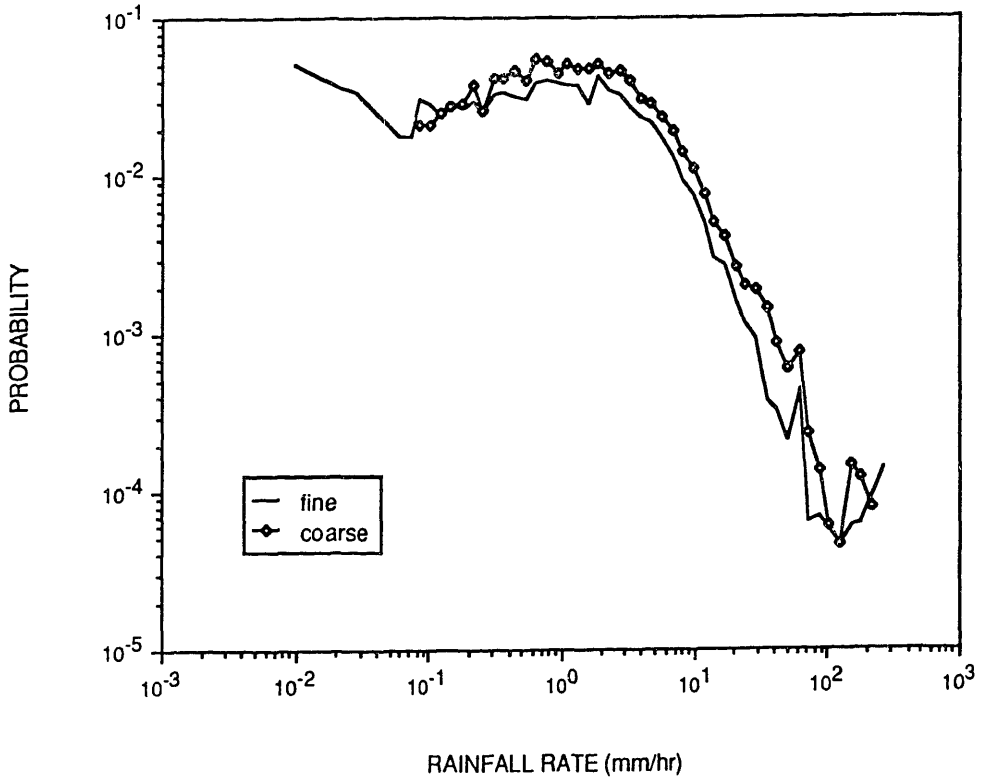

Fig. 1-1 Frequency distribution of rainfall rates. Tipping bucket raingauge data from MIT, coarse and fine gauges. Logarithm of frequency plotted for logarithmic intervals of rainfall rate.

effective dynamic range from less than 1 $mmhr^{-1}$ to over 100 $mmhr^{-1}$. This range is limited by the response of the tipping bucket mechanism, since the duration of rainfall at a given intensity measured by the gauge is inversely proportional to the rainfall rate itself.

Data collected between 1980 and 1983 were included in this study; the sample represents all months of the year, with simultaneous measurements by both gauges. Logarithmic intervals were used to estimate the frequency distribution of rainfall rates. Fig. 1-1 shows this distribution function for the two gauges, plotted in log-log coordinates. Saturation of the tipping bucket mechanism is evident near 100 $mmhr^{-1}$. The observed decrease in the distribution function at rates lower than 1 $mmhr^{-1}$ is clearly not an artifact of the tipping bucket mechanism, since this would tend to produce a negative slope, as observed at even lower rainfall rates. The physical reason for this behavior has not yet been investigated, but it is clear that both evaporation and increasingly

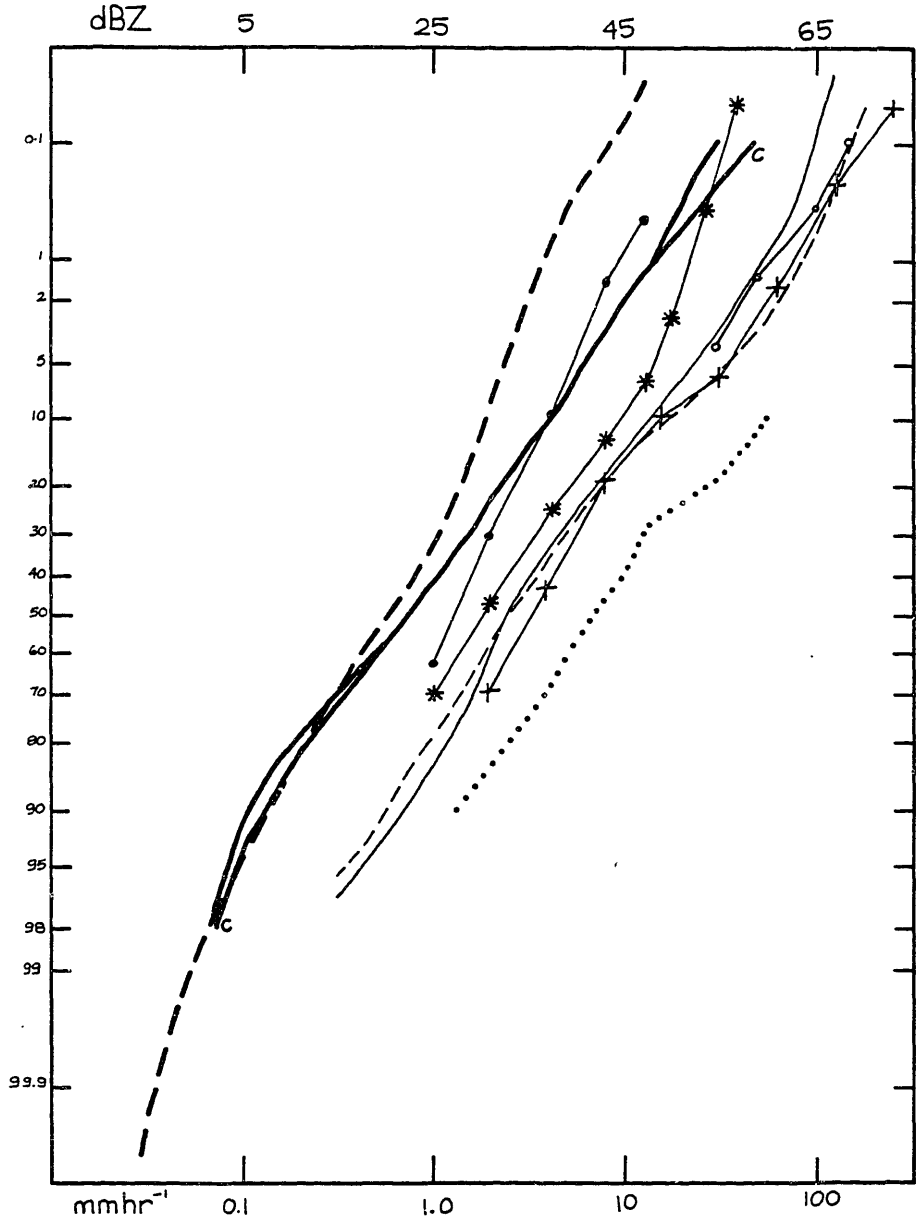

Fig. 1-2 Probability of occurrence of rainfall rates and radar reflectivity. Plotted as exceedence probabilities of the logarithm of the rainfall rate (lower axis), and dBZ (upper axis). Tipping bucket gauge data from Fig. 1-1 are plotted as solid bold line (coarse gauge labelled "C"). For comparison: Austin (1971) thunderstorm cases (asterisks), and all other storms (solid circles); Douglas et al. (1978) for Miami (thin solid line), Illinois (thin dashed); Frenny and Gabbe (1969), (open circles); Drufuca and Zawadzki (1975) for average rainfall rate of independent events (bold dotted line); and Holtz (1983), areal coverage of radar echoes, converted to rainfall rates (crosses). MIT radar reflectivity data (Fig. 1-3) drawn as dashed bold line.

small terminal velocities will be limiting factors for the occurrence of very low rainfall rates. The parabolic nature of the curves in log-log coordinates is an indication that the lognormal distribution is a meaningful approximation to the data, although a hyperbolic approximation may be reasonable over a limited range at higher rainfall rates.

The lognormality of the distribution is confirmed by plotting the cumulative frequency of the logarithm of the rainfall rate on probability paper (Fig. 1-2, solid bold lines). The approximately straight line defines a lognormal distribution with median value and standard deviation $m = 0.7$ mmhr^{-1} and $\sigma = 0.85$ of log(**r**). These values are in agreement with Crane (1985) who obtained $m = 0.79$ mmhr^{-1} and $\sigma = 0.6$ log(**r**) for mid-latitude stations. The analysis is also corroborated by data from several other sources, plotted in Fig. 1-2 for comparison. These include: Austin (1971), who conducted a detailed study of data for Concord, Mass., 1962-1963, using similar gauges but 30 second average rainfall rates; Drufuca and Zawadzki (1975), who analyzed raingauge data from Montreal (10 years); Douglas, Jones and Sims (1978) for data from Illinois and Miami; Frenny and Gabbe (1969) operating an array of rapid response electronic gauges in New Jersey; and Holtz (1983) who collected statistics from radar maps in a manner similar to that pursued in the following section.

ii) Radar Data

Archived MIT radar data from the summer and fall months of 1987 were analyzed to obtain a spatial frequency distribution of reflectivity (Z) values. Because of ground clutter problems in the near field, samples were only considered between ranges of 50 and 100 km. The sample was further limited to echoes with Doppler velocities greater than 0.75 ms^{-1} in order to eliminate any persistent ground echoes. To obtain a sufficiently large sample, each range bin of each map was treated as an independent sample. Nearly 1000 maps were analyzed, providing a total of 6.5×10^6 range bins with reflectivities greater than the minimum detectable (-6 dBZ at 50 km and -3 dBZ at 100 km). In effect, the frequency distribution represents an ensemble average of the frequency distribution of individual radar maps, for which the mean and shape of the distribution may vary considerably, depending on the type and intensity of the precipitation.

The resulting distribution of dBZ values ($10\log_{10}Z$) is plotted in Fig. 1-3. The curve exhibits a pronounced maximum near 25 dBZ, and is consistent with

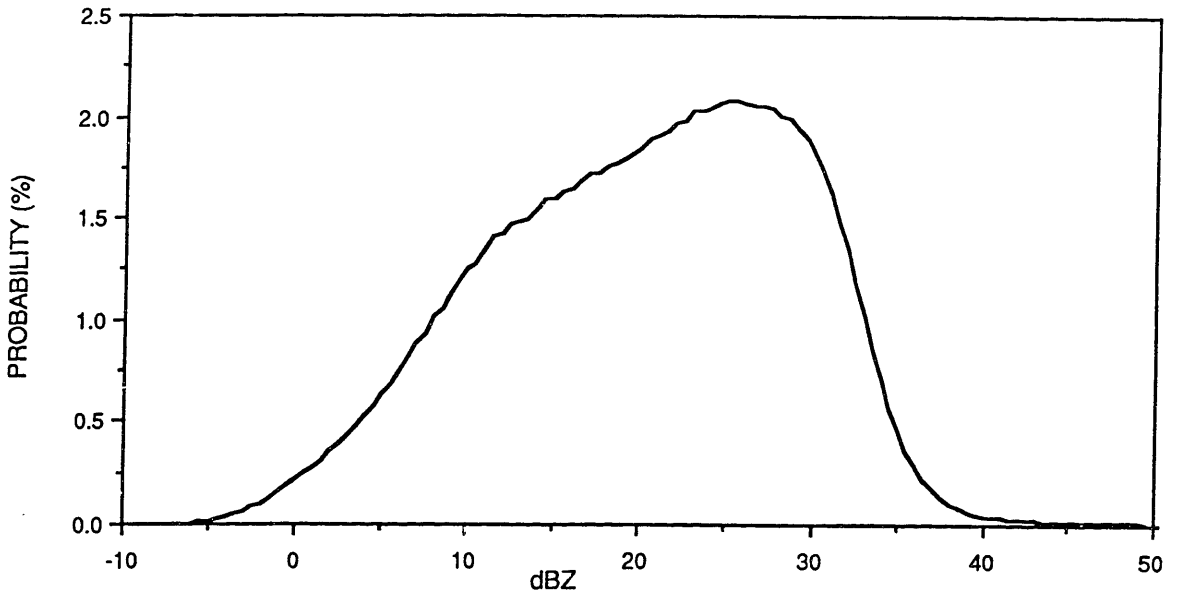

Fig. 1-3. Frequency distribution of reflectivity values. Probability of occurrence of logarithmic reflectivity values (dBZ). Data from 50 to 100 km range gates.

a lognormal distribution for Z. The shape of the probability curve at values less than 20 dBZ is influenced by the signal processing algorithms of the radar. Each sample is scaled by a factor proportional to the signal-to-noise ratio, producing a continuous, but possibly erroneous distribution function at reflectivities approaching the minimum detectable. However, the shape of the distribution and the maximum near 25 dBZ (roughly 1 $mmhr^{-1}$) are consistent with the raingauge analysis. The same distribution plotted on probability paper (Fig. 1-2, dashed bold line) approaches a straight line.

While the medians of the various distributions plotted in Fig. 1-2 vary widely (due in large measure to different averaging intervals), the slopes of the curves, which define the standard deviations, are similar over broad ranges of reflectivities and rainfall rates. The following parameters were fit by eye to the lognormal reflectivity data: $m = 20$ dBZ, $\sigma = 8$ dBZ (over entire range); $m = 25$ dBZ, $\sigma = 6$ dBZ (for $Z > 25$ dBZ). Bell (1987) also reports a lognormal distribution for the radar reflectivity using GATE low-level radar scans on a 4 km grid. The parameters for the GATE data, expressed as equivalent rainfall rates, are $m = 3$ $mmhr^{-1}$; $\sigma = 0.48$.

The lognormal distribution is thus a meaningful description of the probability of occurrence of rainfall rates for both spatial and temporal analyses. However, a physical interpretation of these observations has not yet been advanced. Further analysis of the MIT raingauge data, stratified by storm type, would extend the results of Austin (1971). Also, the radar analysis could be improved by considering data from ranges close to the radar. This is not possible at an urban location because of ground clutter contamination. Examining the range dependence of the probability distribution of reflectivity values might offer some insight into the effects of range on the radar reflectivity measurement, as suggested by Calheiros and Zawadzki (1987).

b) The Spectral Properties of rain

The initial motivation for calculating Fourier transforms of rainfall data developed from a hypothesis that convective rainfall might exhibit a scale, or series of characteristic scales, associated either with the dimensions of the updraft or resulting from a non-linear interaction of raindrops with the rain shaft (c.f., Mollo-Christensen, 1962; Ackerman, 1967; Atlas and Tatehira, 1968; Hosking and Stow, 1987). However, analysis of the raingauge data and subsequent analysis of radar measurements demonstrates quite clearly the lack of any such preferred scale. Transforms of both raingauge and radar data exhibit a power law dependence with the spectral density proportional to $k^{-5/3}$ over a wide range of time scales. An analysis of two-dimensional radar fields by Crane (1986) exhibits a similar dependence for spatial spectra, consistent with Taylor's hypothesis.

The manifestation of a $k^{-5/3}$ power law in the rainfall data is not altogether unexpected. From dimensional arguments, the velocity spectra of three dimensional turbulent fields are predicted to exhibit a sub-range over which

$$S(k) = a\,\varepsilon^{2/3}\,k^{-5/3}$$

as proposed by Kolmogorov (c.f., Tennekes and Lumley, 1972). Energy cascades from larger scales, through the "inertial" range to the microscale, where it is dissipated by viscous effects at rate ε. Kraichanan (1967) showed that a similar inertial range exists for two dimensional turbulence, with the exception that a reverse energy cascade transfers energy from smaller to larger scales.

Observational evidence from the atmosphere indicates that an isotropic, three dimensional description of the turbulent field is only meaningful from scales less than 1 m to somewhat greater than 100 m (MacCready, 1962), although, in strongly convective environments, this range might be expected to extend to several kilometers (Gage, 1979). On the other hand, evidence presented in Lilly (1983) and Gage (1979) demonstrates the extension of the $k^{-5/3}$ dependence of the two dimensional inertial range to scales approaching 1000 km. The ubiquity of the $k^{-5/3}$ power law in atmospheric data is manifest not only in velocity data, but also in the spectra of scalar quantities such as temperature, humidity, and the functionally related refractive index, which act as passive tracers of the flow (cf Lumley and Panofsky, 1964).

i) Raingauge Data

Rainfall time-series for eight storms were selected from the same tipping–bucket raingauge data described in the previous section. The durations of these time series range from 30 minutes to 7 hours. Time series with a time interval of 1 second were derived from the digital data of both the "coarse" and "fine" tipping bucket gauges, and subsequently averaged to longer intervals. Fourier transforms were calculated for each time series, at various levels of aggregation.

Fig. 1-4 shows the coarse gauge data for the storm of October 25, 1980, and the derived Fourier transform (spectral density). A line describing $k^{-5/3}$ is drawn for comparison. The spectrum of the fine gauge data for the same storm (Fig. 1-5) exhibits the same dependence, although the fine gauge mechanism is prone to saturation at higher rainfall rates. Averaging the time series to longer aggregation intervals (2, 5, 10, 25, 50 and 100 seconds) does not significantly affect the slope of the spectral density, as demonstrated in Fig. 1-6. The $k^{-5/3}$ dependence was observed for a variety of storm types, including scattered showers, stratiform rain with embedded convective elements, and for frontal precipitation. Examples of storms of these types are shown in Figs. 1-7,9. In each case the envelope of the spectral density function is consistent with the $k^{-5/3}$ model.

Cavanaugh (1985; c.f., Crane, 1986) conducted an independent study of the MIT tipping bucket raingauge data, with similar conclusions. However, Cavanaugh's analysis considered the logarithm of the rainfall rate, and the ensemble average of the spectra of independent storms. The motivation for

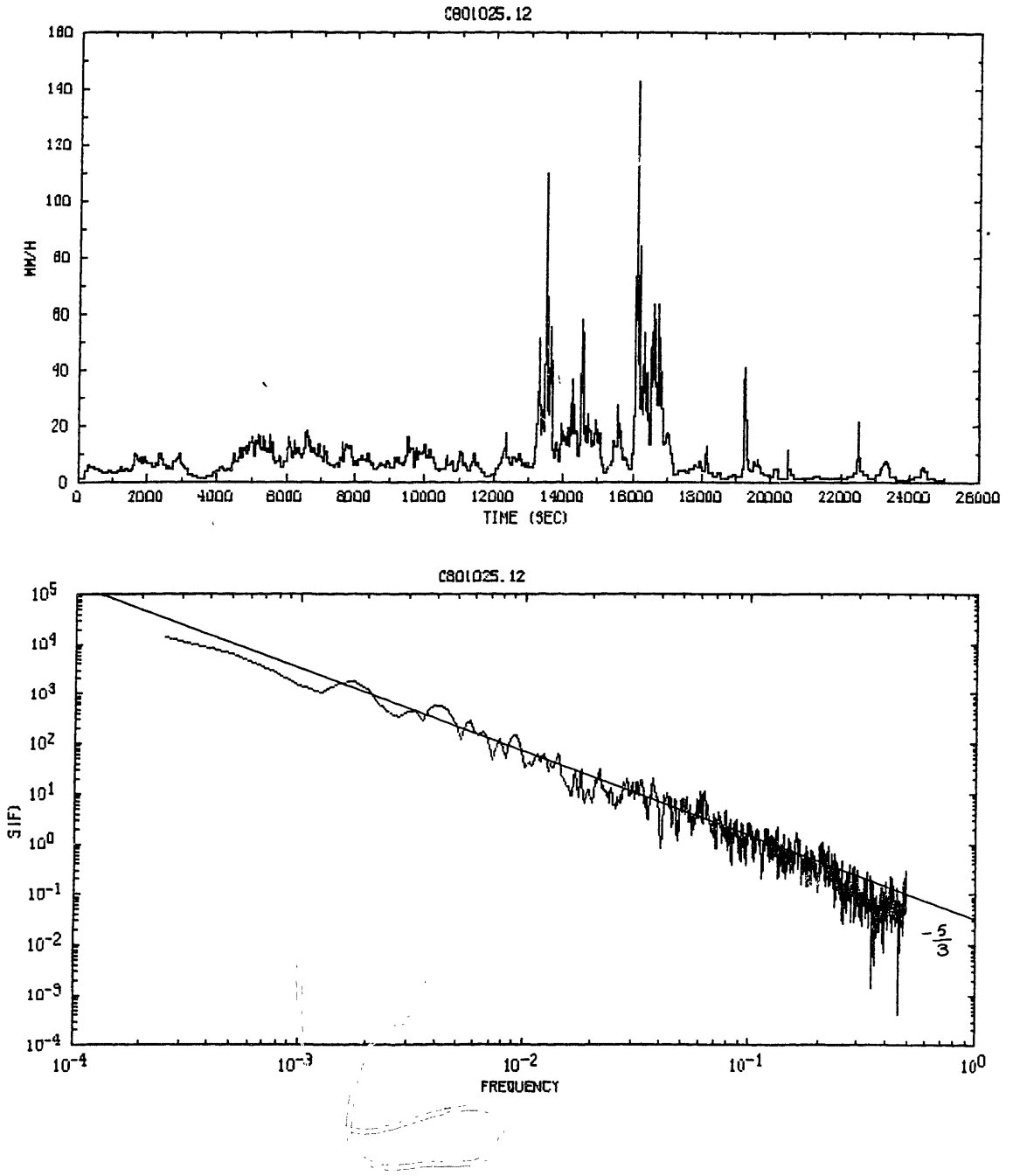

Fig. 1-4. Raingauge data. 25 October, 1980. 7 hour time series of rainfall rate ($mmhr^{-1}$) coarse tipping bucket gauge at MIT. Lower plot is calculated Fourier transform of the data (spectral density). Both axes are logarithmic, frequency in cycles per second. The straight line represents $S(f) \propto f^{-5/3}$.

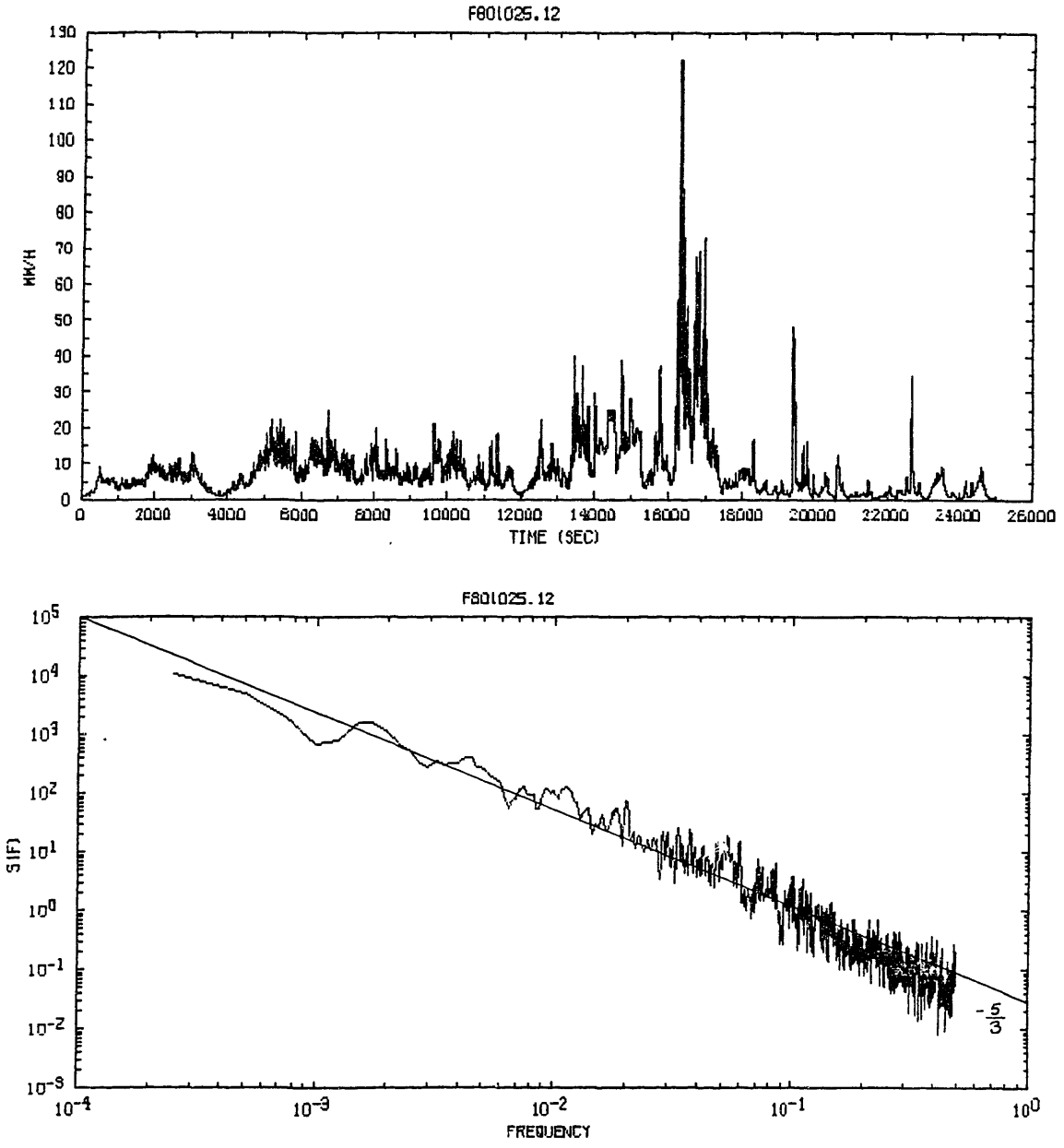

Fig. 1-5. As in Fig. 1-4 for fine tipping bucket gauge.

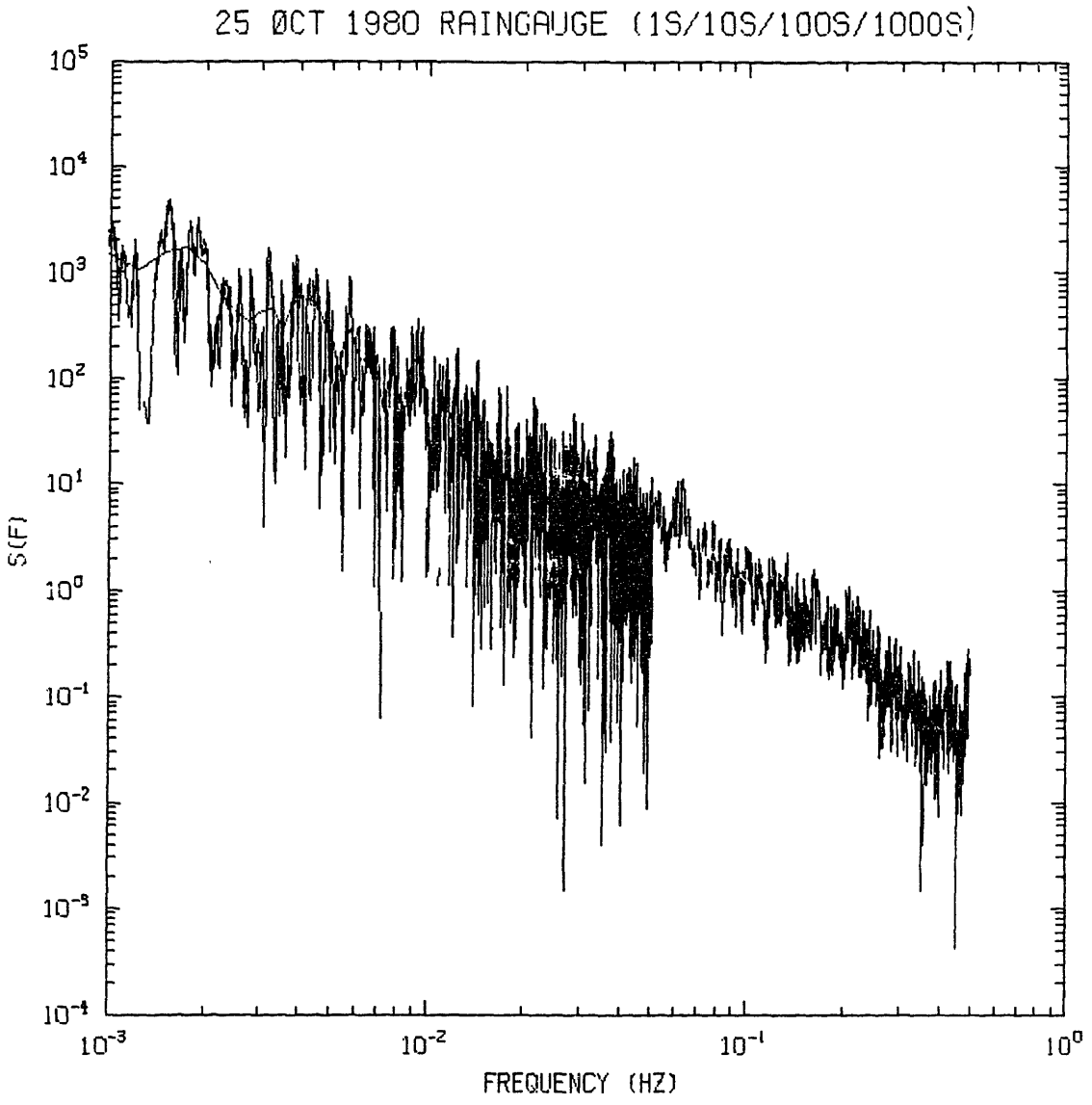

Fig. 1-6. Spectra of data from Fig. 1-4 aggregated at 1, 10, 100 and 1000 second intervals.

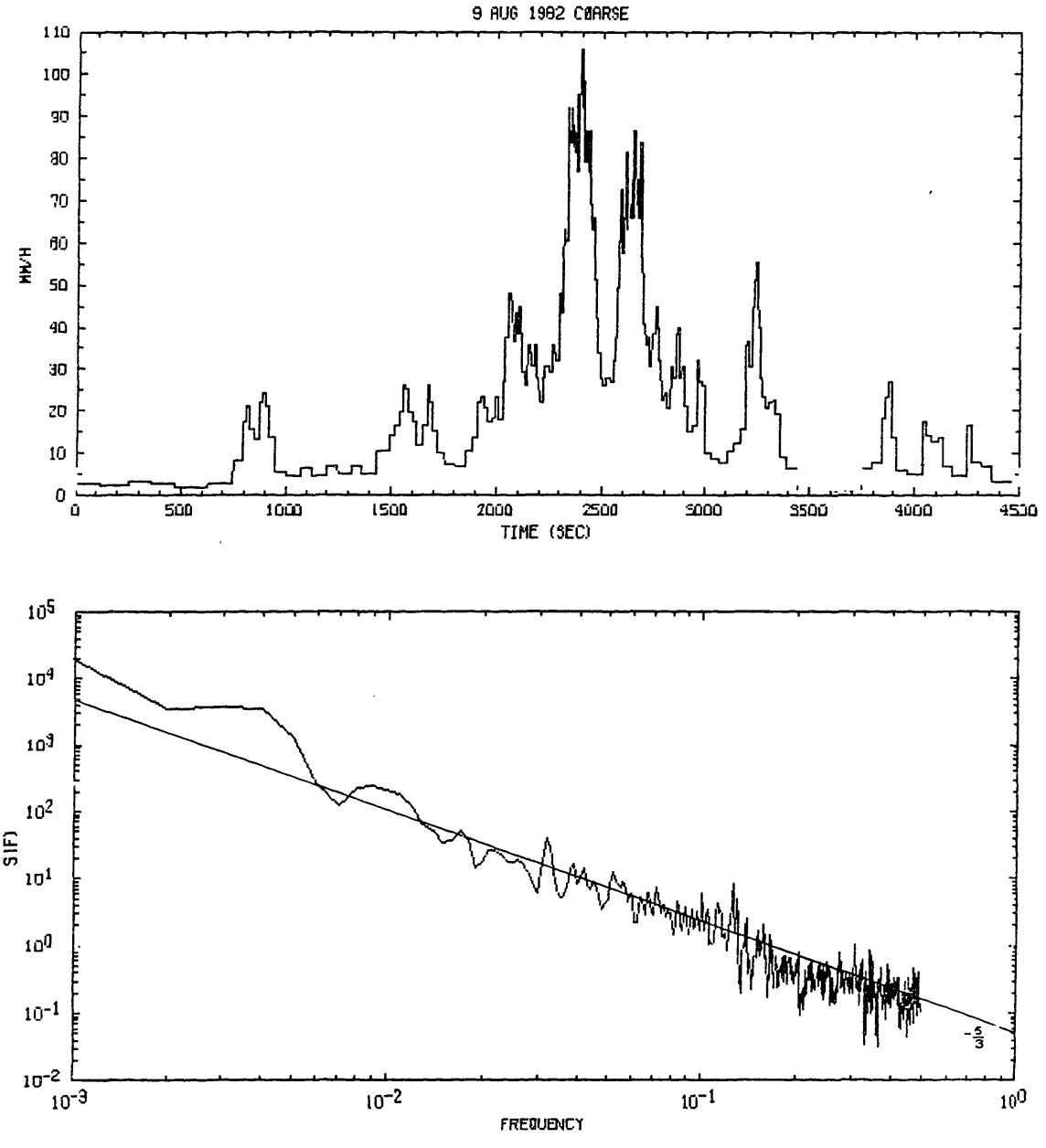

Fig. 1-7. Raingauge data. 9 August, 1982. 1.5 hour time series from coarse tipping bucket; scattered showers.

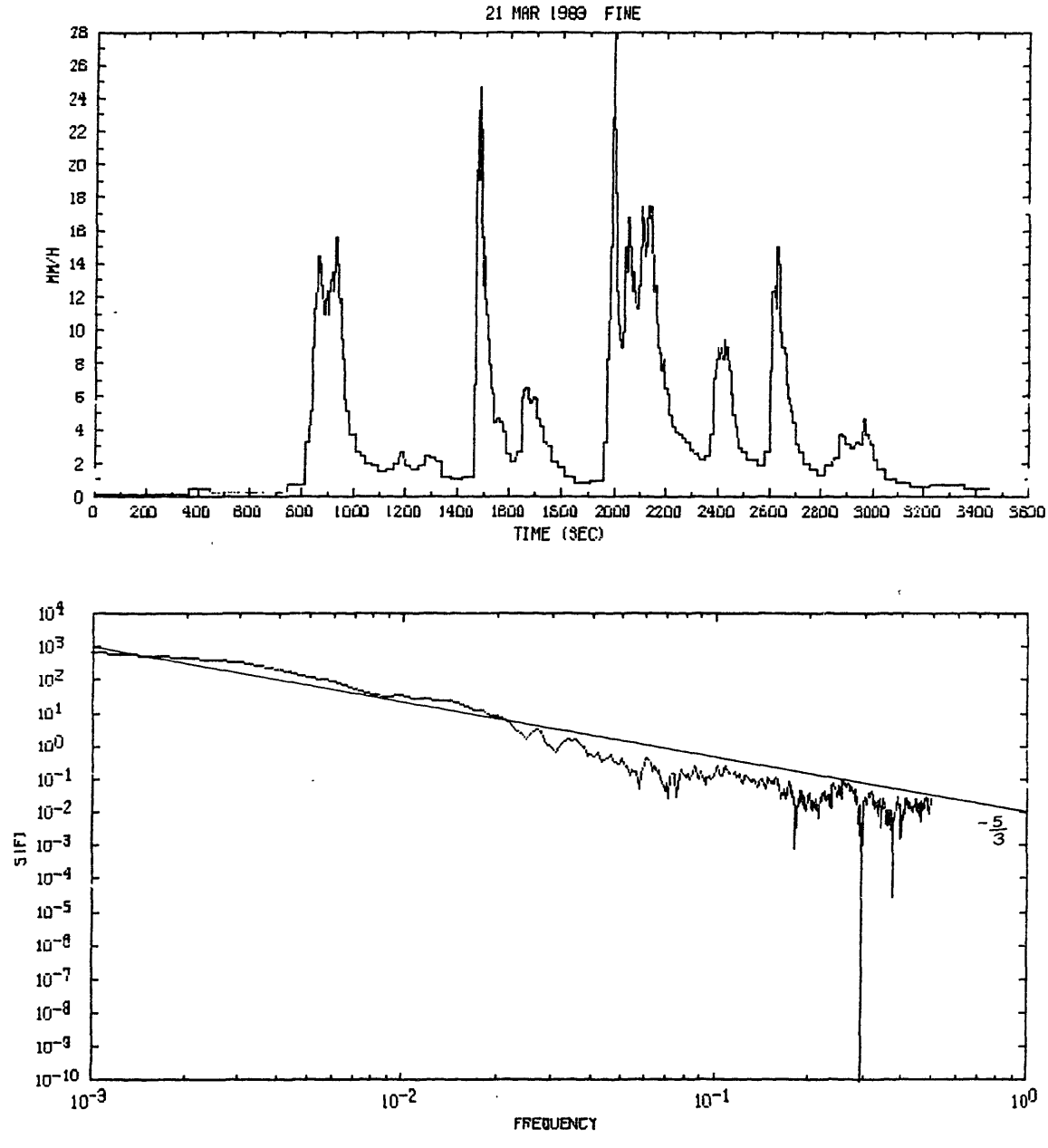

Fig. 1-8. Raingauge data. 21 March, 1983. 1 hour time series from tipping bucket; widespread stratiform rain with embedded showers.

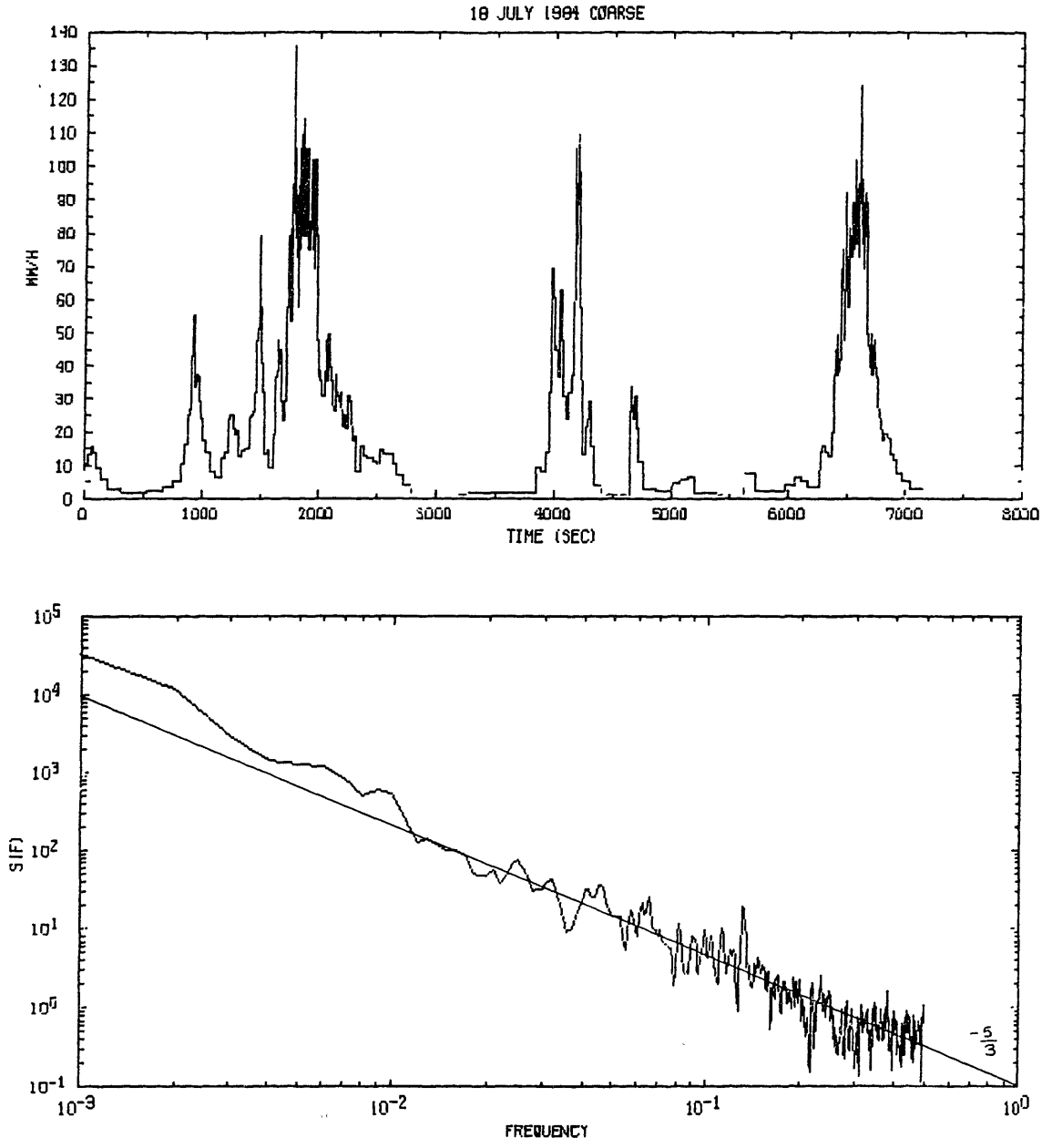

Fig. 1-9. Raingauge data. 18 July, 1984. 2 hour time series from coarse tipping bucket; frontal passage.

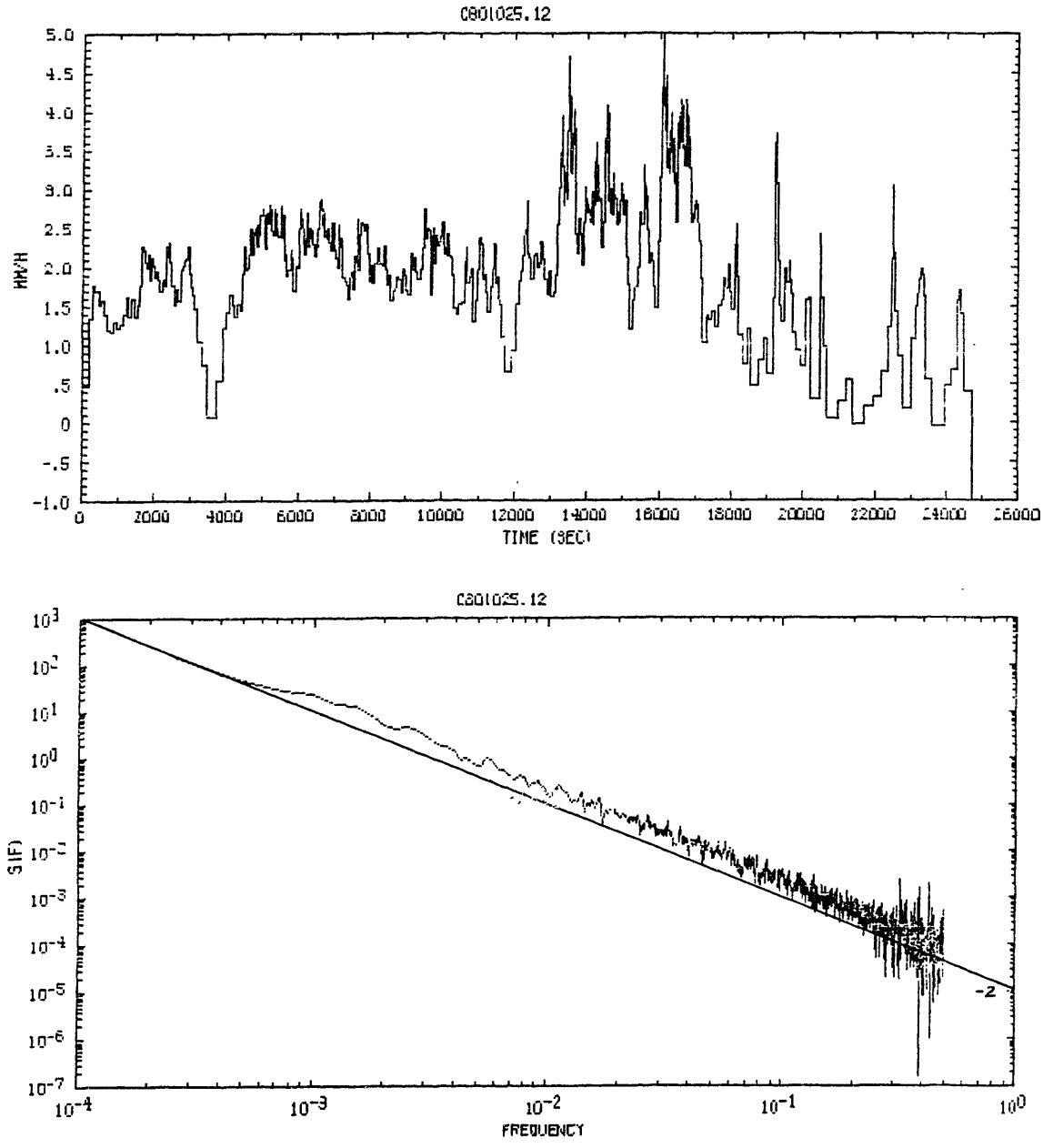

Fig. 1-10. As in Fig. 1-4, for natural logarithm of rainfall rate time series. The straight line represents $S(f) \propto f^{-2}$.

analyzing the logarithm of the rainrate rather than the rainrate itself is not obvious, apart from the observed lognormality of the distribution function. The effects of compressing the dynamic range of the rainfall rate (by taking the logarithm) can be observed in Fig. 1-10 which shows the analysis of the logarithm of the October 25, 1980 time series. In this case the spectrum has steepened to a uniform slope of –2. These effects are possibly compensated for in Cavanaugh's analysis by considering the ensemble average of the calculated spectra. In any event, Cavanaugh and Crane's analysis shows a $k^{-5/3}$ dependence for the coarse gauge over the full dynamic range of the gauge, but only over a narrower range (time scales of 20 min to 75 min) for the fine tipping bucket, possibly due to the sensitivity of the gauge itself.

ii) Radar Data

Time series of the radar reflectivity were obtained for individual range gates by fixing the radar beam in azimuth -- the equivalent of a raingauge point measurement. Data were collected for one hour, the morning of July 2, 1987, in widespread rain with embedded showers. A radar sample (the average of 64 pulses) is recorded every 0.1 seconds. The time series of the reflectivity (plotted as the rainfall equivalent) is shown in Fig. 1-11 for a time series at vertical incidence, 1.5 km above the radar. The spectrum exhibits a marked cutoff at time scales near 10 seconds. At higher frequencies the spectrum contains less power, and is essentially flat, characteristic of white noise. The cutoff frequency corresponds roughly to the translational time scale associated with the radar beam width (50 m with a storm velocity of approximately 5 ms^{-1}). This whitening of the spectrum at spatial scales smaller than the dimensions of the radar pulse volume is discussed in the theoretical work of Srivastava and Atlas (1974) and Sychra (1972).

At spatial scales larger than the pulse volume, however, the radar exhibits the predicted $k^{-5/3}$ dependence. Fig. 1-12 shows the same data plotted with the spectrum obtained from a simultaneous raingauge time series measured at the radar site. The filtering effect of the radar pulse volume on the spectrum is clearly evident at high frequencies. The $k^{-5/3}$ slope is drawn for comparison. The same vertical incidence spectrum is plotted again in Fig. 1-13, along with spectra from fixed beam measurements at low elevation, for range bins at 10 km and 50 km. As the radar pulse volume increases, the region of noise extends to larger spatial scales. The cutoff frequency for the spectra at longer ranges, no

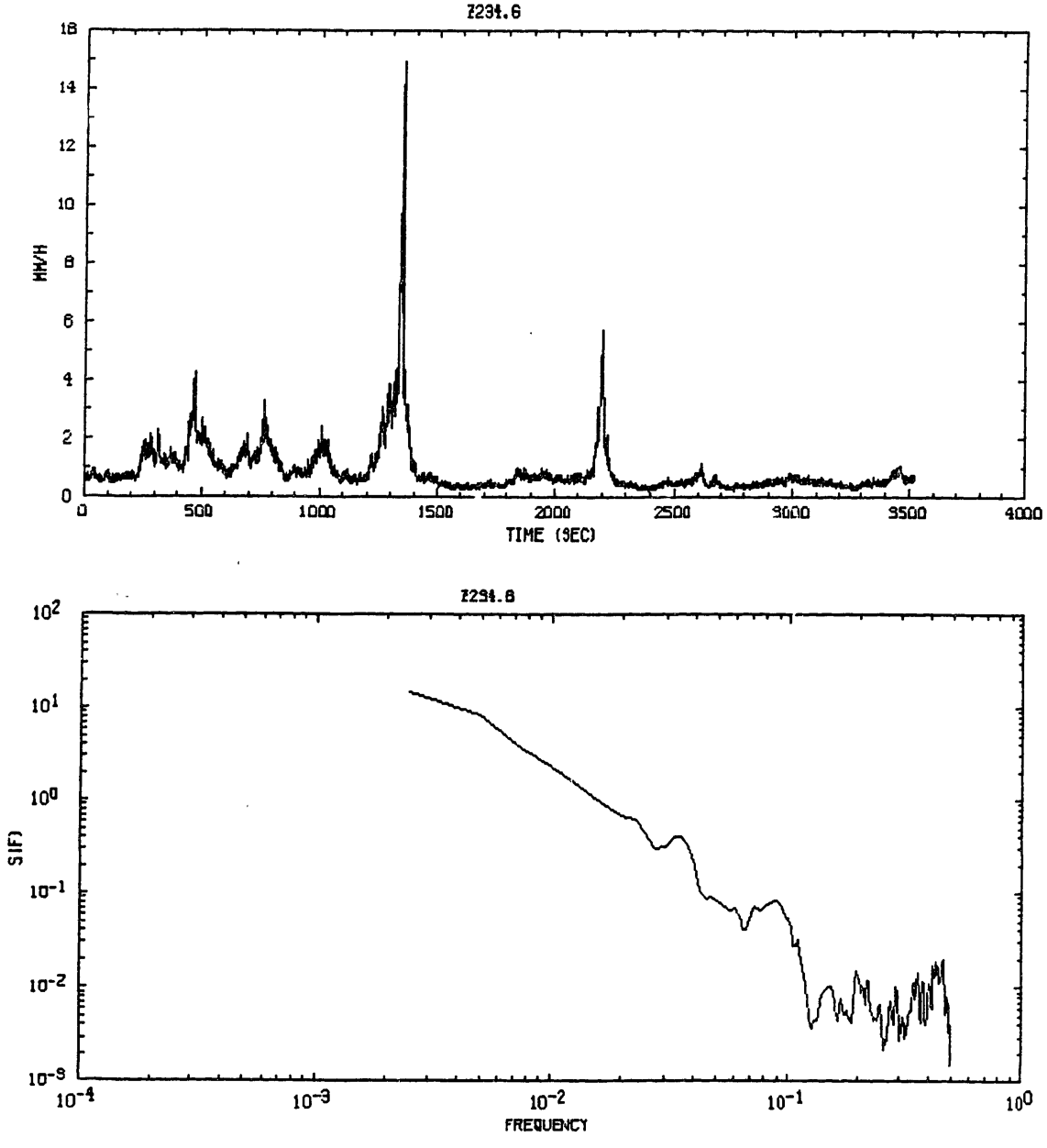

Fig. 1-11. Radar rainfall rate and associated spectral density. 2 July, 1986. Radar reflectivity measured at vertical incidence, 1.5 km above ground, converted to equivalent rainfall rate.

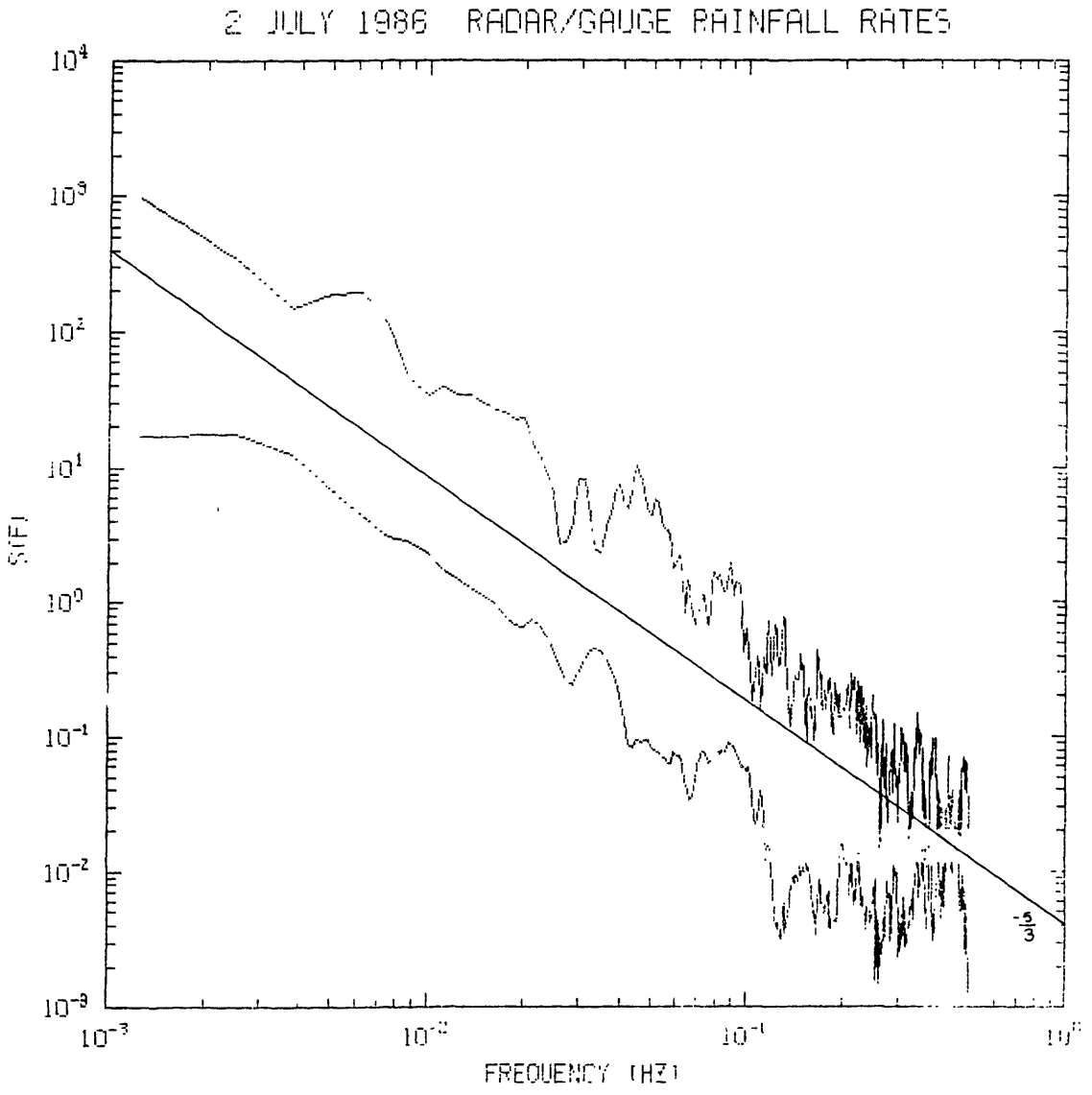

Fig. 1-12. Spectrum of radar rainfall time series from Fig. 1-11 (lower curve) and spectrum of simultaneous measurement of rainfall rate with coarse tipping bucket gauge (upper curve).

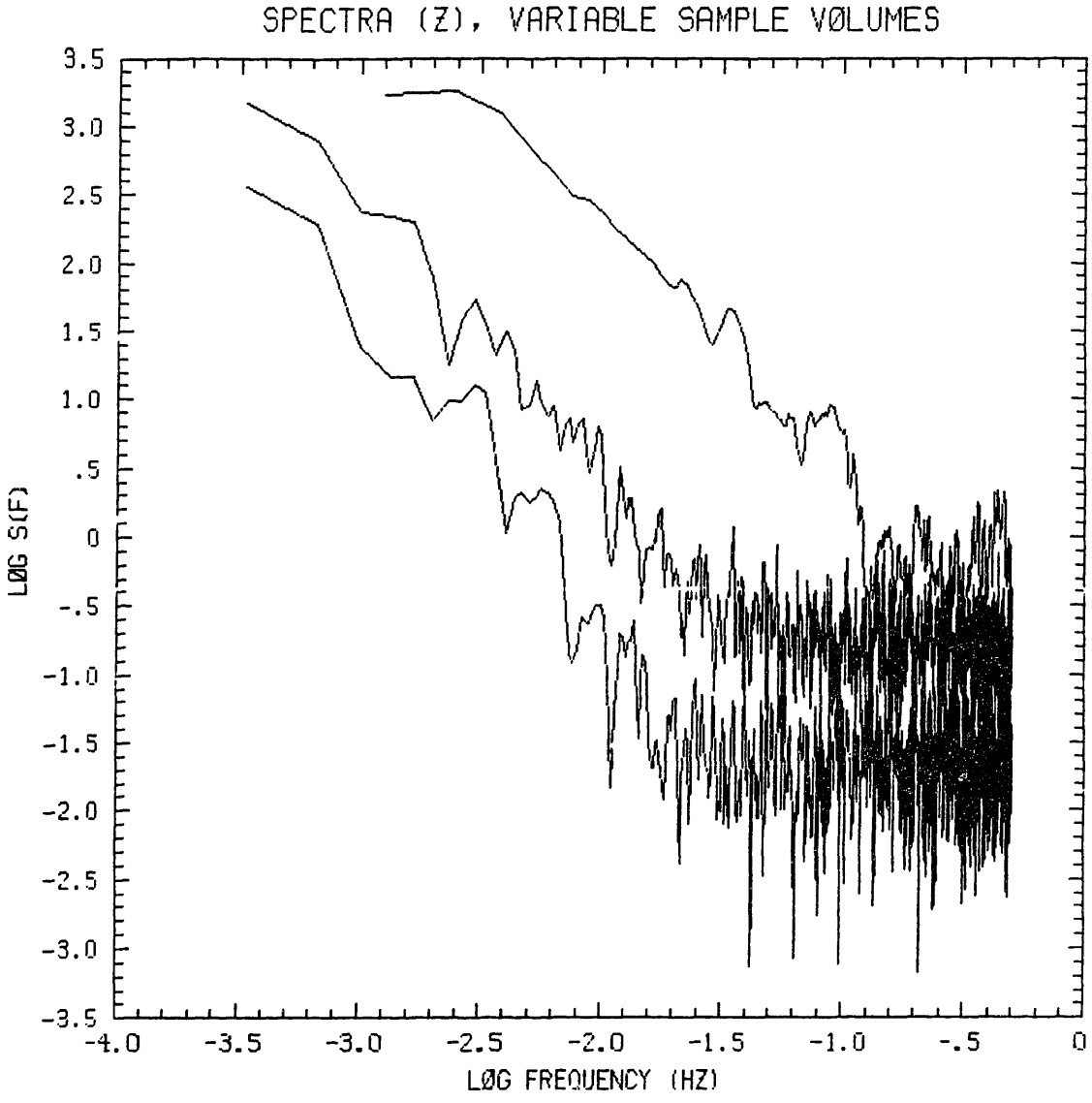

Fig. 1-13. Effect of sample volume on radar rainfall spectra. Upper curve: spectrum from Fig. 1-12 (1.5 km vertical beam); Middle curve: 10 km range; Lower curve: 50 km range. The two spectra at longer ranges are from an hour long time series recorded approximately 1 hour before the data in Fig. 1-11.

longer well defined, is roughly comparable to the radar pulse width (150 m). Because the storm was moving radially, the relevant dimension of the pulse volume is the pulse width, which is independent of range, and there is not a large difference between the cutoff frequencies at 10 and 50 km. The time series for these measurements at longer ranges were recorded the same morning as the data in Figs. 1-11 and 1-12.

Crane (1986) has calculated spatial spectra from radar rainfall maps. He considered azimuthal averages of two dimensional FFTs of the logarithm of the radar derived rainfall field. In data from Tennessee, from the tropics (GATE), and from Boston, a $k^{-5/3}$ dependence was evident at scales larger than 10 km, with a drop-off in the slope at smaller scales.

The $k^{-5/3}$ spectrum and the lognormal distribution of rainfall rates appear to be meaningful descriptions of the rainfall process over a broad range of both spatial and temporal scales. These results might provide the necessary statistical description of the rainfall field for the simulation of rainfall patterns, extending our understanding of errors associated with the radar measurement.

1.2 ERRORS IN RADAR RAINFALL MEASUREMENTS

Numerous studies have analyzed the range of errors associated with quantitative radar rainfall measurements, errors attributable to physical effects such as evaporation of the rain between cloud base and the ground, but also errors associated with the nature of the radar measurement itself. Reviews in the literature include: Kessler and Wilk, 1968; Battan, 1973; Wilson and Brandes, 1979; Doviak, 1983; Huebner, 1985; Zawadzki, 1984; and Austin, 1987. This section will examine selected aspects of these sources of error, specifically with reference to hydrologic applications.

Attempting to incorporate the accuracy of the radar observation of spatial rainfall patterns with quantitative raingauge measurements, some researchers have proposed calibrating the radar measured rainfall with the raingauge catch (c.f., Wilson, 1970; Brandes, 1975; Wilson and Brandes, 1979; Collier, 1986). Others have proposed multivariate statistical techniques for merging the radar and raingauge data sets, for example by cokriging (Krajewski and Ahnert, 1986). The potential for actually increasing the radar error by calibration is obvious, and there is general agreement that in many cases the gauge density required for beneficial radar calibration is in fact so great as to render the radar measurement unnecessary. In this study we have not attempted to calibrate the radar with raingauge data in real time, concurring with the conclusions of Austin (1987) and Zawadzki et al. (1986). The approach adopted here is to consider instead ensemble averages of radar raingauge comparisons to obtain empirical relationships between the radar reflectivity and the rainfall rate.

a) The Z-R Relation

The Z-R relation is both the backbone and Achilles heel of radar meteorology. There are, in reality, two Z-R relationships. The true Z-R relationship relates the drop-size distribution ($Z = \int D^6 dD$) to the rainfall rate ($R = \pi/6 \int N(D) D^3 V_t(D) dD$), as measured by a disdrometer or other suitable technique. Measurements of the drop-size distribution and the terminal velocities (V_t) of the drops define a power law relation of the form $Z = aR^b$, where the coefficients have values close to a = 200 and b = 1.6 (Marshall and Palmer, 1948). When the reflectivity is measured by the radar (called Z_e, for effective reflectivity), the Z_e-R relation is determined by comparison of the radar–derived rainfall with "ground truth", usually obtained from rain gauges.

i) The Measurement of Z_e

The backscattered signal received at the radar is linearly related to the transmitted power, and to the volume reflectivity of the raindrops, but decreases quadratically with range. The constant of proportionality involves various parameters related to the radar wavelength and particular to the radar installation. The characteristics of the radar (WR-66), as configured for this project, are listed in Table 1-1.

Table 1-1. CHARACTERISTICS OF WR-66 RADAR

Wavelength	11 cm
Beam width	1.45 deg
Pulse length	1 μs (150 m resolution)
Sampling (r>50km)	1° x 1km
Recorded precision	0.5 dBZ

Attenuation of the beam by precipitation between the target and the radar is a serious problem for quantitative radar measurements at 3 or 5cm wavelengths, but is negligible at 10 cm. Absorption by atmospheric gases amounts to a fraction of a dB/km, and can be compensated for accurately; the reflectivity is underestimated by about 1 dB at 75 km. This correction is applied during post-processing of the data.

Random fluctuations in the signal, due to noise and the rearrangement of raindrops within the pulse volume, are reduced by averaging a suitable number of samples, in this case 48 (prior to 1987, 64 samples). This averaging reduces the level of fluctuations to about 1 dB. Simultaneous observation of the same target with two radars confirms the calibration of the radar to within about 1 dB (Austin, 1981).

It is worth emphasizing that the accuracy of quantitative radar precipitation measurement relies on careful calibration of the radar to 1 dB tolerances. As increasing use is made of radar in operational settings, and the radar data is used without regard to the possible sources of error, it is imperative that suitable

procedures are developed to ensure the accuracy of the radar reflectivity measurement. Variability in mechanical and electronic components can introduce both random and systematic errors that are not easily detected without careful monitoring. Software errors are equally insidious, and more common with increased signal processing and data manipulation. Simple data consistency checks such as those proposed by Ahnert et al. (1983) should be adopted for all operational radar applications.

ii) Variability in the Z-R Relation

Variations in the drop-size distribution have been recognized to depend on the season and the storm type, and to vary also within the storm. Compensation for variations in the drop-size distribution is accomplished by varying the coefficients of the Z-R relation. Table 7.1 of Battan (1973) lists a selection of the many empirically determined relations. With a knowledge of the probability distribution of the rainfall rate, one can obtain an estimate of the expected variation in the total depth of the rainfall measured with different choices of the Z-R relation coefficients ($Z = aR^b$). Fig. 1-14 illustrates this variability for values of the coefficient **a** between 100 and 500, with the exponent **b** ranging from 1.0 to 2.0. The distribution of occurrences of Z is weighted by a lognormal distribution

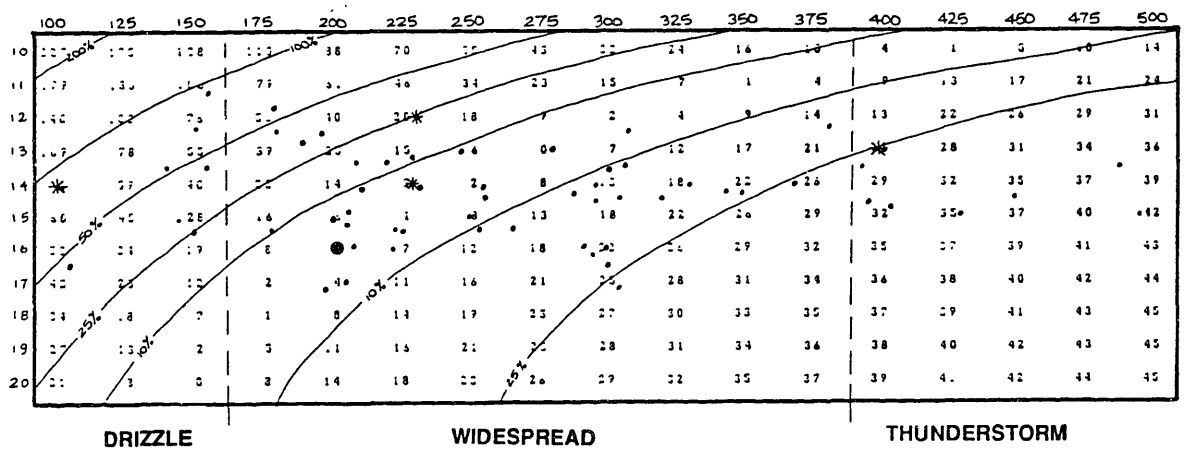

Fig. 1-14. Variability between Z-R relations. Percent difference between $Z = aR^b$ and Marshall-Palmer $Z = 200R^{1.6}$ (solid circle) for total depth, assuming lognormal distribution of Z, with parameters $\mu = 20$ dBZ, $\sigma = 8$ dBZ. Values for Z-R relations reported in Battan (1973) Table 7.1 are plotted as dots. Austin (1987) Z_e-R relationships plotted as asterisks. Broad distinctions between drizzle and thunderstorm cases delineated by dashed lines.

with parameters ($\mu = 20$ dBZ, $\sigma = 8$ dBZ), as calculated in section 1.1. The expected total depth is plotted as the percent difference from the depth obtained for $Z = 200R^{1.6}$, indicated on the plot as a solid circle. Values for **a** and **b** from Battan are indicated by dots. Most of the variability between observed Z-R relations amounts to less than 25 % in the calculated total depth.

Joss and Waldvogel (1970) showed that by selecting three Z-R relations, one each for thunderstorms, drizzle and widespread rain, the average standard deviation of Z-R regressions could be reduced from 30% to less than 20%. However, the observed scatter in Z_e-R plots remains much larger, reaching the factor of two commonly quoted as representing the accuracy of the radar rainfall measurement (c.f., Wilson and Brandes, 1970).

Extending the concept of Z-R relations stratified by storm type to Z_e-R regressions, factors other than the drop-size variability are also incorporated into interpretations of the observed variability. In effect the Z_e-R relationship becomes an empirical calibration equation dependent on the storm type (Austin, 1987), the range (Calheiros and Zawadzki, 1987), the averaging interval (Zawadzki, 1984), and even the particular radar installation.

The results of Austin (1987) are used in this project, since her research was conducted at MIT for New England storms. The relation $Z_e = 230R^{1.4}$ is used in preference to the Marshall-Palmer relation. The relation $Z_e = 400R^{1.3}$ is applied to thunderstorm cases, and $Z_e = 230R^{1.2}$ is used for convective rain associated with cold fronts. Other cases such as drizzle are discussed in Austin (1987; c.f., Table 7), but were not considered here. These Z-R relations are indicated by asterisks in Fig. 1-14.

An example of the effect of different Z_e-R relations on the areal average rainfall rate is shown in Fig. 1-15. The curves represent the average rainfall rate over the Souhegan river basin (440 km^2), at ten minute intervals, for the first eight hours of a strom on 27 June, 1987. The absolute percentage differences between the convective relations and the average relation ($Z_e = 230R^{1.4}$) are plotted in Fig. 1-16, showing the dependence of the differences on the rainfall rate.

The presence of hail in the radar sample volume can enhance the reflectivity by 10 dBZ or more. In this study, rainfall rates are limited to a maximum of 100 $mmhr^{-1}$ (roughly the climatological maximum five minute rainrate) to

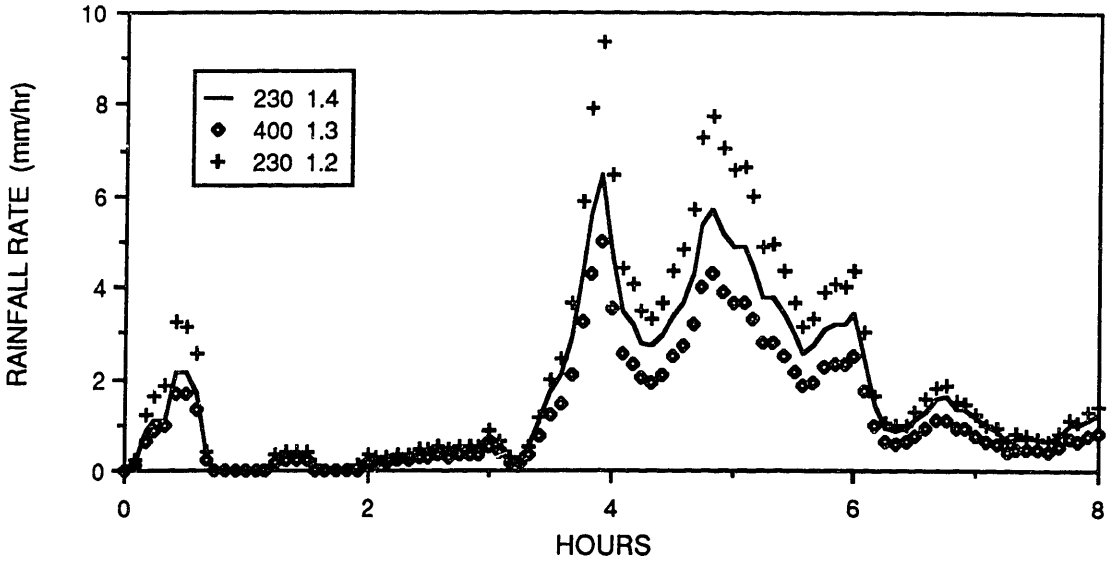

Fig. 1-15. Souhegan areal average rainfall rate for eight hours of 27 June, 1987 storm, assuming: $Z_e = 230R^{1.4}$ (solid line); $Z_e = 400R^{1.3}$ (diamonds); $Z_e = 230R^{1.2}$ (crosses).

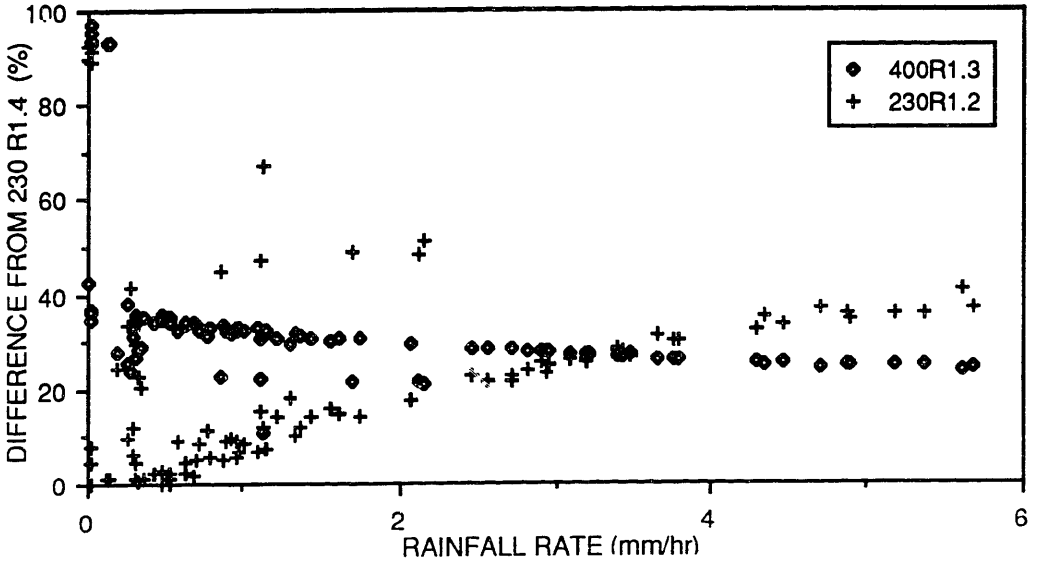

Fig. 1-16. Percent difference between Z-R relations. Absolute value of difference between points in Fig. 1-15 and curve $Z_e = 230R^{1.4}$, plotted as function of rainfall rate.

prevent overestimation of the rainfall under these conditions (Austin, 1987). Also, reflectivities are limited to positive dBZ values in this study (i.e. $r > 0.01$ $mmhr^{-1}$) for computational reasons.

b) The radar sample volume

The explanations presented in the previous section to describe the variability in the Z_e-R relation consider physical mechanisms which affect the rainfall measurement such as updrafts, hail formation etc. For the most part though, they do not address the fundamental differences between radar and rain gauge measurements: the volume nature of the radar sample, and the height of the sample volume above the ground. The consequences of these differences are probably of more consequence for hydrologic applications than the variability of the drop-size distribution. These effects are all the more important because the volume and the height of the radar sample above the ground both increase quadratically with range, effectively limiting the area of radar coverage.

Purely statistical differences between the radar and raingauge sampling modes have been studied with regard to suitable averaging for radar-gauge comparisons (Zawadzki, 1975). It is possible that much of the variability observed in the Z_e-R regressions is attributable to statistical fluctuations alone, as noted by Chandrasekar and Bringi (1986). The results of section 1.1 on the small scale structure of rain might assist in providing some understanding of this problem.

Drifting of the rain between the radar sample and the ground is obviously a large source of error in radar raingauge comparisons. For hydrologic applications, this error is probably negligible compared to the effects of scanning only at intervals of five or more minutes. Dalezios (1982) studied this problem in some detail and found no improvement in the mean storm radar bias when correction for wind drift was applied.

One of the fundamental assumptions of the radar equation is the homogeneity of the raindrop field within the target volume. In reality, strong gradients of the reflectivity field are observed. Torlaschi and Humphries (1983) show that such gradients are exponentially distributed with a mean value between 5 and 10 dBZ/km. Thus "incomplete beam filling", long recognized as a source of error at the edges of radar echoes, is also a major source of error for all

samples, particularly in convective storms. The non-linearity of the radar receiver, and non-uniform illumination of the sample volume both tend to amplify the non-linearity of the Z-R relationship (Zawadzki, 1984).

It is possible that oversampling the rainfall pattern both in range and azimuth might ameliorate the radar sampling problem, to a certain extent. Since the cross-section of the beam is Gaussian, the illumination of the volume is strongly center-weighted, so that sampling in azimuth at intervals smaller than the beam width might yield a more meaningful volume averaged sample. Similar benefits might result from sampling the returned radar signal at 150 m intervals (the pulse width), and then averaging in range, rather than sampling discretely at intervals of 1 km.

Reflectivity gradients in the horizontal are sometimes not as strong as those in the vertical, particularly near the 0°C isotherm where melting snow produces a layer of enhanced reflectivity called the "bright band". In this, as in many other quantitative radar projects, the issue of bright band "contamination" has been side-stepped by considering primarily summer storms, when the bright band, if present, is several kilometers above the ground. To extend radar precipitation measurements into the winter months, and to greater ranges, will require additional research into the nature of vertical gradients of reflectivity. One possible approach to this problem, and to similar problems of evaporation below cloud base and accretional growth in fog, would involve combining radar data with thermodynamic data. Using the full three dimensional data available from volume scans, and incorporating vertical temperature profiles it should be possible to obtain a better estimate of the precipitation actually reaching the ground.

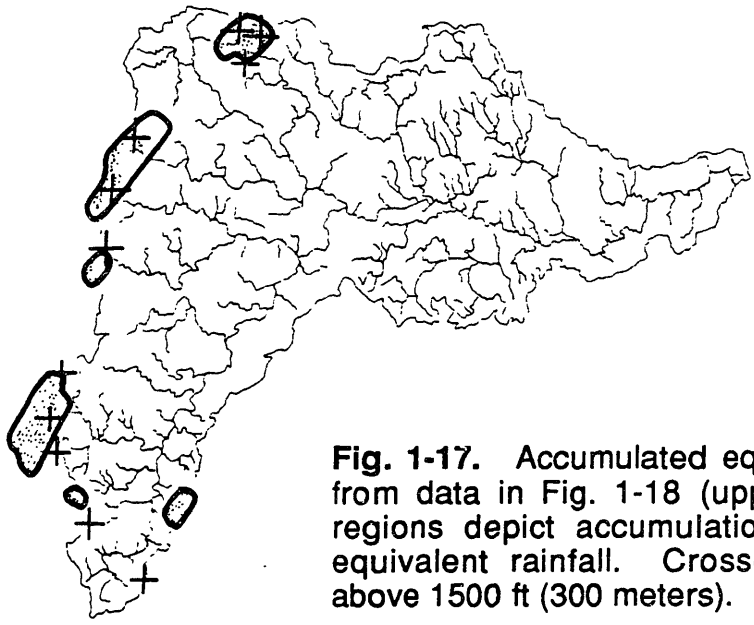

Fig. 1-17. Accumulated equivalent rainfall depth from data in Fig. 1-18 (upper curve). Shaded regions depict accumulations of 1cm or more equivalent rainfall. Crosses mark all summits above 1500 ft (300 meters).

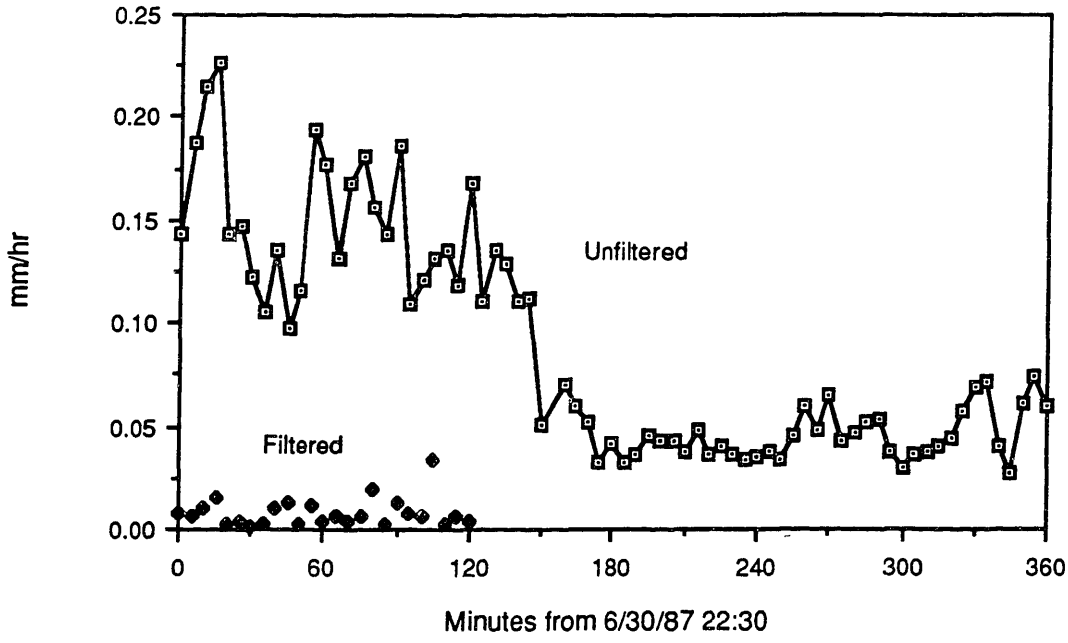

Fig. 1-18. Time series of areal average reflectivity over Souhegan after passage of cold front (expressed as equivalent rainfall rate). Points labelled "Filtered" are first two hours of data with ground clutter filter operating.

1.3 RADAR DATA POST-PROCESSING

a) Ground Echo Rejection

The topography of southern New Hampshire increases considerably west of the broad Merrimack floodplain. On the watershed divides of upland tributaries like the Souhegan, several peaks over 600 meters rise above the ridgeline. The pattern of radar echoes resulting from ground-clutter west of the MIT radar is thus not limited to the urban roof-lines of Boston and Cambridge, but includes the north-south ridge of hills across central Massachusetts and southern New Hampshire at ranges of 50 to 100 km. Isolated peaks, like Mounts Wachusett and Monadnock, appear conspicuously on radar scans if suitable signal processing is not introduced to suppress these ground echoes.

The intensity and spatial distribution of ground echoes depend not only on the elevation angle of the radar beam, but also on the refractive index of the air. Following the passage of a cold front in particular, the air is stably stratified, resulting in a marked refraction of the beam towards the ground, and consequently stronger ground echo returns. This situation is graphically depicted in Fig. 1-18. Six hours of data were collected at 5 minute intervals following the passage of a cold front on June 30, 1987. There was no precipitation over the region during this period. The solid curve in Fig. 1–18 is the time series of the ground echo intensity, averaged over the basin. Reflectivity values have been converted to equivalent rainfall intensities. The values decrease with time, as mixing dissipates the layer of cold air near the ground.

Fig. 1-17 depicts the close relationship between the ground echo pattern and the elevations of peaks along the boundary of the Souhegan basin. The same six hours of data discussed above were integrated to produce this map, on which total depths of equivalent "precipitation" greater than 1 cm have been outlined.

From the above discussion, it is clear that echoes not associated with precipitation must be removed, or significantly reduced in intensity, before the radar map can be used as input to the hydrologic model. The effects of clutter on a distributed model are potentially more serious than they would be if a spatially lumped model were used with areal average rainfall rates as input. With the distributed model, the mountains behave like stationary rain cells aligned on the

ridge, and can, during the course of a storm, saturate specific grid elements that would not have otherwise received any rainfall.

Many clutter rejection schemes rely on pre-recorded maps of the locations of ground targets, such as the one generated in Fig. 1-17. Radar measurements over ground targets are then corrected (usually by some arbitrary factor) to compensate for the clutter. The drawback of this procedure is that the clutter pattern is considered to be fixed in space and time, when in reality the ground echo pattern fluctuates appreciably between scans. By using a Doppler radar, superior clutter rejection filters can be implemented using the velocity information to discriminate between precipitation echoes and stationary ground targets for each scan.

Two different signal processors have been used with the WR-66. Prior to 1987, a sophisticated real-time ground clutter rejection algorithm was in effect. This operated on the principle that the spectrum of doppler velocities recorded from a ground target is narrowly distributed about zero. By analyzing the spectrum, ground echoes can be distinguished from precipitation echoes for which velocity spectra are characteristically broader. Clutter is not simply rejected, but the reflectivity at a given range bin is scaled by a factor related to the ratio of total returned power to the power in the low velocity region of the spectrum. This effectively avoids both the undesirable rejection of real precipitation with low radial velocities, and unwarranted attenuation of precipitation superimposed on ground echoes. The technique performs extremely well, permitting scans at low elevation angles. For all of the archived data used in this study prior to 1987, the elevation angle of the beam was 0.1 degrees. This corresponds to a beam height of less than 1000 meters over the river basins. For typical conditions, only two or three ground echoes are evident on the edge of the Souhegan, with reflectivities of 5 to 10 dBZ.

At present a simpler clutter filter is used with the WR-66. Designed primarily as a means for reducing clutter in the near range, the algorithm acts only as a narrow filter for all echoes with small velocities. Because it cannot distinguish effectively between ground targets and precipitation with no velocity in the radial direction, it can create gaps in the recorded rainfall field. This is unacceptable for quantitative precipitation measurements, and the filters were not used in the region over the watersheds during this experiment.

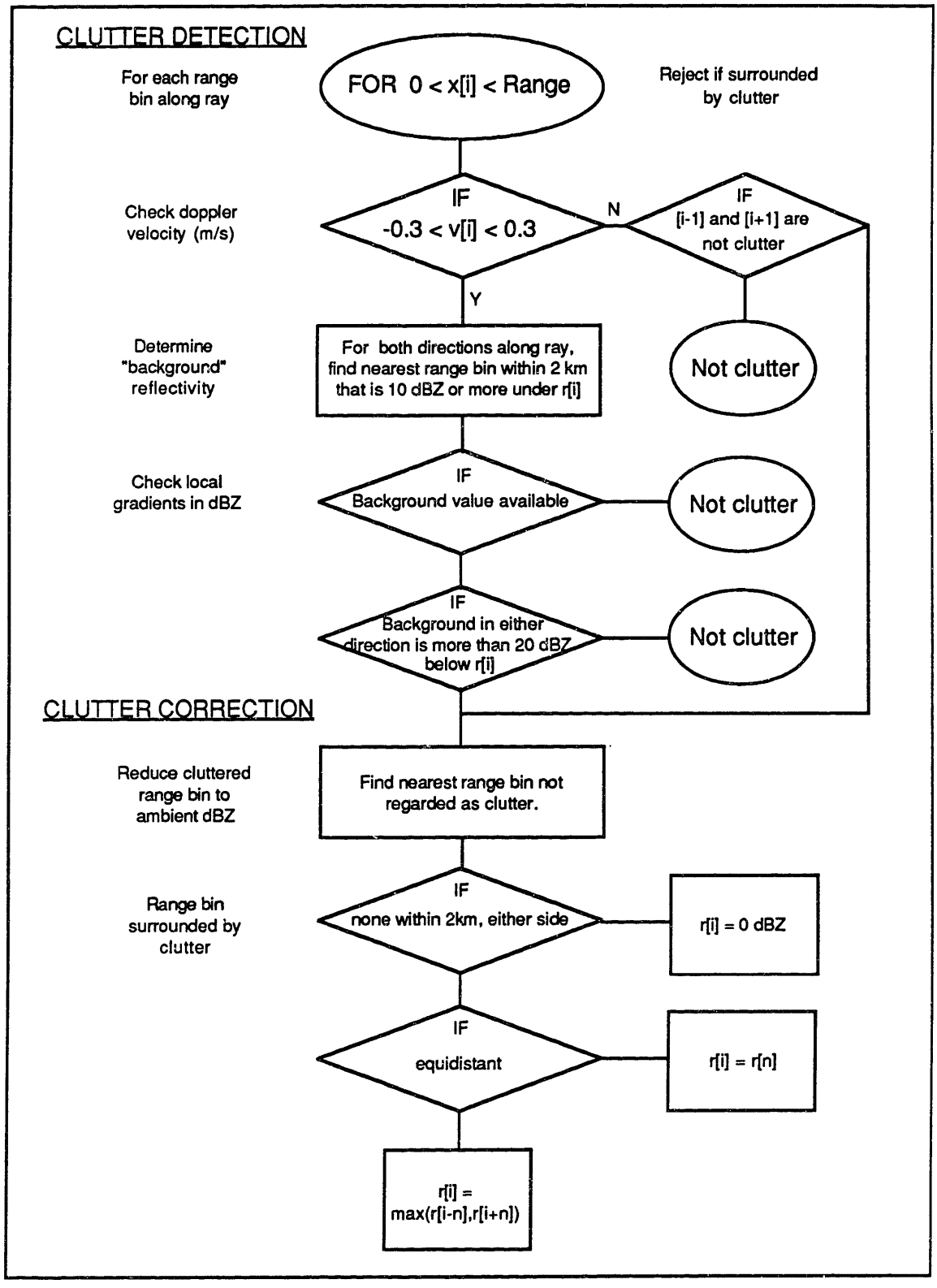

Fig. 1-19. Flow chart of ground clutter correction algorithm.

In order to avoid the strongest echoes from the mountains, the elevation angle of the beam was increased. An angle of 1.4 degrees was selected as providing considerable reduction in ground echoes while keeping the height of the beam (3 km) below the melting layer in most cases. Despite these precautions, considerable ground echo returns are still observed (Fig. 1-18). Two schemes were proposed to overcome this problem. The first involves using a bit–map of normal clutter conditions to determine which range bins are likely to be contaminated. For such range bins, measurements from a higher elevation scan (1.8 degrees) are substituted. This procedure was not adopted because of the reservations expressed above, and because the 1.4 degree scan is itself already close to the melting layer under some conditions.

An alternative approach was developed which relies instead on the recorded Doppler velocities. Criteria are imposed on the mean velocity and on the gradient of the reflectivity, in order to distinguish between ground targets and real precipitation echoes. This procedure proved successful in removing the strong echoes from clutter without significantly affecting regions of precipitation with low radial velocities. Fig. 1-19 provides a description of the algorithm that was implemented during the Cartesian conversion of the radar data. The threshold values of velocity and reflectivity gradients were selected, by trial and error, to produce the most acceptable results over the watersheds, and may not in fact be optimal choices under all circumstances.

The success of the algorithm can be judged by Fig. 1-20. For each five minute interval, the fractional reduction in the areal average of the rainfall rate is calculated for two cases. The time series labelled "Ground echoes" corresponds to the same sequence of maps used to generate Fig. 1-18. With no rainfall present, the reduction is nearly complete. The actual filtered time series is also shown in Fig. 1-18. With rainfall present, (first hour of the 6/27/87 sequence), the filter continues to perform well and the areal average of the rain field does not suffer from any appreciable attenuation. Integrations of rainfall maps over several hours are no longer dominated by the mountain echoes.

As previously noted, the algorithm presented here could be adapted for more general applications. The principal advantage of the procedure lies in its ability to suppress so-called "anomalous propagation" (AP) echoes that result from stronger than normal refraction of the radar beam toward the ground. These AP echoes do not necessarily coincide with topographical or other normal sources of clutter, and would not be detected by a bit-map procedure.

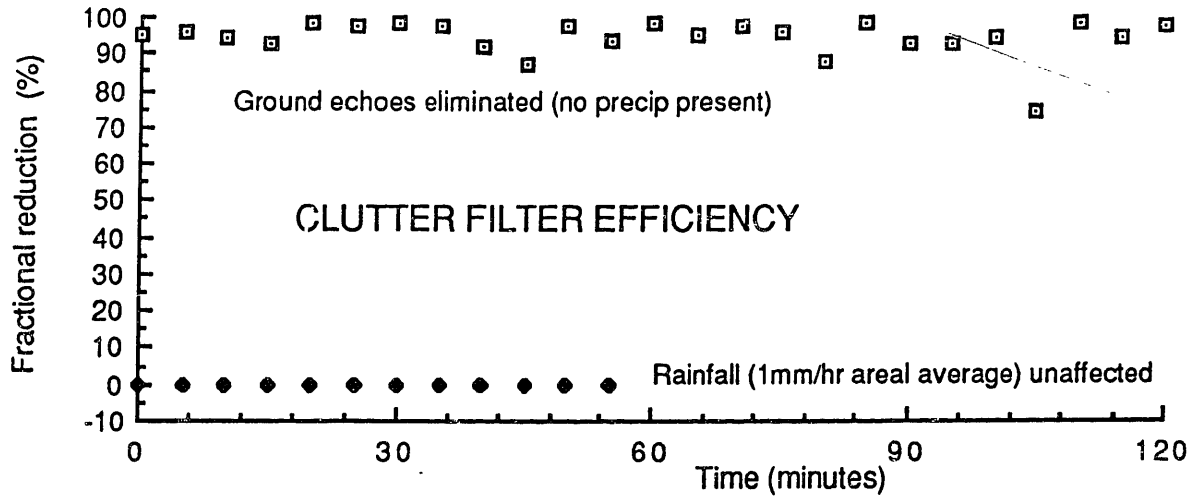

Fig. 1-20. Percent difference between raw and filtered data. Open boxes correspond to first two hours of time series in Fig. 1.18. The contribution of the mountains to the areal average "rainfall" is reduced by nearly 100% with the ground clutter filter. When rainfall is present, (first hour of 27 June storm), the filter removes the mountains without affecting the areal average rainfall rate.

b) Polar to Cartesian Conversion

The radar data must be converted from polar to Cartesian coordinates for input to the hydrologic model. The program POLKA, developed expressly for the purpose, relies on several simplifications justified by the size and location of the river basins relative to the radar. No correction is made for the elevation of the beam, since even at an elevation angle of 2 degrees, the correction for the range is less than 100 m at 100 km range.

There are two possible approaches to performing the conversion from polar to rectangular coordinates, each valid for different relative dimensions of the grid. If the Cartesian grid spacing is large compared to the projected dimensions of the radar pulse volume, an average radar reflectivity can be assigned to each rectangular grid element by performing a weighted average of all radar samples within the element. If, on the other hand, the grid spacing is less than the effective radar sample region, the radar map can simply be digitized at the resolution of the grid spacing without introducing any significant error.

At 75 km range, in the vicinity of the river basins, the radar beam has spread to a width of nearly 1 km. Also, at this range, samples are recorded at 1 km intervals in range, so that the effective radar sample size is nearly 1 km square. Actually, in practice, the radar ray "width" is determined not by the spreading of the beam, but by the angle between successive rays. The antenna controller used with the WR-66 is set to take samples at approximately 1 degree intervals. In the conversion routine, each ray is simply spread to either side of the nominal azimuth in order to cover the entire radar map. Similarly, the radar samples are considered to have an extent in range equal to the sample interval along the ray (e.g. 1 km), although the extent of the radar sample in range is, strictly speaking, given by the pulse width (150 m).

A grid spacing of 100 meters, much smaller than the projection of the pulse volume, was selected for Cartesian conversions of the radar data. This corresponds to the finest grid spacing compatible with the hydrologic model. POLKA, designed for real-time applications, completes the required conversion and storage to disk in approximately 20 seconds. The interactive nature of the routine allows quality–control of the radar map sequence, rejecting scans with missing rays, or maps with no rainfall. An inventory of the map sequence is stored in a separate file.

c) Interpolation and Forecasting

Radar scans are typically recorded at intervals of 5, 10 or even 15 minutes. Assuming a translation velocity of 10 to 15 ms^{-1}, a 10 minute scan sequence would introduce gaps of about 6 km between the locations of echo centers at successive time steps. To reduce this effect, scans at intervals of 5 minutes were recorded on an operational basis during 1987 (normal scan interval is 10 minutes for the archived data). Except in rapidly translating convective storms, there is reasonable continuity between successive scans, and in the integrated maps of total depth.

Since the hydrologic model operates typically with a time step longer than 5 minutes, a procedure for averaging several radar maps is necessary. The algorithm adopted considers each model time step to extend over $t \pm \Delta t$, where t is the nominal time and Δt is half the model time step. Any scans from the inventory which fall within this interval are averaged. If no scans are available for the interval (missing data, hardware malfunction, etc.) the maps previous to and immediately following the interval are averaged, weighting each inversely by

the difference between the nominal time and the time of the scan. This interpolation is not attempted over intervals longer than three times the model time step.

Ideally, the interval between scans should be kept as short as possible for quantitative precipitation measurements. Scans at 1 minute intervals should provide not only a more robust estimate of the accumulation at a point, but also ensure that the storm motion is adequately resolved. The alternative is to consider a procedure for interpolating the rainfall pattern between scans.

Procedures for forecasting radar rainfall patterns have been evaluated by many researchers. Techniques range from simple advection of the pattern (Bellon and Austin, 1978, 1984); advection with provision for development of the rain cells (Tsonis and Austin, 1981); applying different advection velocities to individual cells (Wiggert and Ostlund, 1975), and an objective analysis technique (Takasao and Shiiba, 1984) that incorporates translation, rotation and deformation of the pattern. It is clear from these studies that there is little to recommend procedures more complicated than simple advection of the pattern, since all such forecast schemes are ultimately limited to lead times of little over half an hour, the typical cell lifetime.

It is important to note that these procedures were considered here, not for their predictive value, but to incorporate them eventually into the interpolation scheme proposed for model input. Actual precipitation forecasting was not pursued here because such procedures are typically limited to less than one hour, which is not a significant lead time for river basins which have times to peak runoff on the order of 10 to 20 hours. However, for urban hydrology and flash-flood conditions, even a short-term forecast would be of tremendous value. In all likelihood though, the greatest benefit will be derived not from simple extrapolation forecasts, but from radar data integrated with mesoscale models that consider the storm dynamics and thermodynamics. Such models could conceivably rely either on numerical model results or on conceptualizations of the rainfall process, as proposed by Georgakakos and Bras (1984). The potential shortcomings of simple extrapolation forecasts are graphically illustrated in Fig. 2-12 of the next section.

CHAPTER 2: THE RIVER BASIN

2.1 THE SOUHEGAN AND SQUANNACOOK RIVERS

Several criteria influence the selection of a suitable watershed for radar hydrology research. The most obvious requirements are complete areal coverage of the catchment by the radar, and the availability of near-real-time stream gauge data. Also, the basin should be of sufficient size to demonstrate the utility of radar in situations where there is large spatial variability in the rainfall field. However, the larger the area, the greater the effects of storage on the response of the basin.

Many New England rivers are regulated by dams and other flood control projects. While such elements may, in principle, be incorporated into any model by using standard routing procedures, the response of regulated watersheds tends to be dominated by storage effects, effectively damping the quick-flow components of the hydrograph. The Blackstone River of south-central Massachusetts, one of the basins originally considered, was not selected for these reasons.

Primarily because of the availability of data, the Souhegan and Squannacook Rivers were chosen for this study. Coincidentally, the basins share a common boundary, and are similar in many respects: topography, geology, and climate. Straddling the Massachusetts-New Hampshire border, both are tributary to the Merrimack River: the Souhegan directly; the Squannacook via the Nashua River (Fig. 2-1). Both drainages are oriented roughly west to east (discounting the dogleg of the Souhegan basin), reflecting the general slope of the land towards the Merrimack Valley. Vegetation and soil characteristics are also similar in the two basins, and the following general description of conditions applies to both watersheds. The primary differences between the two basins are size, and certain features of the drainage network that are considered in the section on geomorphology.

a) Soils

The terrain and soils of the region are primarily the result of glacial action. Hills are typically rounded, "drumlin" formations, local regions of rock resistant to the erosive force of the ice-sheet. Outcrops of the exposed granitic bedrock are evident on the flanks and summits of the higher peaks. There, soils are typically thin, supporting a growth of conifers and drought resistant deciduous species. In the valleys, the geomorphology is less a consequence of erosion by

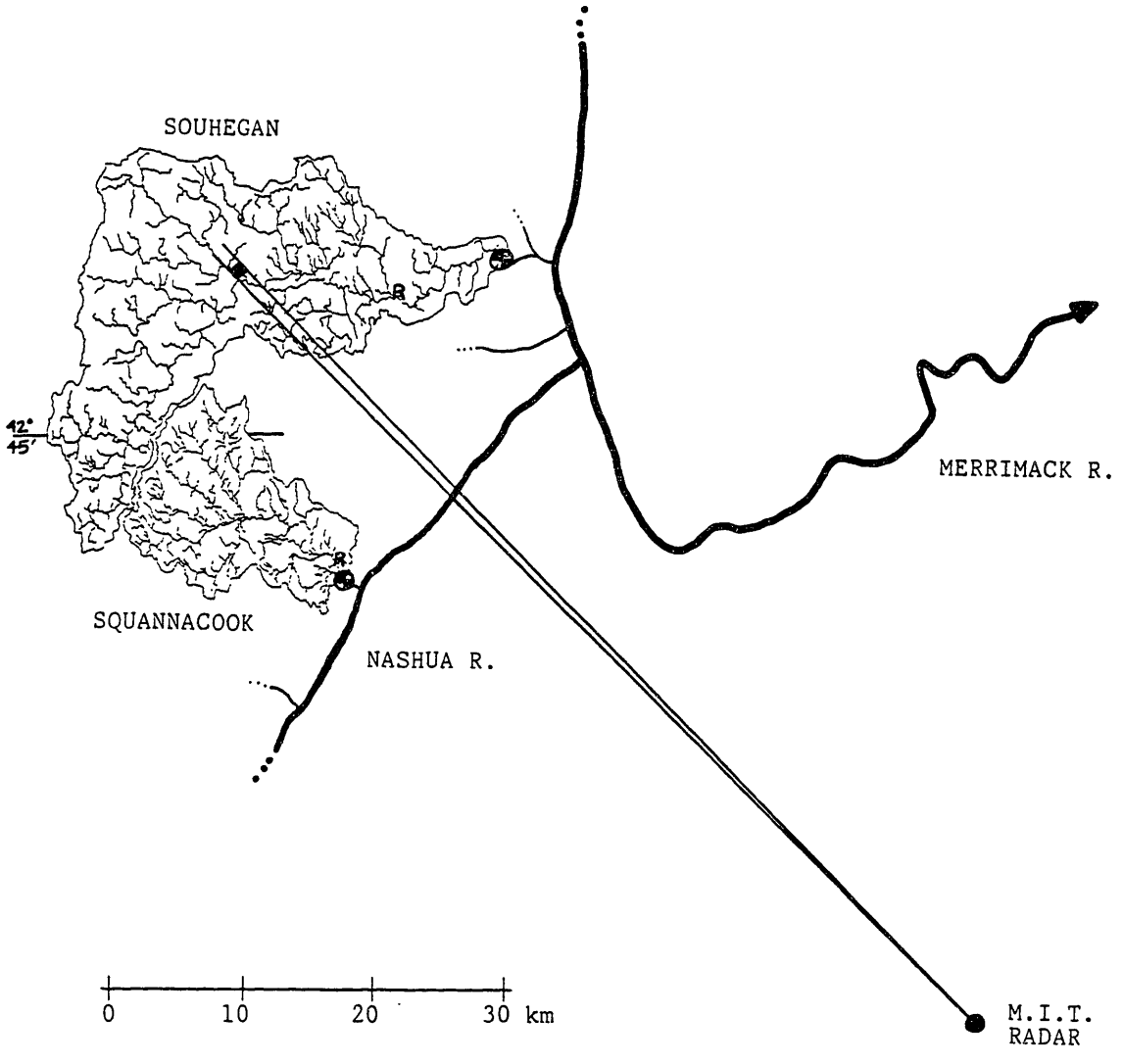

Fig. 2-1. Locations of the Souhegan and Squannacook river basins relative to the MIT radar in Cambridge, Massachusetts. Location of National Weather Service raingauges at Milford and West Groton indicated by **R**. Massachusetts-New Hampshire border at latitude 42°45'. The map is not drawn exactly to scale.

Fig. 2-2. Source of an upland tributary stream to Locke Brook, Squannacook basin. Photographs were taken on the afternoon of August 29, 1987.

the ice itself than of action by glacial meltwater streams. As a result, broad valleys, (e.g. the Merrimack and the lower Souhegan), are covered to considerable depths by sandy sediments, typically mixed with gravels.

Throughout the region, stones and small boulders punctuate the surface at intervals of a few feet, except where they have been arranged in low walls by farmers clearing the land. While forests presently cover more than 85% of both the Souhegan and Squannacook, at the end of the last century, over half of the region had been cleared for agriculture. Currently, the few fields remaining are planted in hay for local dairying, apple orchards, or are used for pasture (Fig. 2-2). A fertile floodplain along the Souhegan near Milford is cultivated for corn and other silage crops. This limited region of rich loamy soils overlays the sand and sandy-loam soils characteristic of the lower elevations of both basins.

Studies by the Soil Conservation Service (U.S. Dept. Agric., 1981, 1985) contain detailed analyses of soils in the New Hampshire section of the Souhegan. Fig. 2-3 and Table 2-1 provide a summary of these results.

Table 2-1. SOIL CATEGORIES OF THE SOUHEGAN

1. FLOOD PLAIN

Near Milford and Amherst in the Souhegan River Valley. Deep (>150 cm), loamy soils (2-6 % clay). Well drained with permeabilities of 1 to 150 mm/hr or greater. In winter, the water table is normally 1 to 2 m below the surface.

2. TERRACES

Along major stream and river valleys; as deep as 10 m in some locations. Excessively well drained (150 to 500 mm/hr) sandy soils with varying fractions of gravel. Clay content less than 5%. The water table is, in all seasons, at least 2 m below the surface.

3. UPLANDS

Loamy soils formed on compact or sandy glacial till. The properties of the soils depend on the nature of the substratum:

3a. Compact Till

Exhibits a perched water table at a depth of less than 1m from November to March. Clay fractions vary from 3 to 10%, with permeabilities between 10 and 50 mm/hr.

3b. Sandy Till

Clay fraction 1 - 8%, with permeabilities similar to compact till types. No perched water table forms.

4. SUMMITS

Somewhat shallow, loamy soils (2 to 10% clay), appearing on the flanks of low mountains. Occasional rock outcrops evident near summits. Permeabilities range from 15 to 150 mm/hr. Soil depths vary from a few centimeters to several meters.

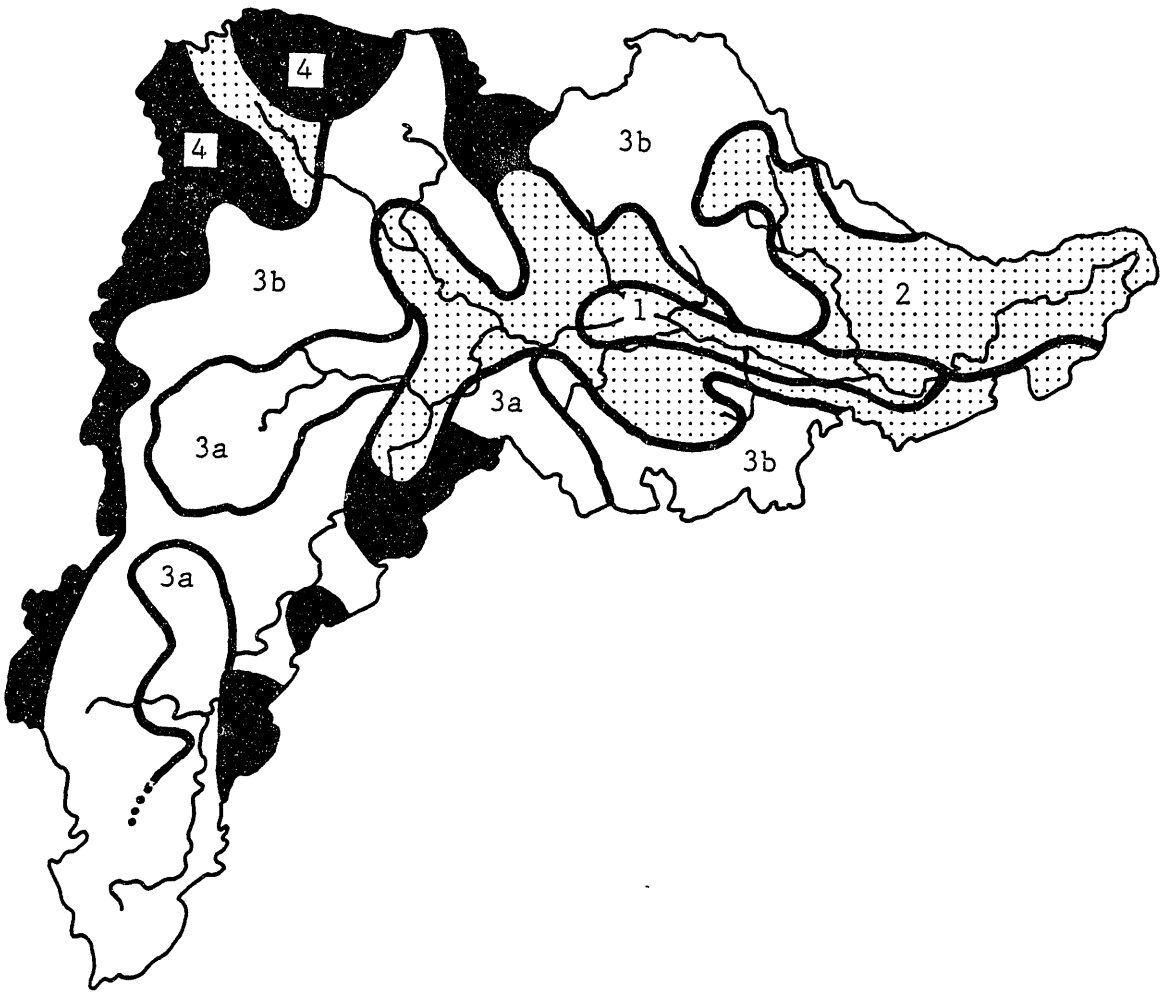

Fig. 2-3. Spatial distribution of soil types described in Table 2-1, based on U.S. Dept. Agric. (1981,1985). Shaded region indicates lowland soils; dark regions are upland soils.

The A horizon, or surface layer, of virtually all soil types in southern New Hampshire is composed of a relatively thick layer of humus. Typically this consists of 2 to 5 cm of fresh leaf litter over a similar depth of decomposed organic matter. This layer is highly permeable.

Within each soil unit, rather different conditions are observed in the vicinity of the rivers and streams. Depressions and drainageways, in all soil units, are characterized by higher water table levels, both seasonally, and throughout the year. Depths to the saturated zone typically vary from about half a meter, up to the surface in swampy regions. The composition of these soils includes a greater fraction of clay and organic matter. Permeabilities, however, are generally comparable to those for the surrounding hillslopes.

The sandy nature of the soils and their considerable depth in both the Souhegan and Squannacook basins is an indication that much of the runoff contributing to streamflow is probably generated by subsurface and groundwater flows, rather than by an overland flow mechanism. The loose upper layers of the soil are protected by a layer of organic debris and by the vegetative cover, preventing compaction which would lead to a less permeable surface zone. This fact was recognized in a study by the USGS (1977) of the Nashua River and its tributaries (the Squannacook among them) which states:

> ... most of the water not evaporated or transpired percolates through the ground to the water table and then moves to the streams, where it becomes the major component of annual streamflow. Ground-water runoff may be as much as two-thirds of the average annual runoff and, in unregulated streams, is frequently the sole supply for streamflow during low flow.

As we shall demonstrate in Chapter 3, an accurate description of subsurface flow is necessary for successful river basin modelling under such conditions. Because this factor was not fully appreciated at the outset of the project, analysis of soils was limited almost entirely to a study of the available literature, when a more thorough investigation would have been desirable.

b) Streams

The character of the stream bed varies with soil type and slope. Headwater (first order) streams in the uplands contain many rocks and small boulders (Fig. 2-4).

Fig. 2-4. First order stream draining from Batchelder Pond, tributary to the Souhegan River near Greenville, N. H. Rocky stream bed and undercut mossy banks are revealed by low summer streamflow.

Fig. 2-5. Dam at Townsend Harbor mill site on the Squannacook.

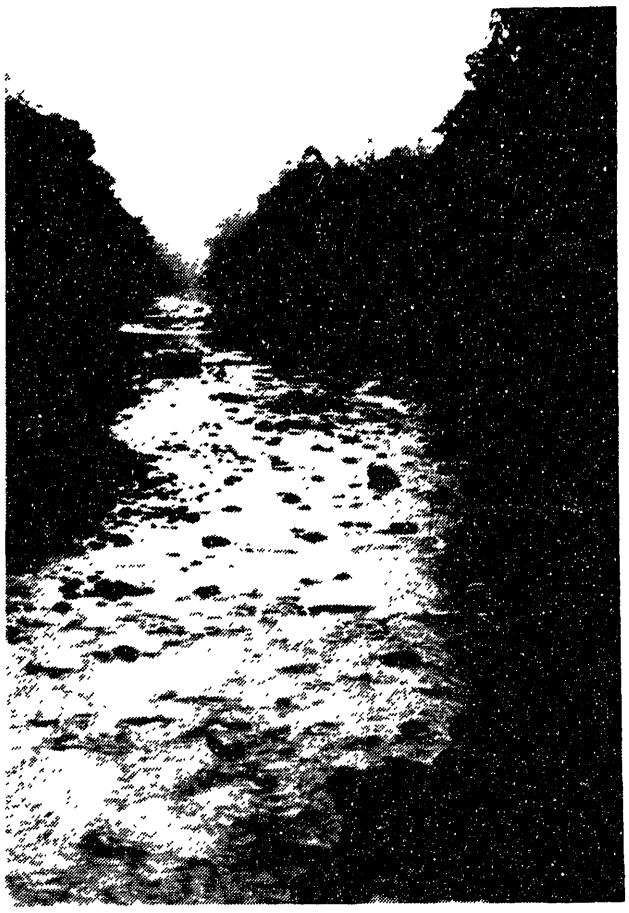

Fig. 2-6. Souhegan River near Milford. View upstream from Purgatory Rd. bridge.

Some streams, for portions of their course, are flumes running in channels eroded from the exposed bedrock. On the floodplain, tributary streams form meandering channels with shallow slopes, often choked by grasses, willow and other vegetation. The main branches of the Souhegan and Squannacook rivers also exhibit some meandering; the stream bed is wide, and relatively shallow. At low flows, boulders and gravel on the stream bed are exposed (Fig. 2-6).

In the Squannacook valley, 5.2% of the basin area is covered by streams, lakes and swamps; 23% of this fraction is reported as being covered by lakes (USGS, 1984). A comparable value for the Souhegan is not available, but is likely to be similar since this figure varies by only a few percent for neighboring

Fig. 2-7. View downstream from ACE stream gauging station on the Souhegan, looking towards Wildcat Falls.

Fig. 2-8. View upstream from the USGS stream gauging station near West Groton on the Squannacook.

drainage basins of similar size. In the past, small dams have been built at locations along both rivers to serve as reservoirs for hydropowered mills at Greenville, Wilton, and Milford on the Souhegan, and at Townsend on the Squannacook (Fig. 2-5). These dams are no longer used for industry, and their presence probably does not have an appreciable effect on flood routing calculations.

i) Stream Gauges

Stream gauge data were generously provided to the project by the U.S. Army Corps of Engineers (ACE), New England Division, for the Souhegan, and by the U.S. Geological Survey (USGS) for the Squannacook gauge.

The Souhegan gauge, located above Wildcat Falls (Fig. 2-7), is one of forty-six remote data collection platforms (DCPs) maintained by the Corps of Engineers across New England. Each gauging station transmits river stage and accumulated rainfall data via GOES satellite at variable intervals determined by the rate of change of the river stage. Because of the lag between the occurrence of the rainfall and the response of the river, the rain gauge data are poorly resolved in time. Bras et al. (1985) derived an optimization procedure for this adaptive random reporting scheme. Due to limitations in the capacity of the communication channels, the sampling rate is normally set to provide flood warning information only (samples 2-3 times a day, more frequently during the rising limb). As a result, there is normally inadequate temporal resolution of the hydrograph for detailed analysis. The sampling rate was increased to transmit reports at approximately hourly intervals for this project during the summer of 1987. Records of the stage and rainfall data from the tipping bucket gauge are available from June 1985 to present. The raingauge data however, are of limited value due to the poor temporal resolution of the record, and because of infrequent maintenance of the collector.

The stream gauge on the Squannacook near West Groton (Fig. 2-8), is maintained by the USGS. Tabulated hourly stage measurements are available from 1949 to present, however, only selected periods, coinciding with the available radar data, were analyzed. Daily mean discharges were examined for the period 1975 to 1987.

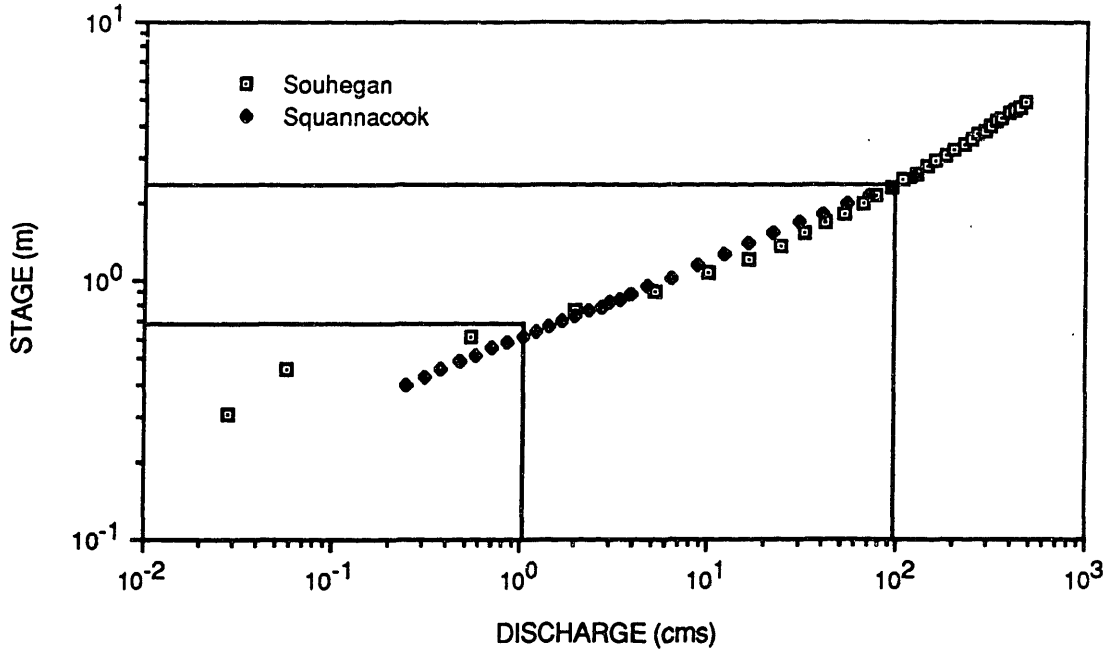

Fig. 2-9. Stage-discharge relations for the Souhegan and Squannacook gauges. Discharge plotted in cubic meters per second. Vertical lines show typical range of discharge values for the Souhegan. Logarithmic axes.

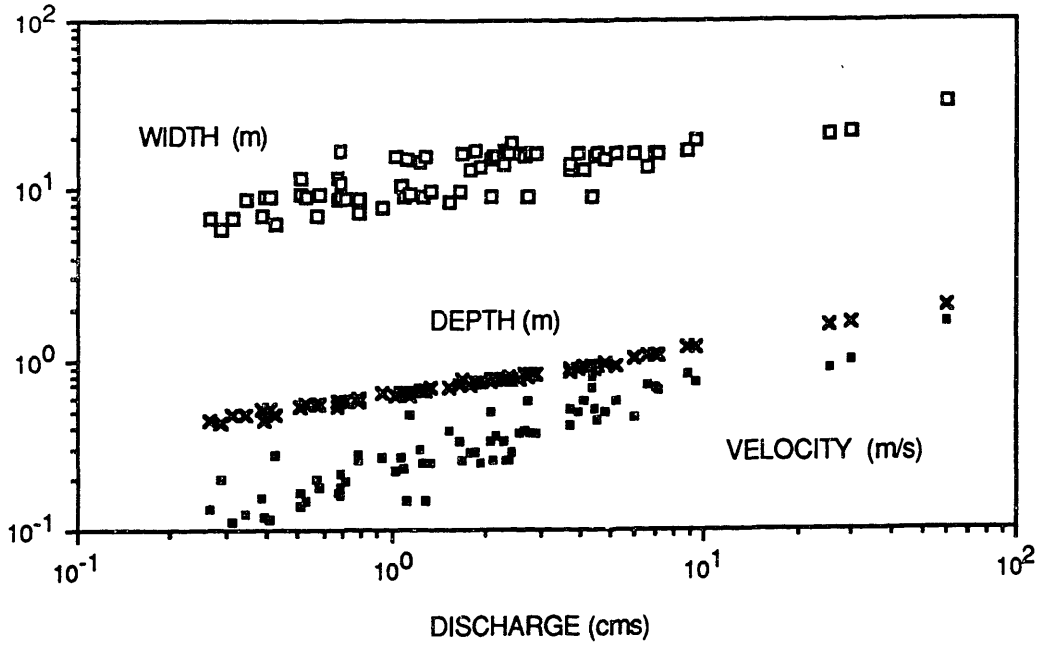

Fig. 2-10. Channel width (meters), depth (meters) and velocity (meters/second) measurements plotted against discharge (cubic meters per second), at the Squannacook gauging station near West Groton. Logarithmic axes.

ii) Discharge Relations

The rating curves (stage-discharge relations) for the Souhegan and Squannacook gauges are plotted in Fig. 2-9. Both curves follow power laws over a wide range of flows, but for practical applications more accurate tables are used for converting the measured river stage values to streamflow in cubic feet per second (cfs) or cubic meters per second (cms).

The measurements used in deriving the rating curve for the Squannacook are available for the Squannacook (but not for the Souhegan). These suggest additional power law relationships between the discharge, the flow velocity and the stream width at the gauge (Fig. 2-10). Linear regression of the logarithms of the data yields the following relations with y and w in meters, u in ms^{-1}, and Q in cms:

DEPTH: $y = 0.623\ Q^{0.275}$ $(r = 0.99)$

VELOCITY: $u = 0.243\ Q^{0.473}$ $(r = 0.92)$

WIDTH: $w = 10.37\ Q^{0.255}$ $(r = 0.79)$

Since $Q = uwy$, the exponents of these three relations must sum to 1.0, and this is observed (1.003). These relations imply that, at the Squannacook gauge, increase in the discharge is accommodated by roughly equal increases in the velocity and the cross sectional area.

These relations, measured at a particular location, do not necessarily apply to downstream increases in the discharge. Considerable research, on a variety of rivers, suggests instead that the channel velocity is reasonably constant throughout the river network (Carlston, 1969). This would imply that the exponent of the power law for the velocity is close to zero. Leopold (1953) found a small increase in the velocity with distance downstream ($V \propto Q^{0.1}$). Pilgrim (1977) observed a similar downstream increase, but concluded from tracer studies that flow travel times were roughly proportional to the length of the channel, implying a nearly constant velocity in the various streams composing the reach. Non-linearity in the velocity was less evident at medium to high discharges. These results are discussed further in Chapter 3, with reference to the model design.

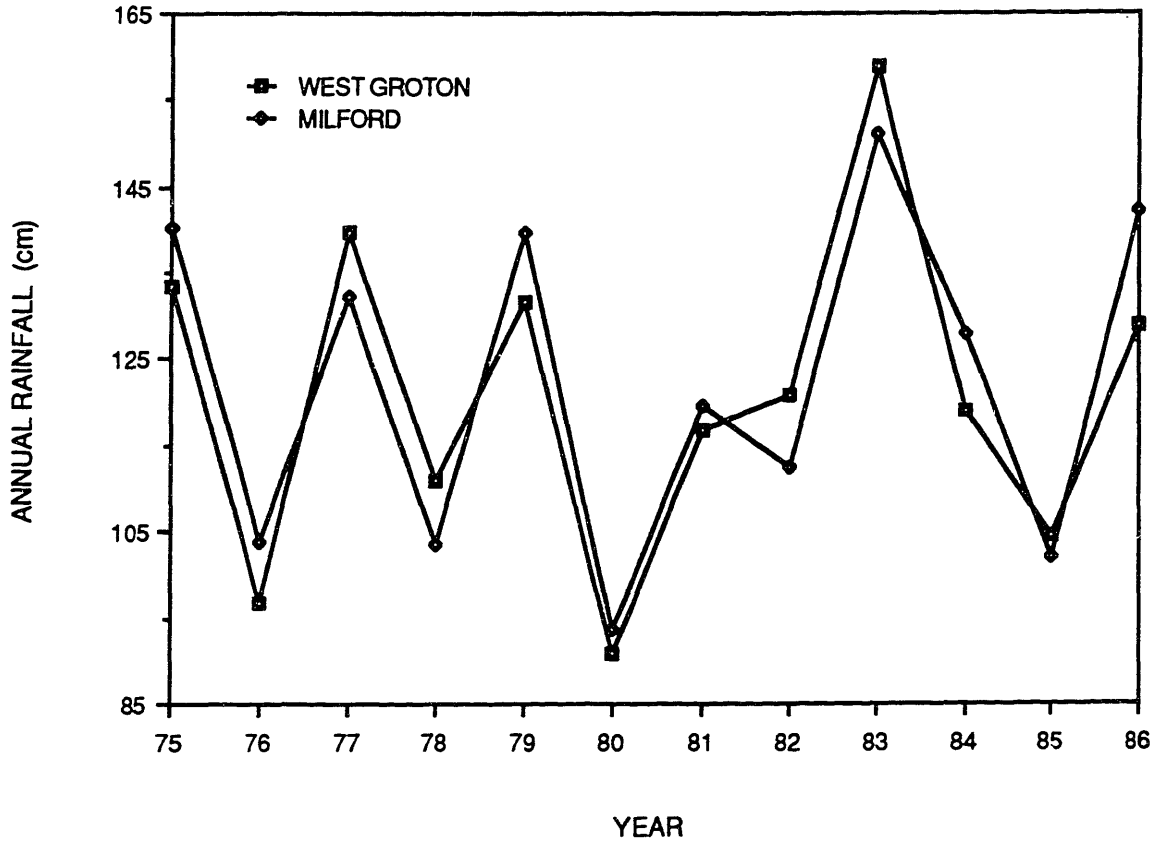

Fig. 2-11. Average annual rainfall depth over calendar years 1975 to 1986, for West Groton (near the Squannacook gauge), and for Milford (in the east-central portion of the Souhegan).

c) Rainfall

Mean annual precipitation over southern New Hampshire varies between 115 and 120 cm depending on the location, with some evidence of local orographic enhancement. This depth is evenly distributed throughout the year, in the climatological mean (9.7 cm/month; σ = 0.9 cm). Interannual variability of the mean annual rainfall at Milford (Souhegan basin) and at West Groton (Squannacook basin) is depicted in Fig. 2-11 for the twelve year period 1975-1986; the data are compiled from Climatological Data Annual Summaries (NOAA, 1986). Differences between the total depth measured at the two gauges are typically less than differences between successive years. The spatial separation between the two stations is approximately 25 km (c.f. Fig. 2-1); elevations of the two stations are comparable.

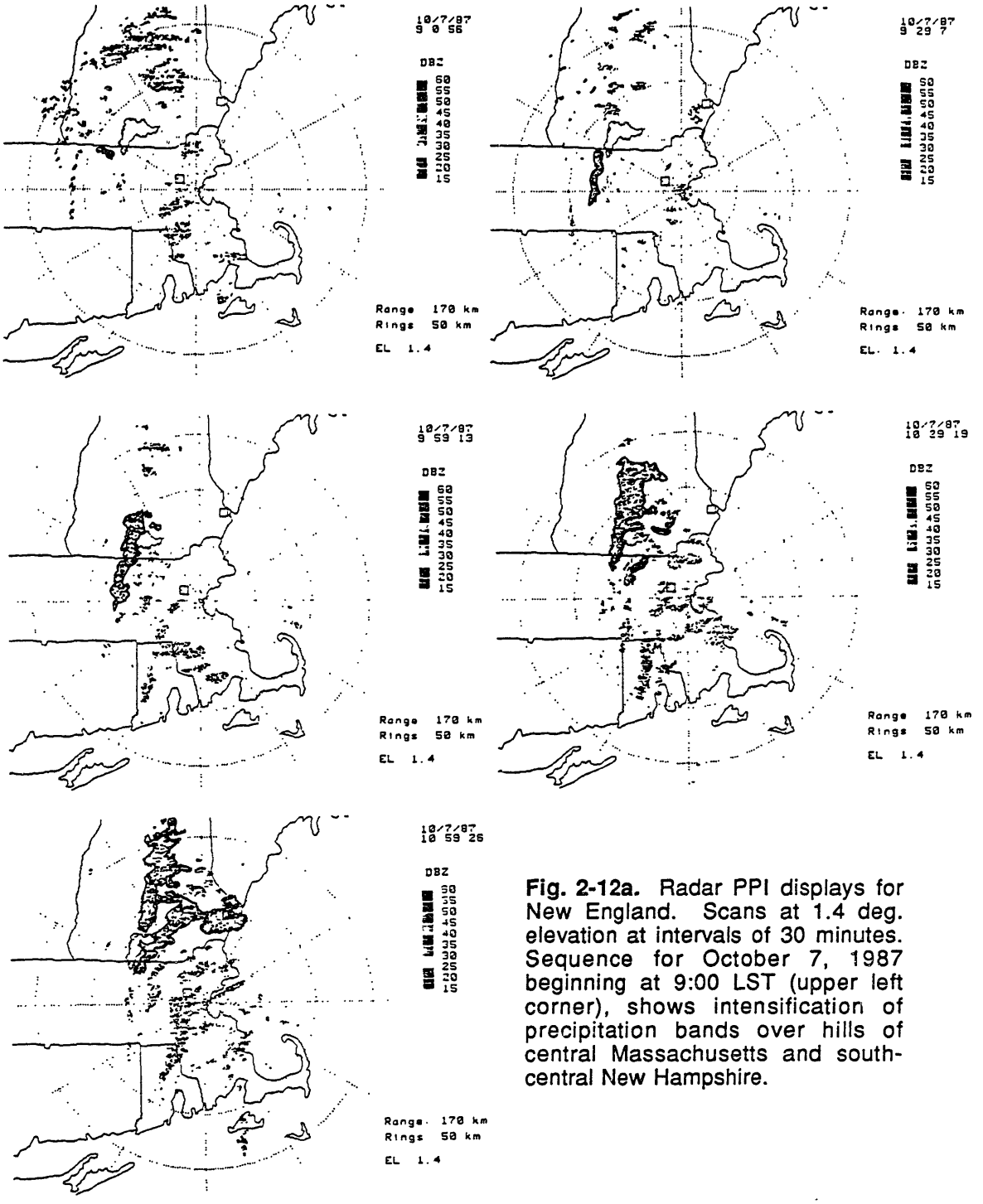

Fig. 2-12a. Radar PPI displays for New England. Scans at 1.4 deg. elevation at intervals of 30 minutes. Sequence for October 7, 1987 beginning at 9:00 LST (upper left corner), shows intensification of precipitation bands over hills of central Massachusetts and south-central New Hampshire.

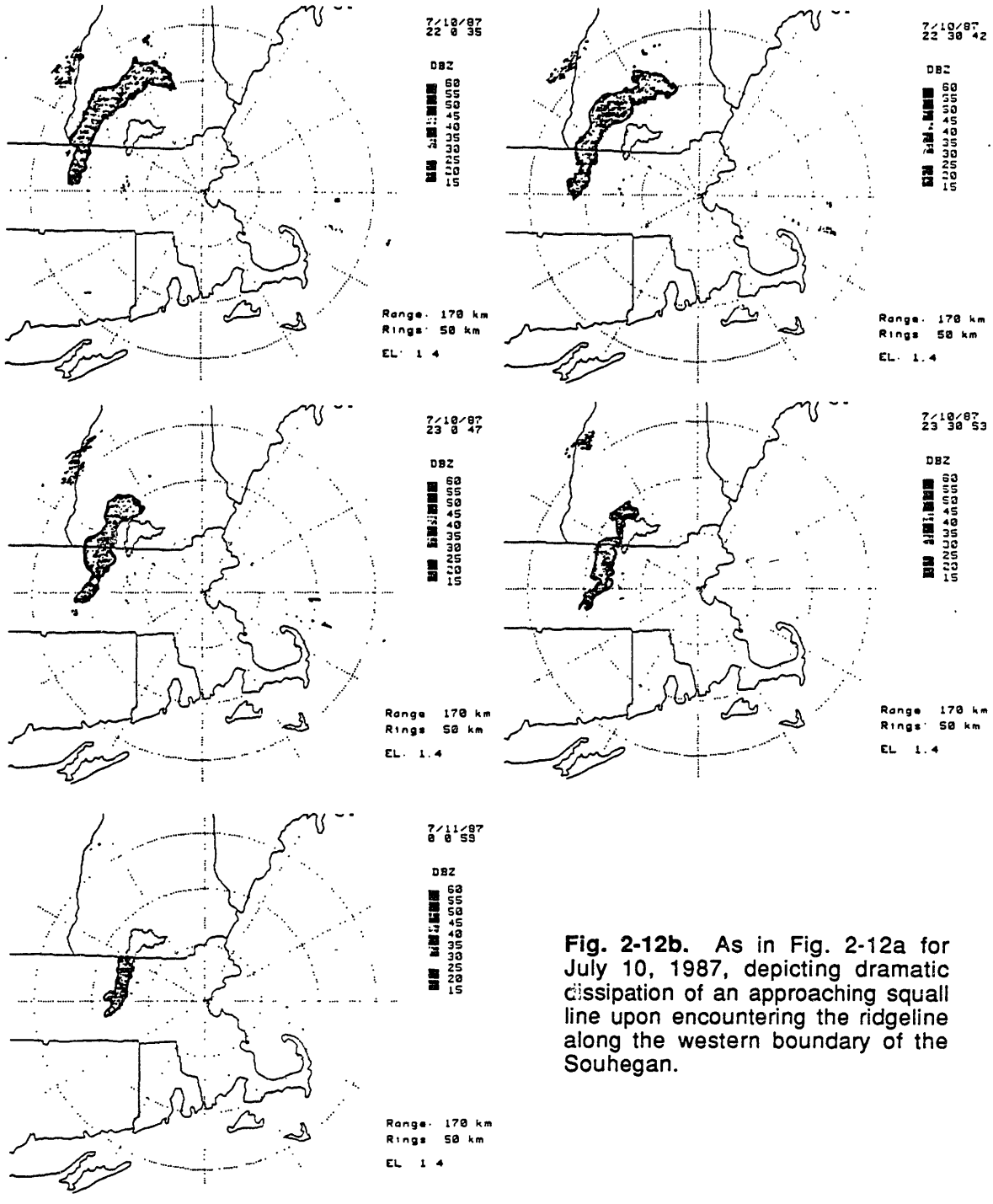

Fig. 2-12b. As in Fig. 2-12a for July 10, 1987, depicting dramatic dissipation of an approaching squall line upon encountering the ridgeline along the western boundary of the Souhegan.

In contrast to the smooth pattern of the spatial distribution of annual mean precipitation, large gradients in the total depth are often observed within individual storms. Such gradients are typically evident as linear features, resulting from the translation of rain cells along preferred tracks. Isohyetal maps of total storm depth presented for case studies in Chapter 3 (e.g. Fig. 3-20), illustrate this observation.

There appears to be considerable interaction of mesoscale convective systems with the topography, perhaps more than we are generally aware of from casual observation of radar patterns. An outline of the Souhegan basin was added for convenience to the normal political features of the PPI display for the duration of this project. Many storm systems showed an uncanny respect for this imaginary boundary. The western edge of the Souhegan basin does of course corresponds to a ridgeline, with several peaks over 500 meters. On several occasions, linear arrangements of rain cells formed along the watershed divide, or, more dramatically, were observed to dissipate completely upon encountering the topography. Two examples of such behavior are illustrated in Figs. 2-12a,b. Each sequence consists of 5 PPI scans at 30 minute intervals; the time of each scan is indicated in the upper right corner of each display.

The maps recorded on October 7, 1987, depict a series of rain bands oriented roughly north-south. One such band intensified rapidly, parallel to the hills of central Massachusetts and southern New Hampshire at 9:30 LST, generating moderate rainfall over the watersheds.

The sequence recorded on July 10, 1987, exhibits a completely different behavior. At 22:00 LST a band of strong convection, with reflectivity cores of 45 to 50 dBZ, approaches the Souhegan. The storm is moving from the north-west at moderate speed, and all indications are that there will be moderate to heavy rainfall over the Souhegan within the hour. However, as the squall line approaches the basin, it stalls just west of the ridgeline. Wrapping around the western edge of the basin, it passes to the south, and eventually dissipates in east-central Massachusetts. No measurable rainfall was observed within the basin boundary. This example clearly demonstrates the potential for errors in short-range (even to one hour) advective precipitation forecasts. In view of these observations, further research on the interaction of precipitation patterns with the topography would be valuable for radar hydrology applications.

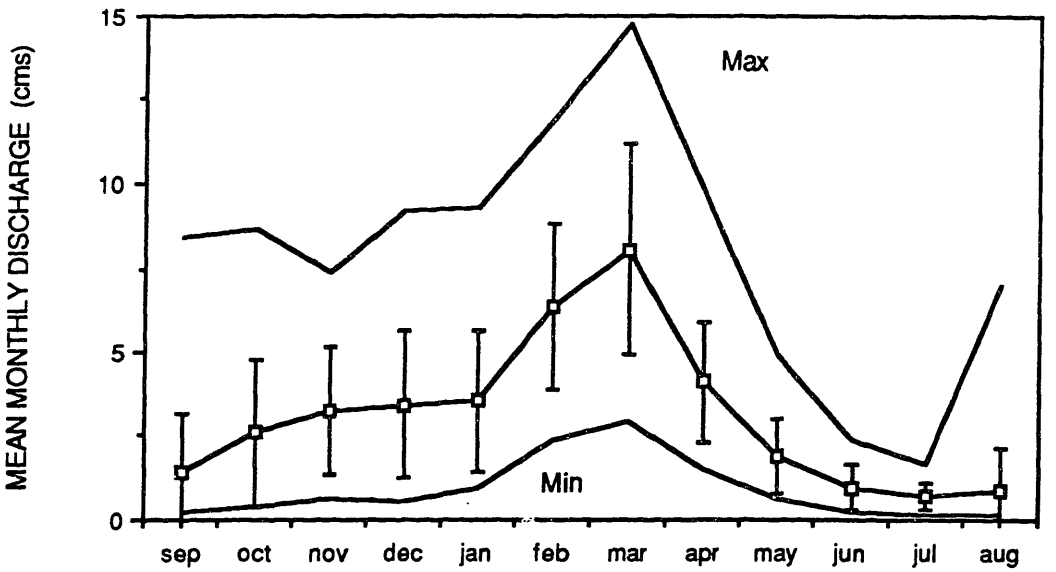

Fig. 2-13. Squannacook average, minimum and maximum mean monthly discharges (cubic meters per second). Standard deviations from the mean are indicated by vertical bars. Data from U.S. Geol. Survey (1984).

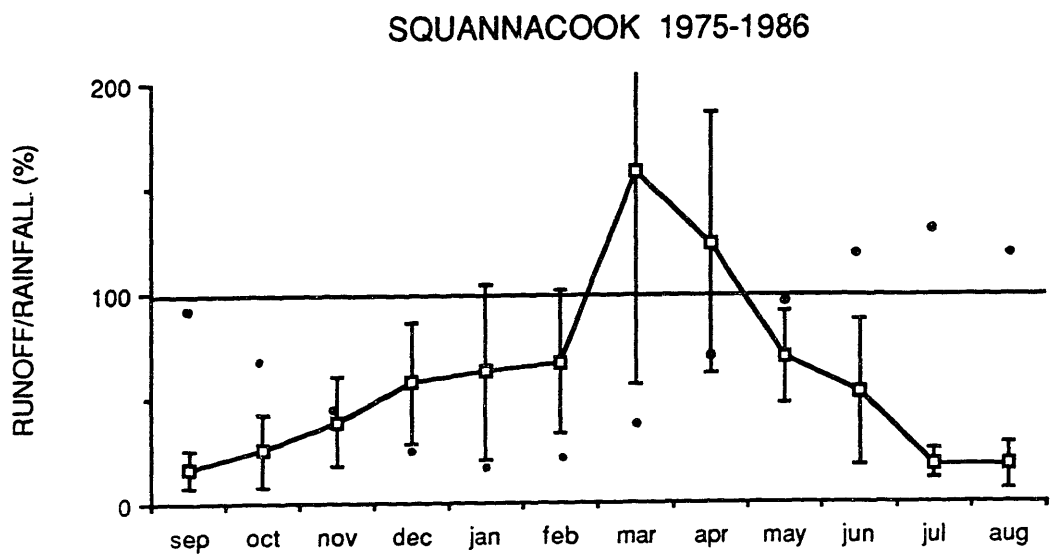

Fig. 2-14. Ratios of mean monthly runoff at the Squannacook gauge to total rainfall at West Groton. The monthly percentages are averaged for the twelve year period 1975 to 1986 (data from U. S. Geol. Survey, 1987; NOAA, 1986). The standard deviations of the averages are indicated by vertical bars. Evaporation data (for lake surface, Coffin, 1950) plotted (dots) as percentage of monthly mean rainfall.

d) Streamflow

Values of the mean monthly discharge of New England rivers exhibit a pronounced seasonal cycle. Data for the Squannacook are plotted in Fig. 2-13, which also displays the standard deviations from the monthly mean, and the minima and maxima for each month. All three quantities exhibit a peak in February-March, and a minimum in mid-summer. Similar behavior is observed for groundwater levels (U. S. Geol Survey, 1968). In a well located on an alluvial terrace near Blodgett Hill in the lower Souhegan. Water levels were observed to fluctuate between 1 meter below the surface in the spring, to about 4 meters in late summer. Despite the nearly constant precipitation input during the year, evapotranspiration during the summer months causes a dramatic drawdown of groundwater levels. Recharge during the winter months is interrupted by freezing temperatures from late November to March.

The close relationship between soil moisture and the runoff volume is implicit in Fig. 2-14. Ratios of the total monthly runoff to the rainfall over the basin have been plotted as percentages. In March and April, during the spring melt, runoff exceeds the rainfall input. In all other months, only a fraction of the rainfall appears as runoff. Integrated over the year, roughly half of the precipitation contributes to streamflow, the remainder is lost through evapotranspiration. The seasonal cycle of the rainfall-runoff ratio is accounted for by the evapotranspiration data plotted in the same figure (Coffin, 1950). Fig. 2-14 will be used in Chapter 3 to relate the radar rainfall volume to the observed storm runoff for storms occurring at various times during the annual cycle.

Despite the buffering effects of the soil capacity, floods can, and do occur in the summer months. For the Squannacook, the largest instantaneous discharge on record is 114 m^3s^{-1} recorded on October 16, 1955. Such floods typically result from prolonged torrential rainfalls associated with tropical depressions. The potential for flooding is greatest though at the time of the spring thaw when rainfall on the snow pack or partially frozen ground can generate a catastrophic volume of runoff. This was observed in the spring of 1987, when the Souhegan gauge crested at 185 m^3s^{-1} on April 6 (Fig. 2-15).

Discharge records for the Souhegan gauge are presented in Figs. 2-15a-d, for calendar years 1986 and 1987. The discharge in m^3s^{-1} is plotted linearly in the upper plot of each pair, and in logarithmic coordinates below. The logarithmic coordinates emphasize the exponential character of the hydrograph

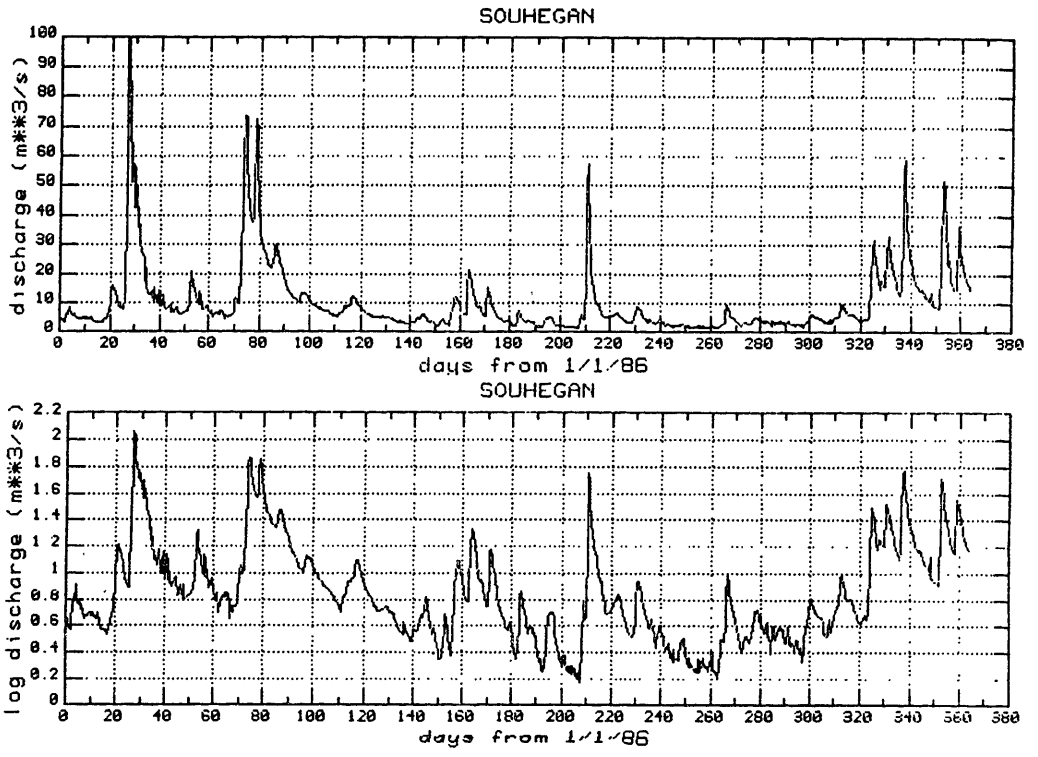

Fig. 2-15. 1985 and 1986 Souhegan instantaneous discharge (cubic meters per second) with variable sampling interval. Figs. a) and c) in linear coordinates, Figs. b) and d) $\log_{10}$(discharge).

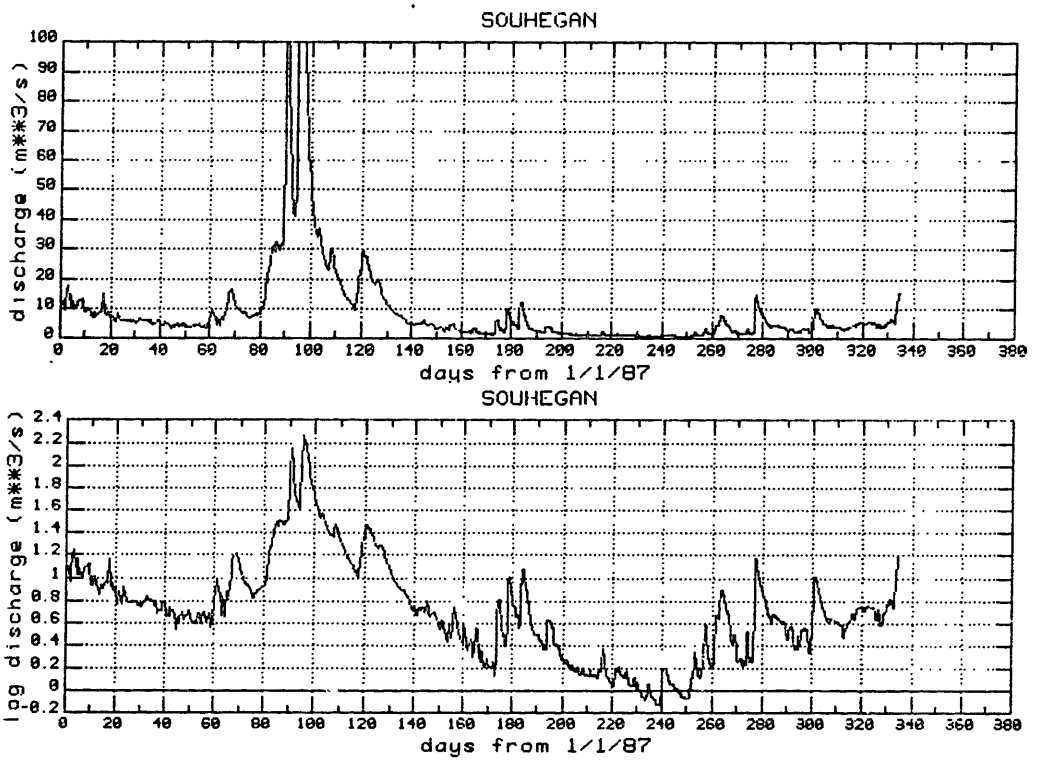

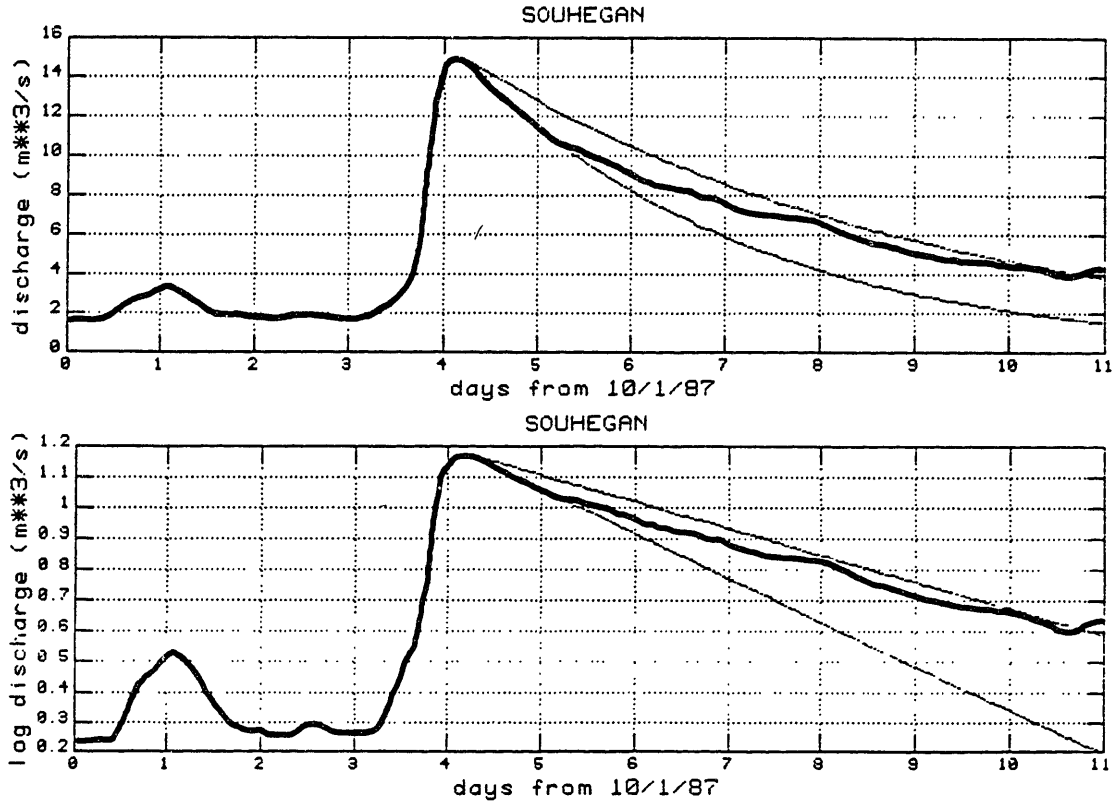

Fig. 2-16. Souhegan gauge, October 1-12, 1987. Example of exponential recession. Bold curves are gauge data as in Fig. 2-15; light curves are exponentials with times scales (e-fold) of 3 and 5 days.

recessions of individual events, which can be identified by the straight line segments in the logarithmic plot. Fig. 2-16 shows the first half of October 1987 in greater detail. Exponential curves with time scales of 3 and 5 days (e-folding) have been drawn for comparison.

The hydrograph recessions do not in fact appear as true exponentials characterized by unique time constants. The principal reason for this is that the gauge record depicts a superposition of many individual events. While all events may in fact share a common time scale for the recession portion of the hydrograph, the total hydrograph exhibits the lagged summation of these events, with corresponding adjustments of the slope of the decay. For a meaningful comparison of individual events, it is necessary to separate the hydrograph of interest from the previous history of the streamflow. The procedure adopted in Chapter 3 for comparison of gauge data to the model results involves subtracting a series of exponential curves, corresponding to previous hydrograph recessions, from the time series preceding the period of interest.

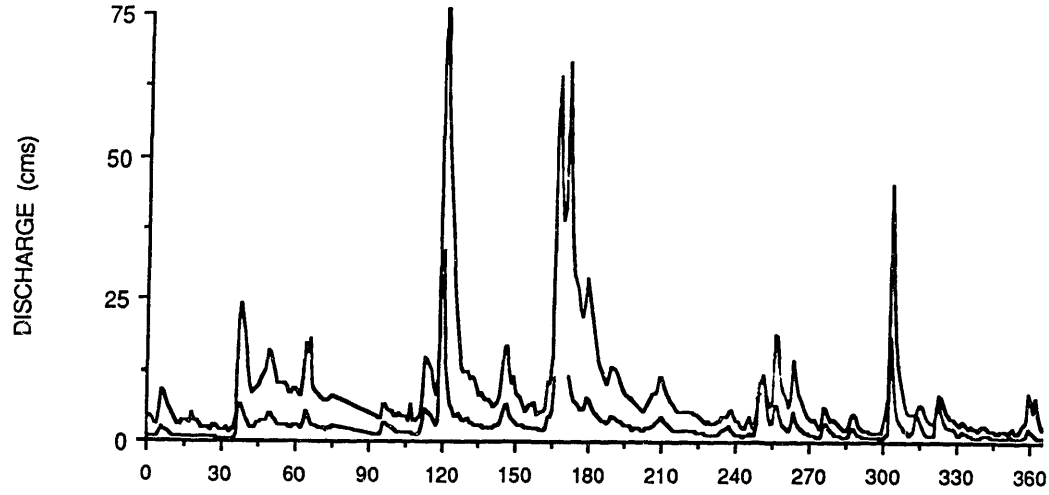

Fig. 2-17. Souhegan and Squannacook daily mean streamflow for the 1986 water year (October 1985 - September 1986).

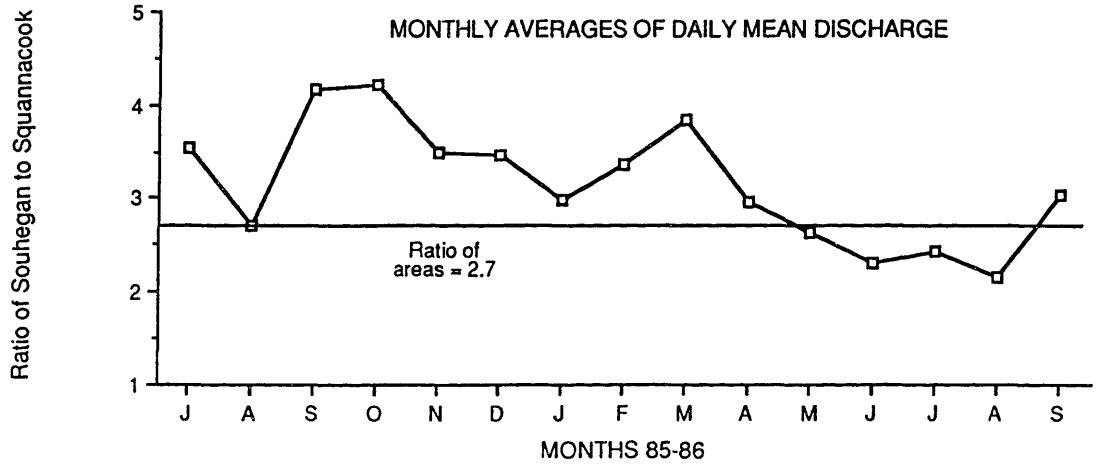

Fig. 2-18. Daily mean discharge at Souhegan gauge divided by discharge at the Squannacook gauge, averaged by month for June 1985 - September 1986. Horizontal line indicates ratio of basin areas (2.7).

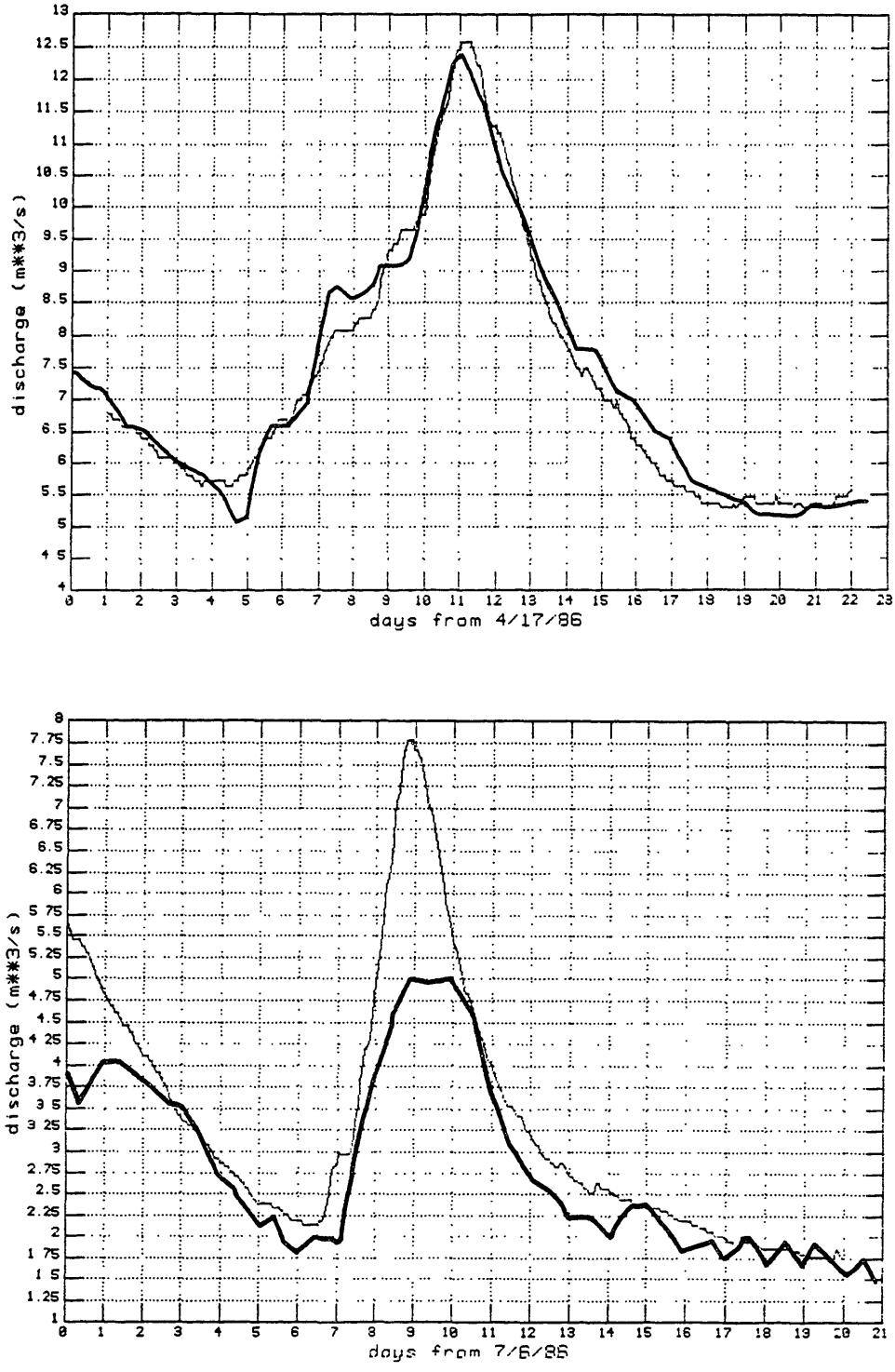

Fig. 2-19. Instantaneous discharge hydrographs for the Souhegan (bold) and Squannacook (light line). The Squannacook data have been scaled by the ratio of basin areas (2.7). Upper plot: April-May, 1986; lower plot: July, 1986.

Although the complete time series of hourly streamflow data available for the Squannacook was not analyzed here, comparisons of daily mean discharge data revealed a striking correlation between the records for the Souhegan and Squannacook gauges. Data for the 1986 water year (October 1 1985 - September 1986) are plotted in Fig. 2-17. Each hydrograph peak is mirrored by a corresponding peak at the other river basin gauge. This, in itself, is not particularly noteworthy, since the two basins are in effect nothing more than giant raingauges responding to the same climate; the correlation between the curves is greatest during the winter months (Oct-April; $r = 0.91$), when stratiform rain is typical, and least during the summer months when localized convection can, on occasion, produce runoff in one basin without affecting the other (May-Sept; $r = 0.79$). The scale factor yielding the greatest correlation between the two gauges is close to the ratio of the basin areas. Fig. 2-18 depicts the ratio of the daily mean discharge at the Souhegan to that measured at the Squannacook gauge, averaged by month. There is no significant seasonal variation for these ratios, however the Souhegan appears to produce slightly more runoff per unit area than the Squannacook, assuming equal rainfall inputs.

The close agreement between the responses of the two basins is even more striking when the records for individual events are compared. Fig. 2-19 illustrates this for two events. The first, (April-May 1986), shows nearly perfect agreement between the two records when the Squannacook data (light curve) are scaled by a factor of 2.7, the ratio of the basin areas. The data for July 1986, however, are not nearly as well correlated, presumably because the rainfall was less uniform in this summer storm case. Nonetheless, the agreement between the peaks, times to peak, and the shapes of the hydrographs is, in general, remarkable. Apart from the similarity of the times to peak (which is indicative of different streamflow velocities in the two basins), these examples suggests that the response of the watershed is coupled to characteristics of the basin that are similar in the two cases, i.e. relatively independent of the size and shape of the basin, but linked to common features such as the spatial arrangement of streams within the basin.

2.2 GEOMORPHOLOGY

The structure of the river network reflects the dynamic interaction of climate and geology. Since the spatial geometry of the streams is the most readily observable property of the drainage basin, it is certainly tempting to believe that the key to understanding the streamflow process might be latent in the pattern of the streams themselves. It is because the morphology of the streams and rivers is the result of erosional processes linked to the rainfall and streamflow, that this is a useful approach.

A detailed analysis of the geomorphologic character of the Souhegan and Squannacook drainage basins was motivated by several considerations. Certainly such analyses provide a means for describing and comparing drainage patterns that result from similar geologic and climatological conditions. Differences, or similarities, between the responses of two basins might be linked to certain readily parameterized characteristics of the drainage network. This reasoning provides the rationale for a basin response function related solely to the channel network characteristics, as in the geomorphologic unit hydrograph proposed by Rodríguez-Iturbe and Valdés (1979). Primarily, however, this analysis of the drainage network serves to highlight length and time scales relevant to modelling the basin response.

The following sections describe the derivation of a variety of morphometric parameters from digitized map data. Many of the original studies of the geomorphology of river basins were conducted prior to the advent of digital computers, and typically required laborious calculations from maps and field surveys. The approach adopted here relies on the computer analysis of digitized maps, and represents a considerable savings in time and effort. Streams are recorded as sequences of links connecting stream junctions and sources. The data are thus amenable to statistical analyses of both the Hortonian type, relating stream statistics to the stream order, and of the sort advocated by Shreve (1969), in which the stream link is considered as the fundamental morphometric unit of the basin.

a) Topographic Map Data

Topographic maps from the USGS were used to delineate the watershed divide above the gauging station, and to map the spatial distribution of stream

channels within the basin. The Squannacook is covered by four maps at a scale of 1:25,000, but large scale maps are not available for the full area of the Souhegan. Instead, a combination of seven sheets at scales of 1:62,500, 1:24,000 and 1:25,000 was used. The larger scale maps are available for all but the northwest quadrant of the basin. Whenever possible, the large scale maps were used, and stream channels were considered to coincide with the streams as drawn on the maps. In that section of the basin for which large scale maps were not available, additional streams were included on the basis of the topography. These additions were made after comparing maps for a region where maps at both scales were available.

Researchers in geomorphology (e.g. Smart and Werner, 1976) have drawn attention to errors that can result from the subjective biases of both cartographer and analyst, particularly with regard to the determination of the number of stream sources. The need to resort to maps of smaller scale for a section of the Souhegan might have resulted in such an error. However, partial field verification of the maps in that region revealed no serious discrepancies between the observed and the analyzed stream networks.

A digitizing table, connected to a personal computer, is used to transfer the information from the maps to a computer-compatible format. Each recorded stream segment consists of a series of numbered, ordered, points. Additional information, such as the elevations of coordinate points, had to be recorded separately and keyed in later. Post-processing of the data is necessary in order to correct for slight offsets between adjacent sheets and other distortions of the digitized map. In all, about 8000 points were recorded for each basin. All meandering of the streams is faithfully represented to within an accuracy of about 20 meters. Also, points are digitized at each intersection of contour lines by streams. The contour intervals are 10 feet and 20 feet (3 and 6 m) on the large and small scale maps respectively. Elevations of all intermediate points along the streams are linearly interpolated from these values.

In order to join the separate map sheets and to ensure that all of the stream segments connect with the network, an interactive computer program is used to check each segment, forcing tributary streams to meet at a single node. The recorded stream elevations are also entered at this time, and verified to decrease with distance along the stream.

The coordinate system used for this analysis, and in the hydrologic model, is a cartesian grid with the origin located at the radar site. For the geomorphometric analysis, a 100 m grid was used in determining basin and sub-basin areas. Grid points which do not coincide with a stream channel are connected to the nearest stream by a simple algorithm which determines the closest stream element to the grid point in question. The distance of any point from a stream is thus minimized. Stream lengths, however, are calculated directly from the network of digitized points, i.e. with better resolution than the grid-scale.

In both basins, the stream gauge is located a few kilometers upstream of the true basin outlet. Since the digitized watershed corresponds to the gauged portion of the basin only, statistics of the principal channel will be underestimates of the true values of length and area for the purposes of geomorphologic analysis. In the case of the Squannacook, no tributaries join the stream before its juncture with the Nashua River. However, downstream of the Souhegan gauge but prior to discharging into the Merrimack, the Souhegan is joined by Baboosic Brook which drains a watershed roughly one third the size of the Souhegan itself.

b) Horton Analysis

Analyses of networks depend on a system of ordered stream segments: following Strahler (1952), a second order stream is here defined by the juncture of two first order streams; third order streams are formed when two streams of second order combine etc.. Statistics such as the average stream length or the average sub-basin area, may then be calculated for streams of a given order. This procedure has come to be known as a "Horton analysis", and general discussions of the seminal studies by Horton, Strahler and Shreve may be found in Eagleson (1970), Chorley (1969), and Smart (1978).

The Horton analysis scheme is based on the observation that mean properties such as the number of streams, their length, and contributing areas, tend to form geometric series when the streams are stratified by order. Shreve (1966) proposed that Horton's "laws" might be viewed simply in terms of a random sampling of networks from the set of all possible networks of a given magnitude. The specified magnitude (μ) is simply the number of first order streams (external links) of the network. The number of topologically

Table 2-2. Number of topologically distinct networks of order μ, $N(\mu)$, and probability that network is of order Ω, $p(\mu,\Omega)$.

$\mu = 10$	$\mu = 25$	$\mu = 50$	$\mu = 100$	$\mu = 177$	
$N(\mu)$	4862	1.29×10^{12}	5.10×10^{26}	2.28×10^{56}	2.2×10^{102}

$p(\mu;\Omega)$	$\mu = 10$	$\mu = 25$	$\mu = 50$	$\mu = 100$	$\mu = 177$
$\Omega = 2$	0.053	6.50×10^{-6}	5.52×10^{-13}	1.39×10^{-27}	2.17×10^{-50}
$\Omega = 3$	0.923	0.357	0.019	2.01×10^{-5}	2.40×10^{-10}
$\Omega = 4$	0.024	0.642	0.874	0.361	0.043
$\Omega = 5$		7.72×10^{-4}	0.106	0.638	**0.893**
$\Omega = 6$			2.43×10^{-8}	1.22×10^{-3}	6.40×10^{-2}
$\Omega = 7$				1.15×10^{-17}	5.08×10^{-9}
$\Omega = 8$					9.50×10^{-43}

distinct networks, $N(\mu)$, is calculated using the following recursion formula (Shreve, 1966):

$$N(\mu) = \sum_{i=1}^{\mu-1} N(i)N(\mu-i) \quad ; \quad N(1) = 1$$

Also, the number of topologically distinct networks of a given order Ω, $N(m;\Omega)$, is given as:

$$N(\mu;\Omega) = \sum_{i=1}^{\mu-1} \left(N(i;\Omega-1)N(\mu-i;\Omega-1) + 2N(i;\Omega) \sum_{\omega=1}^{\Omega-1} N(\mu-i;\omega) \right)$$

with initial terms $N(1;1) = 1$; $N(\mu;1) = 0$; and $N(1;\Omega) = 0$.

Solutions of the recursion formula are presented in Table 2-2, for various values of μ and Ω, with $p(\mu,\Omega) = N(\mu;\Omega)/N(\mu)$. For the Souhegan with 177 sources, the most likely configuration is clearly a network of order 5, as observed, (with probability 0.89). The Squannacook, with 133 sources is also

observed to be a fifth order network. Maps of the stream orders are presented for both basins in Fig. 2-21.

i) Stream Numbers

The number of streams of given orders are tabulated for the two basins in Table 2-3. Following the Horton analysis scheme, the distribution of the stream numbers forms a geometric series with ratio $R_B = N_\omega/N_{\omega+1}$, the bifurcation ratio. Linear regression of log(N) versus the order (ω) is shown in Fig. 2-20, from which $R_B = 3.6$ for the Souhegan (correlation coefficient, $r = 1.00$). For the Squannacook, regression yields $R_B = 3.5$ ($r = 0.98$).

Shreve (1967) showed that for topologically random networks the expected value of the bifurcation ratio is 4. Also, the expected value of the bifurcation ratio calculated for the distribution of links (stream segments) is 2. For the Souhegan, this ratio is approximately 1.9; for the Squannacook, close to 1.6. The statistics of links are discussed further in Section 2.3d.

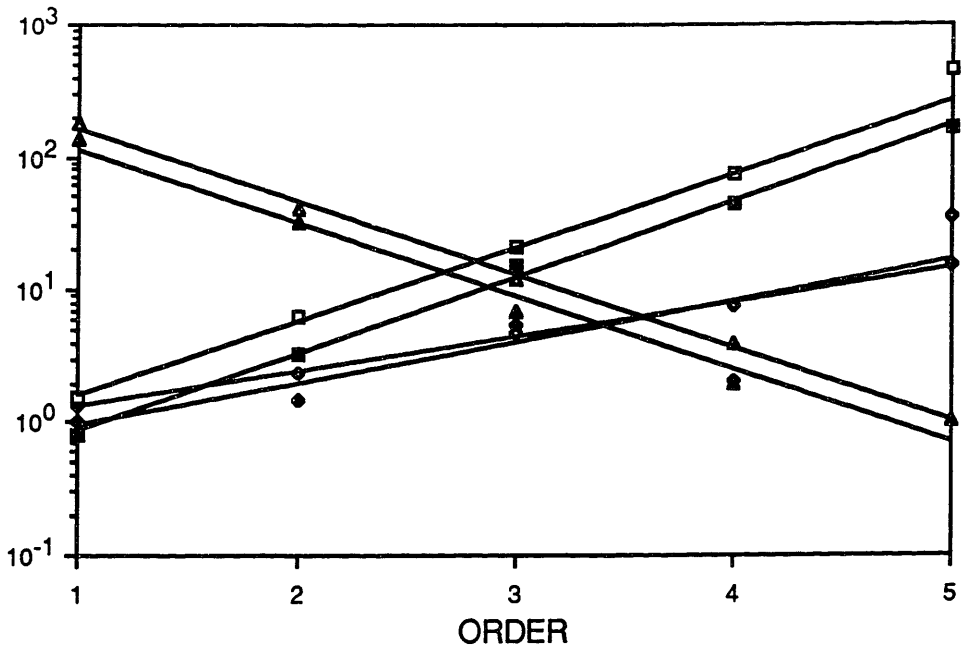

Fig. 2-20. Horton diagram for Souhegan (empty symbols) and Squannacook (filled symbols): number of streams (triangles); mean stream length measured in kilometers (diamonds); and mean contributing area (squares) for streams of all orders. Log-linear regression curves (bold line for Souhegan). Data tabulated in Table 2-3.

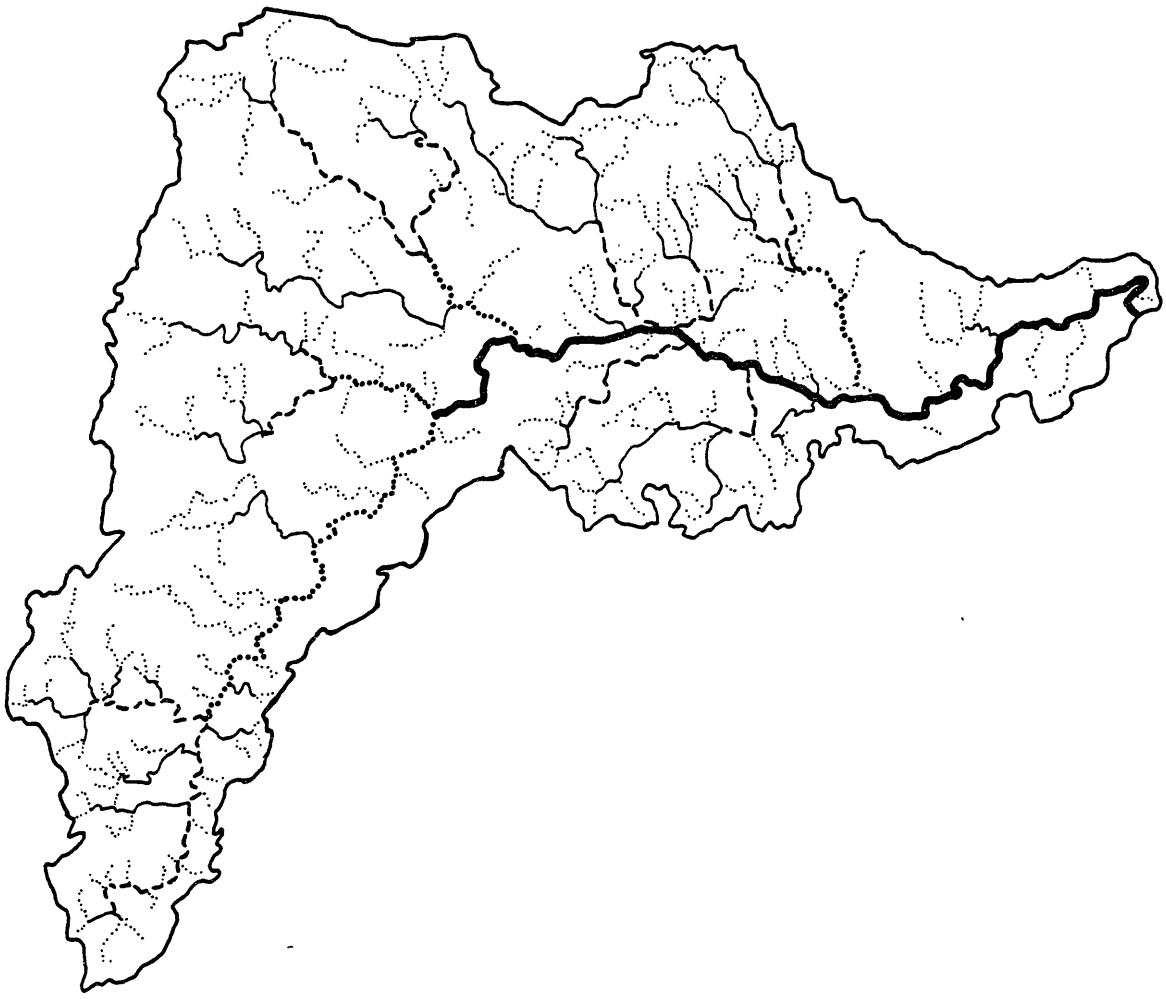

Fig. 2-21a. Souhegan Strahler stream orders. First order streams (fine dotted); second order (thin solid); third (dashed); fourth (bold dotted); and fifth (bold solid).

Fig. 2-21b. As in Fig. 2-21a for the Squannacook.

Table 2.3. Stream statistics for the Souhegan (left column) and Squannacook river basins (right column), by Strahler stream order (ω): number of streams (N_ω); mean length of streams (L_ω); total length of streams (Total L_ω); and area of basin contributing to streams (A_ω). Horton ratio (log-linear regression for all orders) is indicated below each column.

ω	N_ω		L_ω (km)		Total L_ω (km)		A_ω (km^2)	
1	177	133	1.35	1.01	239.3	134.7	1.54	0.81
2	40	32	2.36	1.51	94.59	48.37	6.20	3.30
3	12	7	4.85	5.47	58.16	38.30	21.01	15.44
4	4	2	7.69	2.05	30.74	4.09	72.77	44.40
5	1	1	35.66	15.11	35.66	15.11	443.1	162.9
Ratio	3.55 R_B	3.51	1.81 R_L	2.03	0.29 R_T	0.47	3.59 R_A	3.88

ii) Stream Lengths

By analogy with the law of stream numbers, the law of stream lengths may be expressed as a length ratio $R_L = L_{\omega+1}/L_\omega$. Values for the Souhegan and Squannacook are tabulated in Table 2-3. Representative regression lines are drawn in Fig. 2-20: for the Souhegan $R_L = 1.8$ ($r = 1.00$); for the Squannacook $R_L = 2.0$ ($r = 0.98$). The expected value of R_L for topologically random networks is approximately 2, reflecting the observation that the mean length of stream links does not vary appreciably with order (Shreve, 1967).

If instead of considering the mean stream lengths, the total length of streams is plotted as a function of order, a ratio comparable to the reciprocal of R_L is obtained (Table 2-3). Regression for the Souhegan yields $R_T = 0.29$ ($r = 0.99$), and $R_T = 0.47$ ($r = 0.94$) for the Squannacook.

iii) Stream Areas

Calculated from the 100m grid, the average areas of the sub-basins of various orders exhibit the distribution given in Table 2-3. The area drained by each stream includes the areas drained by all tributary streams. The area ratios are obtained from the regression lines drawn in Fig. 2-21: for the Souhegan $R_A = 3.6$, ($r = 1.00$); for the Squannacook $R_A = 3.9$, ($r = 1.00$). For random networks, R_A is approximately 4, (Shreve, 1967).

iv) Sub-basins

Bifurcation, length and area ratios were also calculated for each fourth order sub-basin of the Souhegan and Squannacook watersheds. These results are presented in Table 2-4. The averages of the ratios for the sub-basins are, in most cases, within 10% of the ratios calculated above for the full stream network of order 5. The significance of this result with regard to self-similarity of the network structure is, however, limited by the small sample size of the number of streams in each sub-basin, and by the arbitrary nature of the Strahler ordering system. Indeed, it is questionable whether Horton's laws, which rely on average statistics, can be expected to apply at the level of a single basin, where the regression relations are often not well defined (c.f., the third order streams of the Squannacook basin).

Table 2-4. Horton ratios for Souhegan and Squannacook sub-basins of Strahler order 4 (A, B, ...): bifurcation ratio, R_B; length ratio, R_L; and area ratio, R_A. Averages of these ratios (Avg) are compared with the ratios calculated for the full stream network of order 5 ($\Omega = 5$).

SOUHEGAN							SQUANNACOOK				
	A	B	C	D	Avg	Ω=5		A	B	Avg	Ω=5
R_B	2.67	2.69	2.31	4.01	**2.92**	**3.55**	R_B	3.35	3.60	**3.48**	**3.51**
R_L	1.74	1.37	1.36	2.53	**1.75**	**1.81**	R_L	1.23	1.58	**1.41**	**2.03**
R_A	3.26	3.06	2.70	4.57	**3.40**	**3.59**	R_A	3.91	4.19	**4.05**	**3.88**

c) Geomorphologic IUH

Representation of the basin response in terms of Horton's ratios (GIUH) was proposed by Rodríguez-Iturbe and Valdés (1979). The theory has been tested by Valdés et al. (1979) against model results for several real basins, modified by Gupta et al. (1980), and expressed in terms of linear reservoir theory by Rosso (1984). Rodríguez-Iturbe et al. (1982) derived the probability distribution functions of the GIUH variables subject to climatic variability in the rainfall input.

The theory predicts the time to peak (t_p, [time]) and peak discharge (q_p, [time^{-1}]) for the basin instantaneous unit hydrograph. Since a constant velocity in all streams is assumed (v), these variables incorporate basin length scales: t_p corresponds to the mean distance of travel to the gauge (k); while q_p is related

to the time base of the hydrograph (θ^{-1}), i.e. the farthest distance from the outlet (assuming a triangular hydrograph for which $(q_p t_p)/2 = 1$). The variables t_p and q_p are expressed in Rodríguez-Iturbe and Valdés (1979) as:

$$t_p = k/v = \frac{0.44\, L_\Omega}{v}\left(\frac{R_B}{R_A}\right)^{0.55} R_L^{-0.38}$$

$$q_p = \theta\, v = (1.31\, v) / (L_\Omega\, R_L^{0.43})$$

Both equations involve a factor multiplying the length of the highest order stream (L_Ω). Unfortunately, in the Souhegan, as is likely to be the case for many basins, the measured length of the highest order stream is not consistent with the Horton ratio analysis (Fig. 2-20). The value of L_Ω might instead be estimated from the regression analysis: for the Souhegan this corresponds to L_Ω = 15 km (compared with the measured 36 km); for the Squannacook L_Ω = 17 km (in agreement with the 15 km measured). The values of k and θ^{-1}, the basin length scales for the Souhegan and Squannacook basins are presented in Table 2-5. The predicted value of θ^{-1} is in better agreement with the measured mean distance to the gauge (c.f., Section 2.3h), than with the maximum distance to the gauge.

However, as Rodríguez-Iturbe and Valdés (1979) suggest, the value of IR = $q_p t_p = k\theta$ is possibly a more useful description of the shape of the triangular hydrograph since it is independent of L_Ω, and the velocity. This parameter is approximated by

$$IR = 0.58(R_B/R_A)^{0.55}$$

Table 2-5. Predicted basin length scales from GIUH theory. Length of highest order stream (L_Ω) measured, and estimated from Horton regression. IR = $k\theta$ is a measure of geomorphologic similarity.

SOUHEGAN	(R_B/R_A)	IR	L_Ω (km)	K (km)	θ^{-1} (km)
L_Ω measured	0.99	0.58	36	13	35
L_Ω estimated	---	---	15	5	15
SQUANNACOOK	(R_B/R_A)	IR	L_Ω (km)	K (km)	θ^{-1} (km)
L_Ω measured	0.91	0.55	15	4.8	16
L_Ω estimated	---	---	17	5.4	18

Table 2-6. Parameters for direct calculation of the geomorphologic IUH. $P_n(\omega)$ expresses the probability of water effecting the transition from a stream of order ω to a stream of order n; $P_\omega(0)$ is the probability that the rain originates in a stream of order ω. $P_\omega(0)$ is calculated on the basis of the fractional basin area of order ω and on the fraction of total stream length of order ω.

SOUHEGAN	1	2	3	4	5
$P_2(\omega)$	0.6780				
$P_3(\omega)$	0.1525	0.8250			
$P_4(\omega)$	0.0904	0.0750	0.6667		
$P_5(\omega)$	0.0791	0.1000	0.3333	1.0000	
$P_\omega(0)$ Area	0.6135	0.1579	0.0939	0.0703	0.0645
$P_\omega(0)$ Length	0.5221	0.2061	0.1269	0.0671	0.0778
SQUANNACOOK	1	2	3	4	5
$P_2(\omega)$	0.7368				
$P_3(\omega)$	0.1805	0.7813			
$P_4(\omega)$	0.0000	0.0625	0.5714		
$P_5(\omega)$	0.0827	0.1563	0.4286	1.0000	
$P_\omega(0)$ Area	0.6614	0.1576	0.1261	0.0120	0.0429
$P_\omega(0)$ Length	0.5599	0.2011	0.1592	0.0170	0.0628

since $R_L^{0.05}$ is nearly equal to 1. For the Souhegan and Squannacook, IR = 0.58 and 0.55 respectively. This would imply that almost 60% of the basin runoff arrives before t_p.

There is, in practice, little to recommend the above procedure for estimating the parameters of the IUH. As noted by the authors themselves (Rodríguez-Iturbe and Valdés, 1979), using Horton's ratios to obtain the GIUH may well provide some insight into the relationship between geomorphology and the rainfall-runoff process, but is of limited practical value since a complete analysis of the basin geometry must be made in order to derive these ratios. In the next section we shall consider the basin geometry directly.

On the other hand, it is worth looking again at the basis for the GIUH model, without introducing the unifying assumptions of Horton's ratios. The basic premise of the model is that each drop of rain, depending on the order of the sub-basin into which it initially falls, arrives at the outlet of the basin with a time delay whose probability distribution function is given by the sum of exponentially distributed "waiting times" in each stream. The IUH is thus based on a matrix describing the probability of drops originating in a stream of order ω (the fractional area of the basin contributing directly to streams of order ω, assuming uniform rainfall over the basin), and by the probability of the water flowing from a stream of order ω to a stream of order $\omega+n$. These probabilities, calculated directly from the basin data, are tabulated for both basins in Table 2-6.

It is worth noting that the probability of a drop flowing into a first order stream ($P_1(0) = A_1/A_\Omega$) is estimated by Horton's ratios as $(R_B/R_A)^{\Omega-1}$ which yields a considerable overestimate of $P_1(0)$ for the Souhegan (0.96), but almost exactly the observed value for the Squannacook ($P_1(0) = 0.67$). This, and the preceding comparisons, point to the sensitivity of the GIUH analysis to the parameter (R_B/R_A), which for random topological networks will be approximately equal to 1.

A further comment is in order regarding the applicability of the GIUH theory to the basins studied here. This concerns the assumption that the distance of "overland travel" is small compared to the total distance travelled in the stream network. For regions where soils are permeable, this assumption is probably only valid for a narrow zone adjacent to the streams where saturated overland flow can occur. In this case the relevant parameter for partitioning the rainfall between stream orders would be the length ratio rather than the area ratio, since the area of the contributing saturated zones will be expressed as a function of the length of the streams. These initial probabilities, based on the total lengths of streams rather than the sub-basin areas, are included in Table 2-6.

d) Link Statistics

An alternative system to Strahler's ordering system considers the link (a stream segment between the nodes of the network), as the fundamental morphometric unit.

Table 2-7. Statistics of links for the Souhegan (left column) and Squannacook river basins (right column), by Strahler order (ω) of parent stream: number of links (N_ω); mean link length (L_ω); ; and area of basin contributing to streams (A_ω).

ω	N_ω		L_ω (km)		A_ω (km^2)	
1	177	133	1.352	1.013	1.536	0.810
2	80	66	1.181	0.733	0.875	0.389
3	48	42	1.211	0.911	0.867	0.489
4	23	4	1.336	1.022	1.353	0.487
5	25	20	1.426	0.755	1.143	0.349

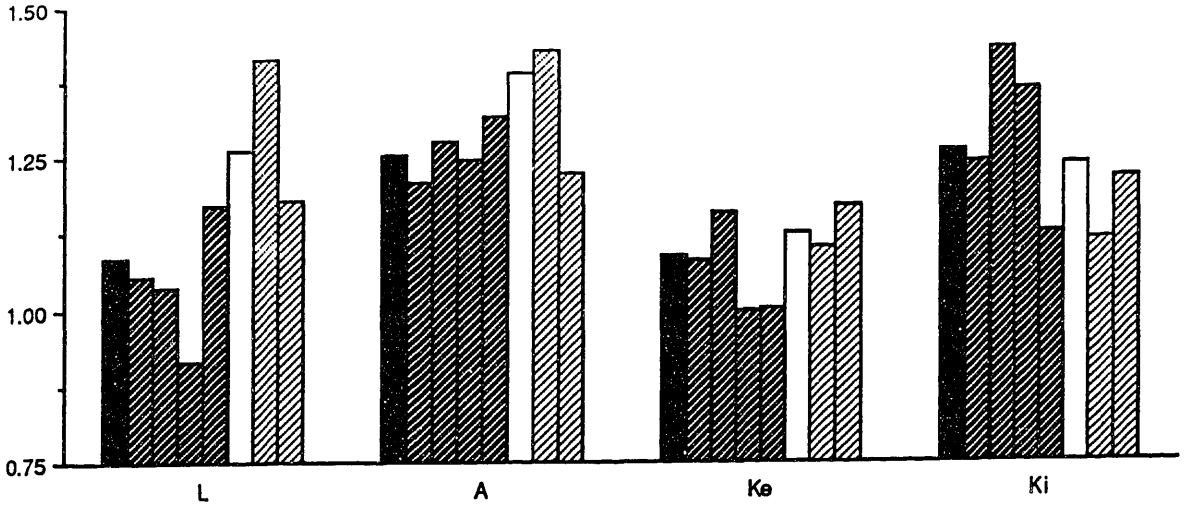

Fig. 2-22. Link parameters from Smart (1973), plotted relative to 1.0, for Souhegan (dark columns) , Squannacook (light columns), for entire basin (solid) and fourth order sub-basins (shaded). Ratio of lengths of external links to internal links (L); square root of the ratio of mean area contributing to external links, to internal areas (A); square root of ratios of the squared mean length of external links to external contributing areas (K_e); and K_i, as K_e for internal links.

Table 2-7 summarizes the statistics of link parameters, stratified by Strahler order. No significant differences are observed between mean lengths and contributing areas of different orders. Smart (1973) proposed a description of dendritic networks based on the four dimensionless parameters:

$$\lambda = \frac{l_e}{l_i}\ ;\quad \alpha = \frac{a_e}{a_i};\quad K_e = \frac{l_e^2}{a_e};\quad \text{and } K_i = \frac{l_i^2}{a_i}.$$

This parameterization is based on the observation that link lengths are approximately equal throughout the basin. Networks are composed of *n* external links (first order streams; subscript "e"), and identically (*n* -1) internal links (subscript "i"); "a" and "l" represent the mean area contributing to, and the mean length of each link, respectively. The values of λ, $\alpha^{1/2}$, $K_e^{1/2}$, and $K_i^{1/2}$ are plotted in Fig. 2-22 for both complete basins, and for each of the fourth order sub-basins. In both basins the mean area contributing to external links is greater than the average area contributing to internal links; in the Squannacook the lengths of the external links are themselves greater than those of internal links. Otherwise, differences between the parameters for the two basins, and differences within the two basins, are not particularly significant.

e) Basin Topography

Since the earliest drainage basin surveys, researchers have remarked on the concave upward profile of stream gradients, observing that channel slope decreases in the downstream direction. Stream gradients were calculated for the Souhegan and Squannacook basins by dividing the total elevation drop along a channel by the length of the channel. Table 2-8 lists these statistics, determined both for streams and for links. The mean drop along streams appears to be independent of the stream order, while the mean drop along links decreases with order.

Table 2-8. Channel slope statistics for Souhegan (left column) and Squannacook river basin (right column), by Strahler stream order (ω), for streams and for links: mean drop in elevation (meters) along channel (D_ω); mean slope of channel (S_ω).

	STREAM STATISTICS				LINK STATISTICS			
ω	D_ω (m)		S_ω (m/km)		D_ω (m)		S_ω (m/km)	
1	43	34	35.2	34.5	42.7	34.1	35.2	34.5
2	40	29	16.7	19.7	20.0	14.0	17.6	20.1
3	47	83	10.2	13.2	11.7	13.8	7.6	15.3
4	67	19	9.1	6.6	11.6	9.4	8.6	7.1
5	89	20	2.5	1.3	3.5	1.0	2.1	1.2

Channel slopes, determined for both streams and links show a systematic decrease with order, which can be parameterized by a Horton slope ratio, $R_S = S_{\omega+1}/S_\omega$. Regressions for these parameters yield $R_S = 0.55$ ($r = 0.96$) for the Souhegan, and $R_S = 0.45$ ($r = 0.96$) for the Squannacook. The highest order streams have a particularly shallow slope relative to the remainder of the basin. This is a reflection of the broad, nearly level conditions characteristic of the lower elevations of both the Souhegan and Squannacook basins.

Although a complete digitization of the basin topography was not attempted, the elevations of points along the streams themselves provide a reasonable representation of the topography of the river basins. Knowledge of the stream gradients and the incorporation of a simple assumption concerning the relationship between stream and valley hillslopes make it possible to generate a synthetic map of the catchment relief. Strahler (1950) obtains the following regression between valley slope (θ_V) and stream slope (θ_S), from the analysis of several sites throughout the United States:

$$\log\theta_V = 0.6 + 0.8\log\theta_S$$

where θ_V and θ_S are measured in degrees. Using this relationship together with the known elevations at points along the streams, approximate maps of the topography are obtained (Fig. 2-23). These maps exhibit the observed demarcation between the upland sections of the basins to the west, and broad floodplains near the basin outlets. This distinction is even more obvious in Fig. 2-24 which depicts the distribution of basin area as a function of elevation.

Considering the basin as a dynamic system, subject to landform-modifying forces, the relationship between altitude and area is an indication of the stage of the basin in the cycle of erosion. In the "inequilibrium" (young) stage, a large fraction of the area is at a relatively high elevation; with time, the topography is eroded yielding the opposite, "Monadnock", configuration. Fig. 2-25 shows the relative area of each basin as a function of the normalized height above the basin outlet. These hypsometric curves (Strahler, 1950) are characteristic of basins at an equilibrium, or "mature", stage.

f) Sinuosity

The meandering of streams, particularly in the lower reaches of the basin, can contribute significantly to the delay of the hydrograph peak relative to the

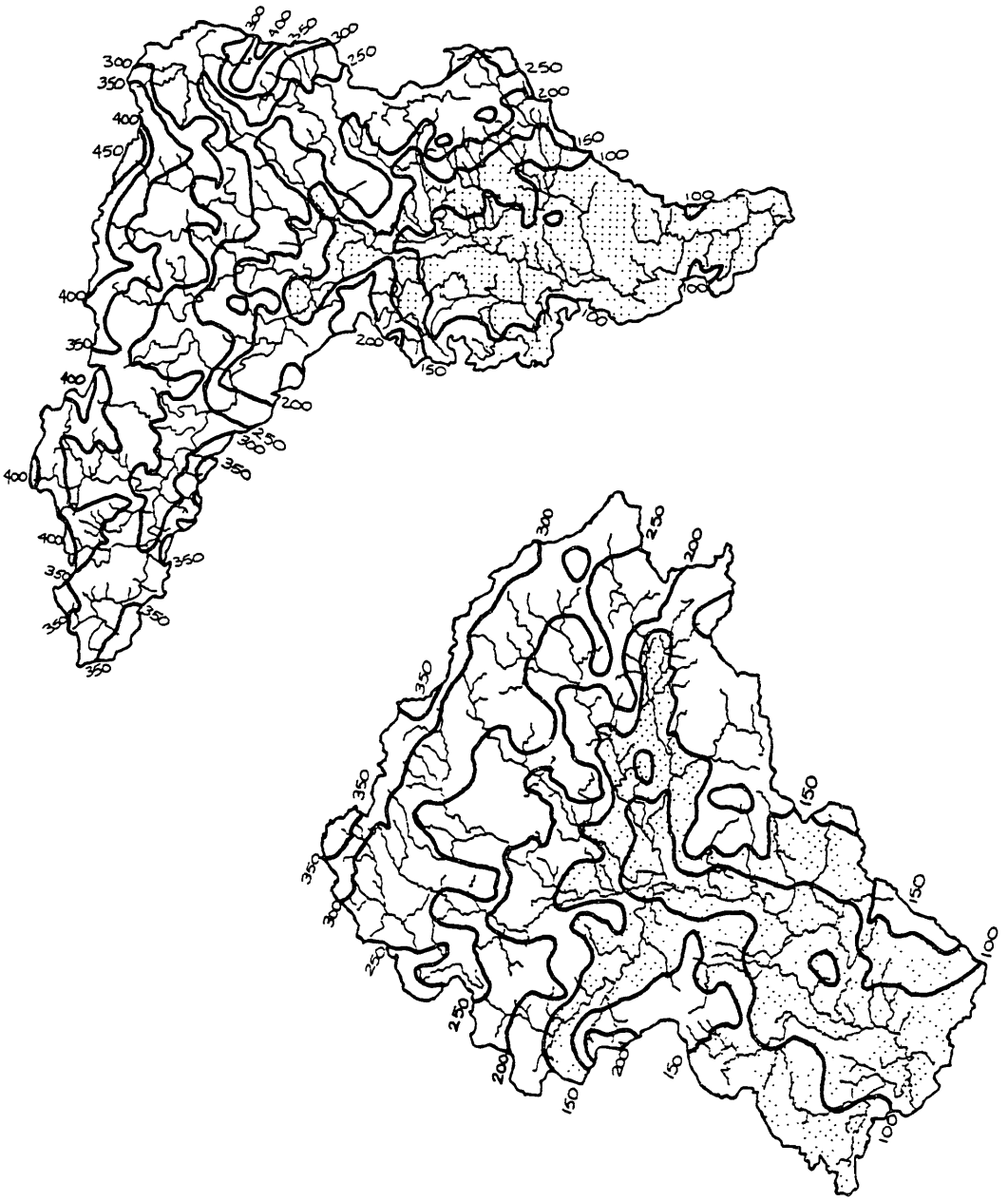

Fig. 2-23. Maps of elevation (m) above mean sea level, generated from digitized elevation points on streams and parameterized valley slopes. Region below 150 m is shaded.

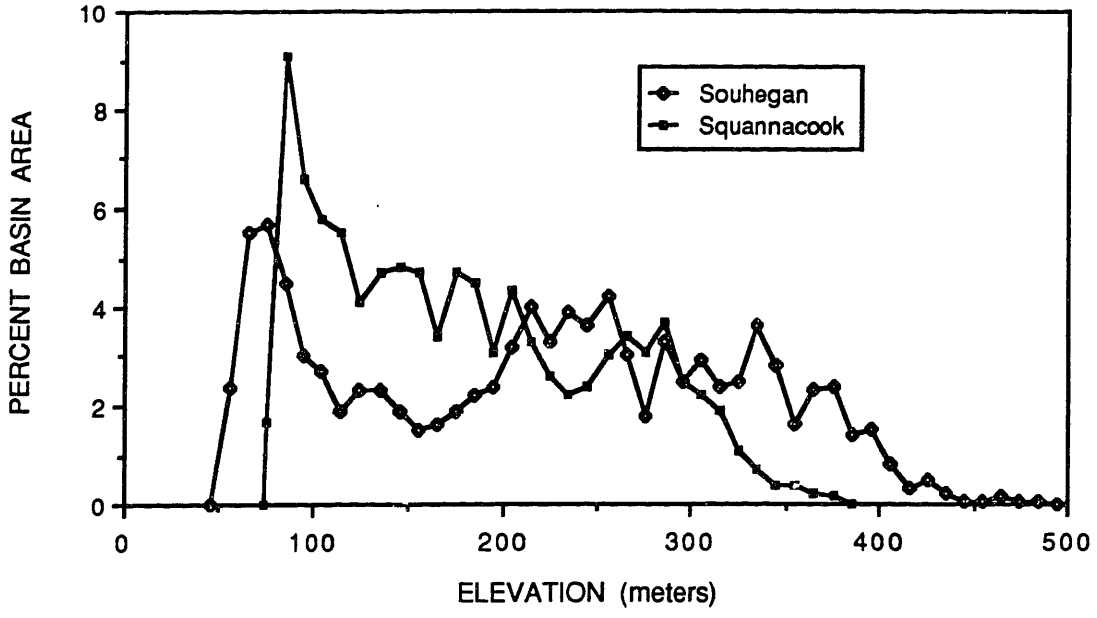

Fig. 2-24. Percentage of basin area at elevation (meters) above sea level.

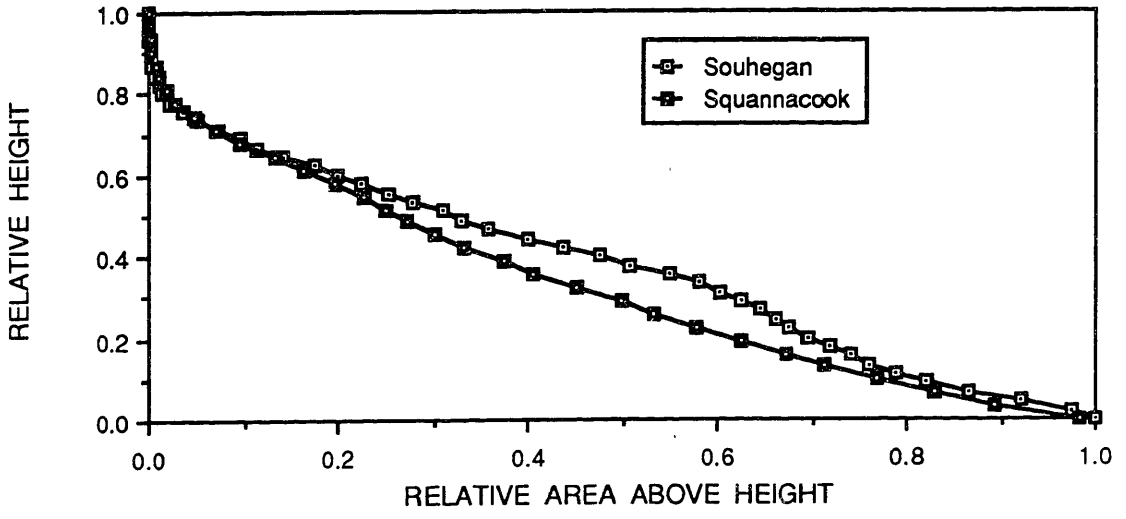

Fig. 2-25. Hypsometric curves. Percentage of basin area above height measured from gauge datum (normalized).

Table 2-9. Channel and stream sinuosities for Souhegan and Squannacook stream networks, stratified by Strahler order. Channel sinuosity defined as ratio of measured link length to straight-line distance; stream sinuosity defined as measured stream length (sum of links) divided by straight-line distance for complete stream.

SOUHEGAN	1	2	3	4	5
Channel Sinuosity (%)	117	115	118	119	131
Stream Sinuosity (%)	117	122	134	125	165
SQUANNACOOK	1	2	3	4	5
Channel Sinuosity (%)	116	111	116	127	132
Stream Sinuosity (%)	116	115	141	127	164

response of a similar basin with straight channels. A measure of this effect is the channel sinuosity or stream sinuosity. These parameters are defined separately here, the first as the ratio of the actual link length to the straight-line distance between nodes, and the second as the actual length of the Strahler stream divided by the distance between start and end points of the stream. The mean channel sinuosity is thus a measure of the tortuosity of the channel (true meandering), while the stream sinuosity is a measure of the deviation of the stream from a straight course (as a result of topographic or geologic obstructions). These values are tabulated for the Souhegan and Squannacook streams, stratified by Strahler order (Table 2-9).

In both basins the sinuosity increases with stream order. For the highest order streams the increase in distance due to meandering approaches 50 %. There is a marked difference between the sinuosity of the 5th order streams, and that of the upland tributaries of lower order. Values for both the channel sinuosity and stream sinuosity of the 5th order streams are nearly identical for the two basins.

If the salient features of the basin morphology could be obtained from an analysis of straight links only, with an appropriate factor applied to account for the sinuosity, the task of digitizing the river network would be simplified considerably. In practice, decreasing the channel velocity would be equivalent to scaling the straight link network by a suitable sinuosity.

Table 2-10. Drainage densities (km^{-1}) for the Souhegan and Squannacook basins, calculated as the mean of the drainage densities for sub-basins of each order. The drainage density of the whole basin (order 5) is indicated in boldface.

	1	2	3	4	5
SOUHEGAN	1.161	1.169	1.156	0.974	**1.034**
SQUANNACOOK	1.495	1.504	1.512	1.510	**1.476**

g) Drainage Density

The drainage density is defined as the ratio of the total length of streams to the basin area. The area of the Souhegan basin above the gauging station is 443 km^2 (as determined from the 100 m grid); the area of the Squannacook is calculated as 163 km^2. The total lengths of streams in the basins (determined from the digitized data and not from the grid) are 458.4 km and 240.6 km respectively. The drainage densities are thus determined to be 1.03 km^{-1} for the Souhegan, and 1.48 km^{-1} for the Squannacook. Average values of the drainage density were also calculated for each Strahler order, and the results are presented in Table 2-10. There is no apparent relation between the order of the sub-basin and the drainage density.

Drainage density is a highly variable parameter in nature (1 - 10^3 km^{-1} according to Chorley, 1969). Of course this parameter is scale dependent, and can only be compared with other values derived by the same analysis method. Qualitatively though, the drainage density is closely related to the "peakedness" of the hydrograph: regions with a high drainage density will efficiently concentrate runoff into channel flow, resulting in a rapid basin response.

Within a particular basin, the drainage density provides an estimate of the distance of overland (or subsurface) flow, $L_o = 1/2D$. For the Souhegan, L_o = 480 m; for the Squannacook L_o = 340 m. Smart (1973) postulates that the inverse of the drainage density should be comparable to the mean link length. For the Souhegan, the average link length is 1300 m, (compared to D^{-1} = 970 m), while for the Squannacook the mean link length is close to 900 m (D^{-1} = 680 m). The inverse of the drainage density underestimates the mean link length by 30% in both basins.

h) Basin Length Scales

Many early studies in hydrology considered the distribution of travel times over the watershed, as a means of understanding the basin response to rainfall. Zoch (1934), Clark and others (c.f. Eagleson, 1967), applied the term "isochrones" to curves connecting points in the basin with equal travel times to the outlet. Since these studies considered overland flow to be the primary runoff generation mechanism, travel times to the stream were neglected compared with the time of travel in the streams.

In regions with permeable soils however, infiltration and subsequent movement of the rainfall to the streams occurs at a velocity which may be orders of magnitude slower than the flow velocity in the streams. Thus, although the distance of travel to the streams is indeed short compared to the length of the streams themselves, for basins of moderate size the time required for the water to reach the streams is often greater than the time spent in the streams. This two velocity conceptualization of the watershed response provides the basis for the model discussed in the next chapter. In this section we present a discussion of the distribution of distances to the gauge and to the streams, independent of any assumptions regarding relative flow velocities.

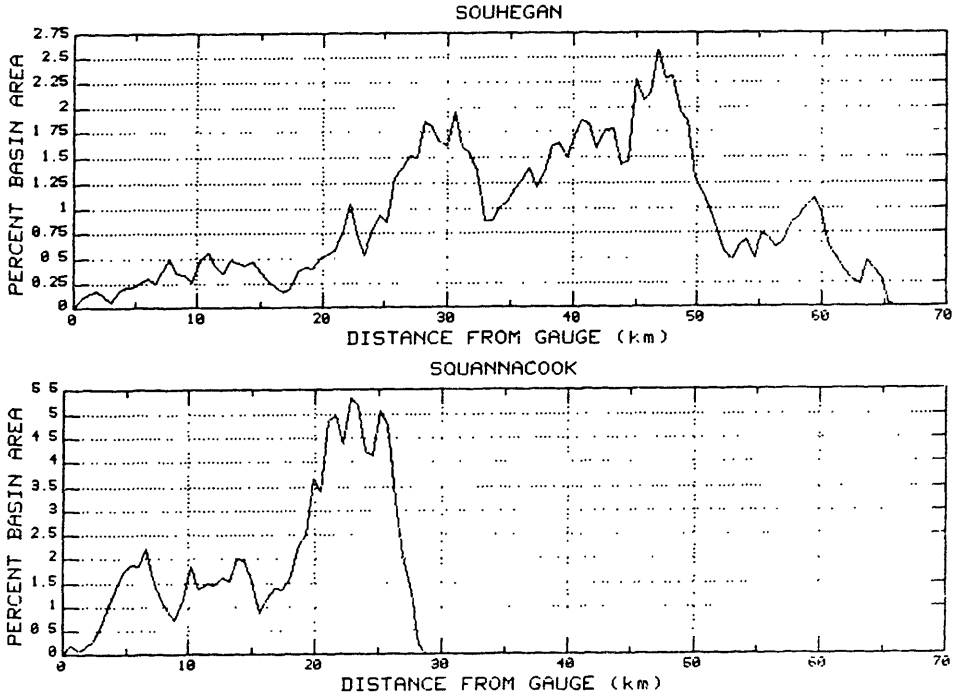

Fig. 2-26. Distribution of distances from the gauge. Percentage of basin area at given distance from basin outlet.

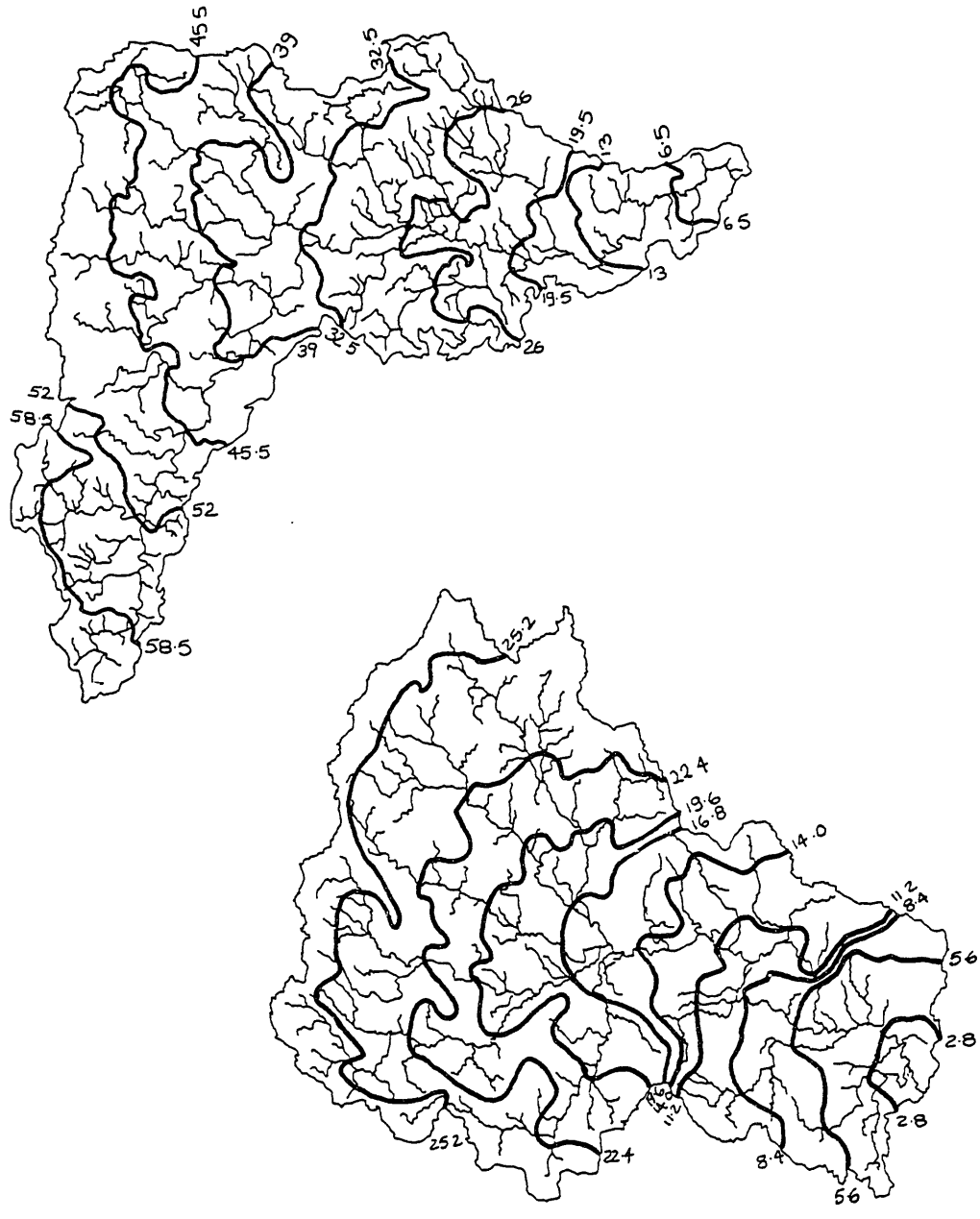

Fig. 2-27. Isometric curves. Contours of constant distance from the basin outlet (km). Ten equal intervals, normalized by the maximum distance to gauge.

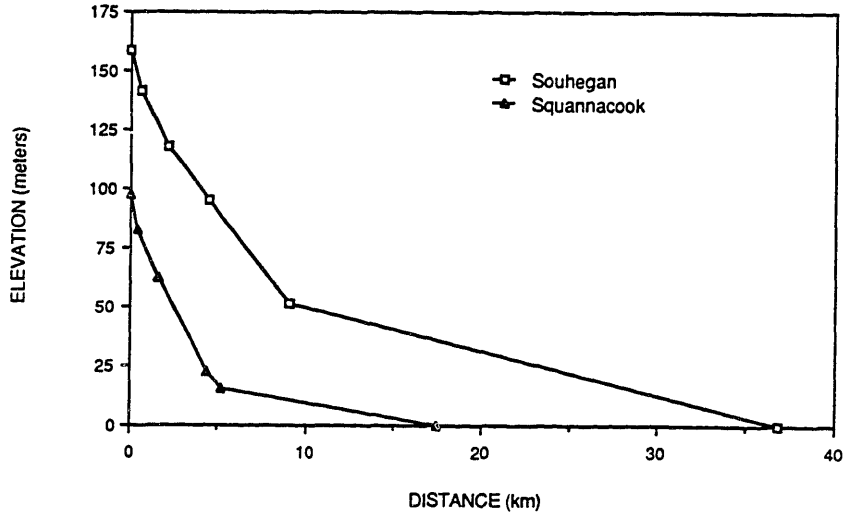

Fig. 2-28. Mean stream profiles. Average flow paths to the gauge (elevation drop (m) and distance (km)) considered by Strahler stream orders.

i) Distance to Gauge

Figs. 2-27 depicts "isometric" lines of equal distances to the basin outlet, for the Souhegan and Squannacook basins. These plots correspond to the familiar "isochronal" analyses if a constant velocity is assumed for overland flow and for channel flow in all streams. The distribution function describing the distance of points in the basin to the gauge (Fig. 2-26) is a function primarily of the shape of the basin. For the Souhegan, with a nearly linear basin structure, each maximum in the distribution function corresponds to a widening of the basin contour, the "width function" (c.f., Troutman and Karlinger, 1985). The distribution function for the Squannacook, on the other hand, is dominated by a single sharp peak, resulting from a peculiar, nearly radial, convergence of streams in the upland section of the basin.

The mean distance from the gauge for points in the Souhegan is 37 km; for the Squannacook, 18 km. Maximum distances are 65 km and 28 km respectively. Averaging the distances travelled in streams of different orders, we obtain a picture of a typical flow path in the system. The profiles in Fig. 2-28 also consider the elevation drop along the streams; the path followed to the gauge from each grid point in the basin contributes to the mean profile.

ii) Distance to Streams

In the foregoing discussion on geomorphology, the contributing areas of the stream segments were calculated after finding the nearest grid element with a stream for each hillslope grid element. Each grid point thus has a calculated distance to the nearest stream (zero for grid elements with streams). The distribution functions of the area of the basin at a given distance from the stream are shown in Figs. 2-29 and 2-30 for the Souhegan and Squannacook basins. Fig. 2-29 depicts the cumulative basin area as a function of distance from the streams, while Fig. 2-30 shows the derivative of these curves, plotted in log-linear coordinates. The distribution of distances to the stream exhibits an exponential behavior over a wide range of distances from the stream.

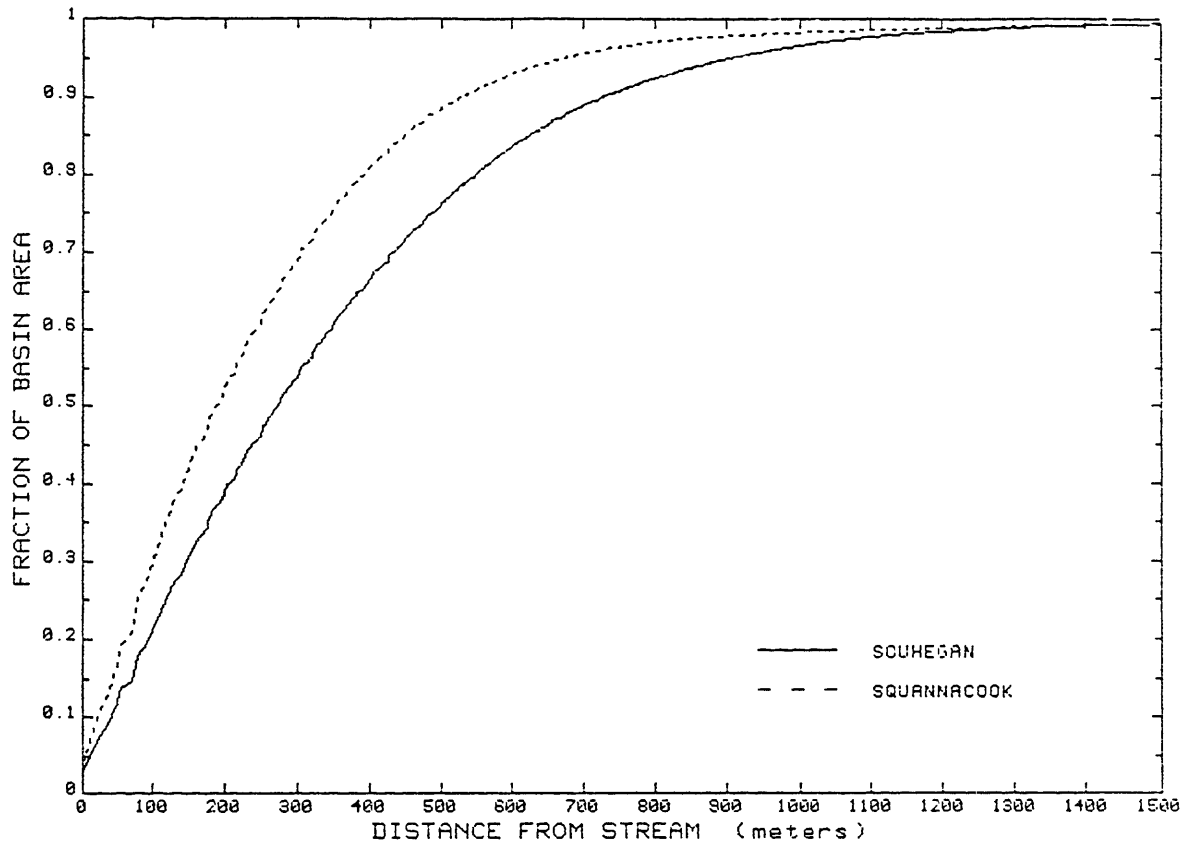

Fig. 2-29. Cumulative distribution of distances to the nearest stream, as measured using 25 meter grid.

It is worth noting that this smooth exponential behavior was not initially observed when using the 100 meter grid. That analysis produced a maximum in the distribution that was only later recognized to be an artifact of the grid, roughly explained by points on streams being counted once, while neighboring pixels are counted twice, for each side of the stream. This difficulty is avoided by considering a finer grid (25 meters), which is treated in the same fashion, but then averaged to 100 meter resolution. This sidesteps the discretization problems of the single grid which can provide only measures of distance from a prescribed sequence (x, $x\sqrt{2}$, 2x, $x\sqrt{5}$, etc.). Previous attempts to use a nested grid (a 10 m sub-grid for 100 m grid elements containing streams) were not successful in avoiding the numerically produced maximum.

It is perhaps not obvious that the basin area within successive contours of distance to the stream should in fact decrease with distance. A simple geometrical relationship, however, confirms that for all networks above a certain magnitude, the differential area, at any, even infinitesimal, distance from the network, is a decreasing function of distance (assuming that the region containing the network is bounded).

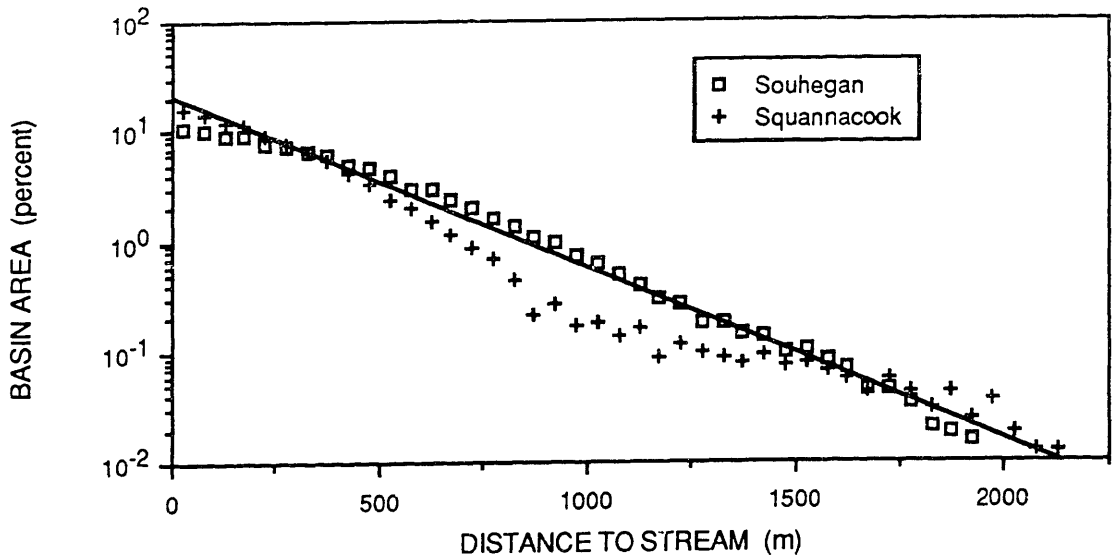

Fig. 2-30. Distribution of distances to stream. As in Fig 2-29, but increment in area located at given distance from stream. Calculated from 25 grid, averaged to 100 m. y-axis is logarithmic.

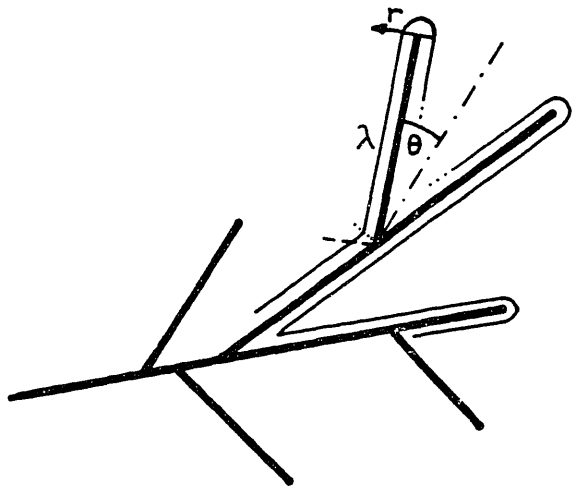

Fig. 2-31. Definition sketch for expanding network: area (A) within a distance (r) of the initial line network. The angle between neighboring branches is 2θ, the link length is λ.

Fig. 2-31 shows the geometry of the expanding network schematically. We shall consider the rate of growth of the basin area contained within a distance r of the streams. For each side of each branch of the network (length λ), there will be a quarter-circle contribution to the growth at the tip (growing to radius r), while the area on each side of the branch increases to rλ. Because of the angle formed at the juncture of two branches, there will be a deduction for the triangular piece lost due to the overlap of neighboring segments at the apex of the angle (half-angle measured by θ). For each half-limb, the area within radius r is then given by

$$A(r) = \frac{\pi r^2}{4} + r\lambda - \frac{r^2}{2\tan\theta}$$

For a network composed of N sources, with identically 2N -1 total links (the root, or outlet, of the network is not free to grow at the tip)

$$A(r) = 2N\left(\frac{\pi r^2}{4}\right) + 2\sum_{i=1}^{2N-1} r\lambda_i - 2\sum_{j=1}^{3(N-1)} \frac{r^2}{2\tan\theta_j}$$

where $\sum_{j=1}^{(N-1)}\theta_j$ must equal $2(N-1)\pi$.

Although the above formula allows any combination of link lengths and angles (they are independent summations), for simplicity we will consider a

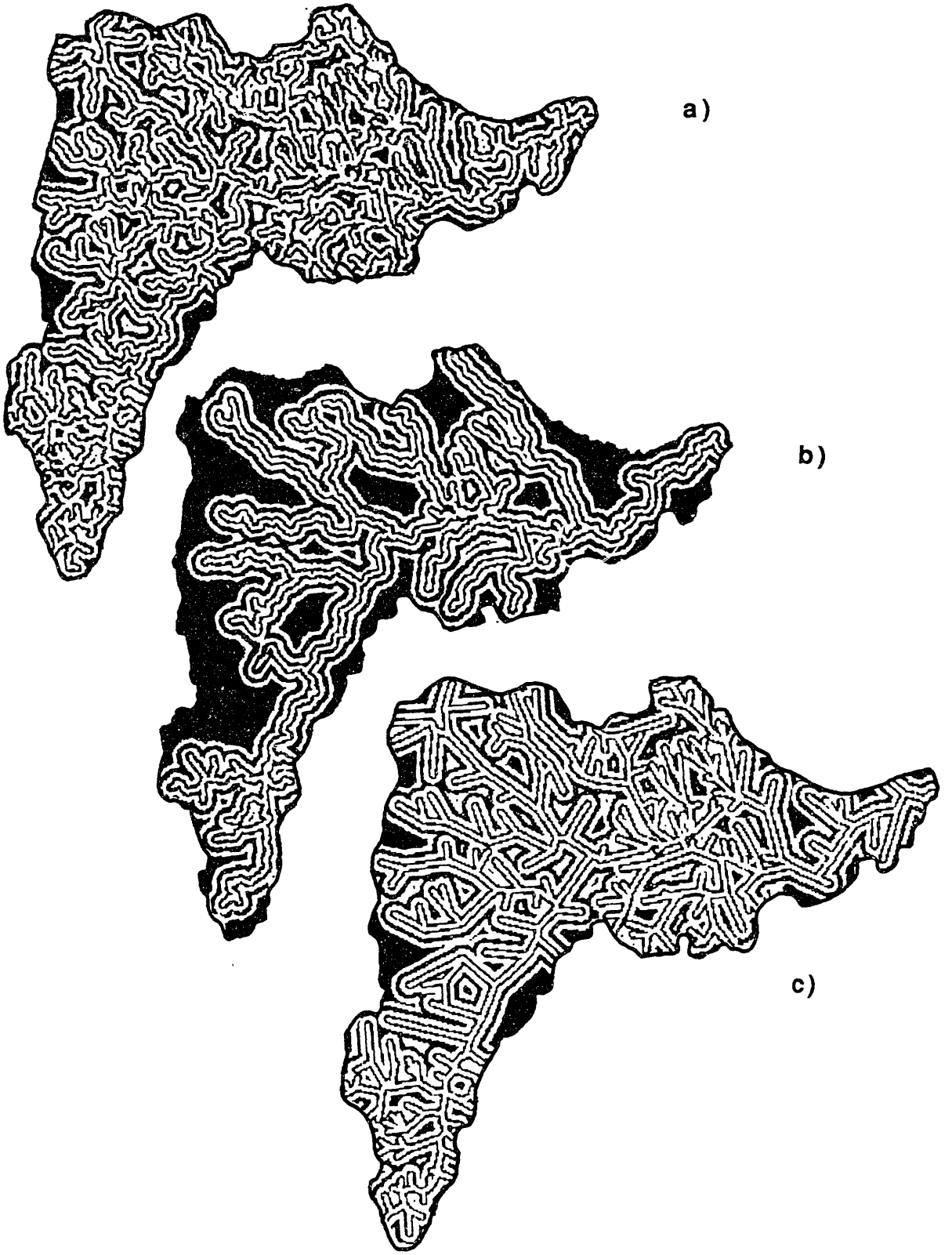

Fig. 2-32. Contours of distance to the nearest stream for the Souhegan. 100 meter intervals. a) Complete basin (5th order); b) first order streams omitted (4th order basin); c) Complete basin, but streams composed of straight links.

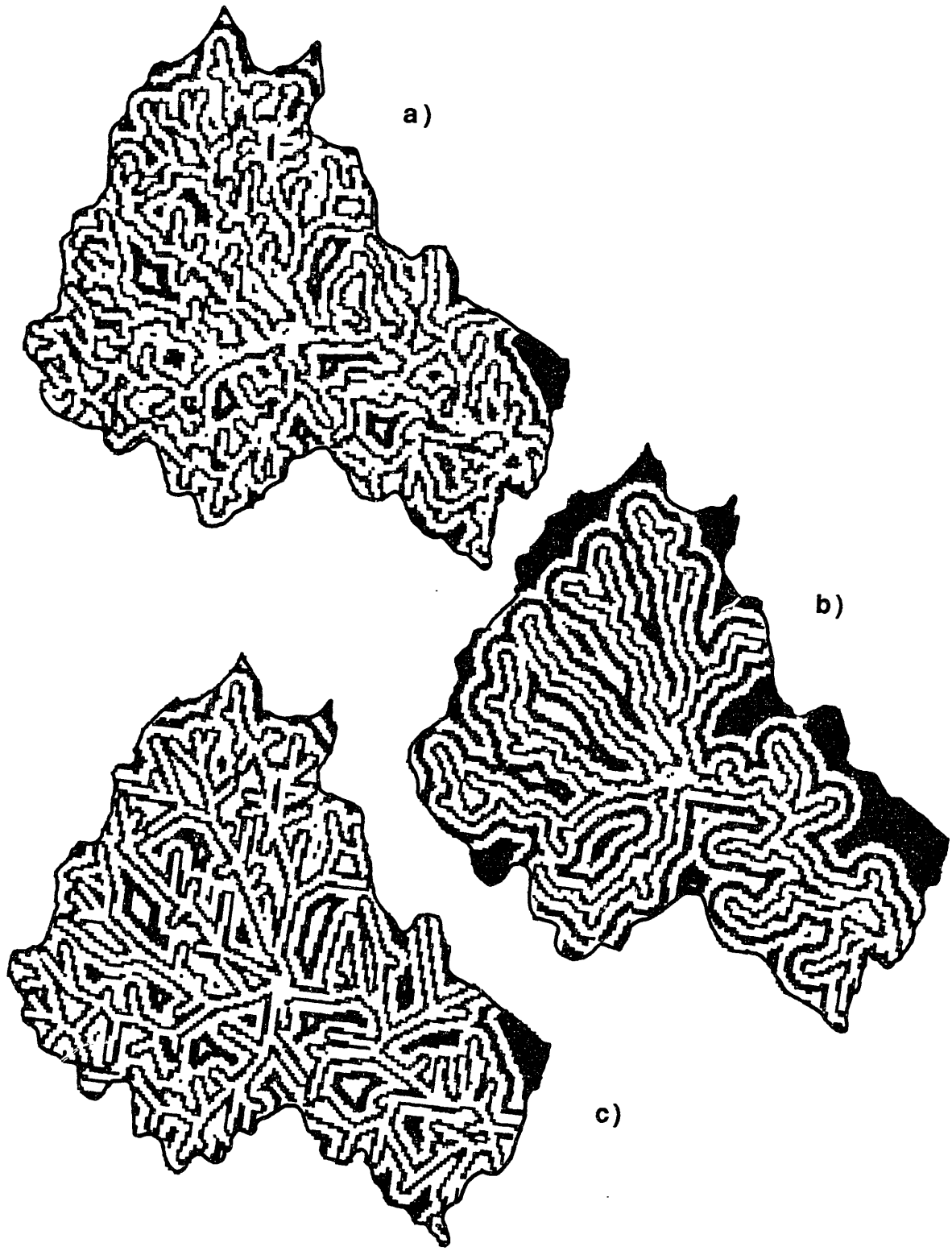

Fig. 2-33. As in Fig. 2-32, for the Squannacook.

network with N sources, equal link lengths λ, and the property that each new source joins the network consistently at an angle of 2θ. Then

$$A = 2\left(\frac{N\pi r^2}{4} + (2N-1)r\lambda\right) - 2(N-1)\left(\frac{r^2}{2(\tan\theta + \tan(\pi/2-\theta))}\right)$$

$$= \frac{N\pi r^2}{2} + (4N-2)\,r\lambda - (N-1)\left(\frac{1+\tan^2\theta}{\tan\theta}\right)r^2$$

Differentiating twice with respect to r, the distance from the stream, we obtain

$$\frac{dA}{dr} = (4N-2)\lambda + N\pi r - 2(N-1)\left(\frac{1+\tan^2\theta}{\tan\theta}\right)r$$

$$\frac{d^2A}{dr^2} = N\pi - 2(N-1)\left(\frac{1+\tan^2\theta}{\tan\theta}\right)$$

If the second derivative of the area with respect to r is less than zero, the differential area $(\frac{dA}{dR})$, will decrease with increasing distance from the network. The critical number of sources (N) required for this behavior depends on the angle θ. For angles less than about 20 deg, this will be true for networks of any magnitude. Moreover, if there are more than four sources, the differential area will decrease with distance away from the network regardless of the combination of angles. This is clearly the case for any natural stream network.

While the previous analysis does show that the distribution of basin area must decrease away from the streams, it does not predict the observed exponential behavior. The exponential is a property of the spatial arrangement of the network, and does not depend simply on the topology. The process which produces the exponential can be understood by visualizing an expanding river network of the sort depicted in Figs. 2-32 and 2-33 where distances from the streams have been contoured at intervals of 100 meters for the Souhegan and Squannacook basins. Considering the expanding network as a space filling process, we observe regions which become "pinched" off - the hydrologic equivalent of cell division, an exponential process. The cells between streams become filled by further subdivision of the region, and the basin continues to fill, at an exponential rate. An analytic description of this process is certainly desirable, but is unlikely to be forthcoming on account of the complexity of the geometry.

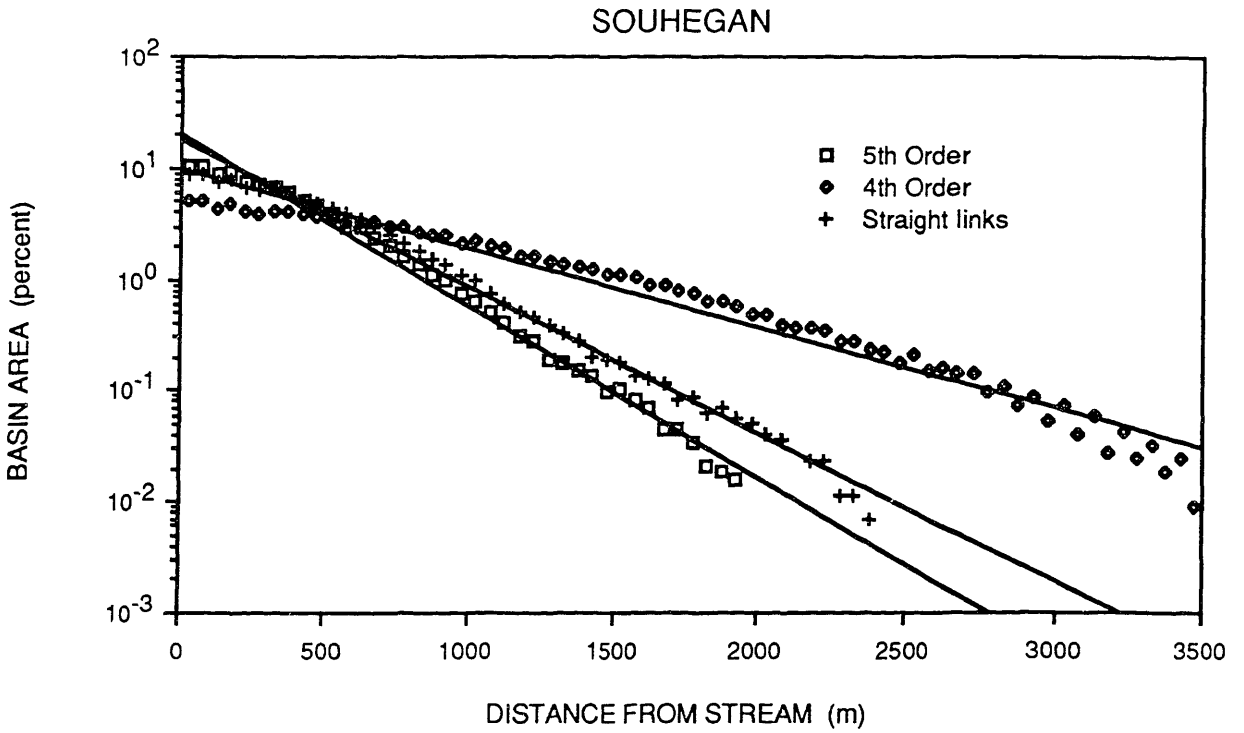

Fig. 2-34. As in Fig. 2-30, for the networks in Figs. 2-32 and 2-33. Upper plot for Souhegan; lower for Squannacook.

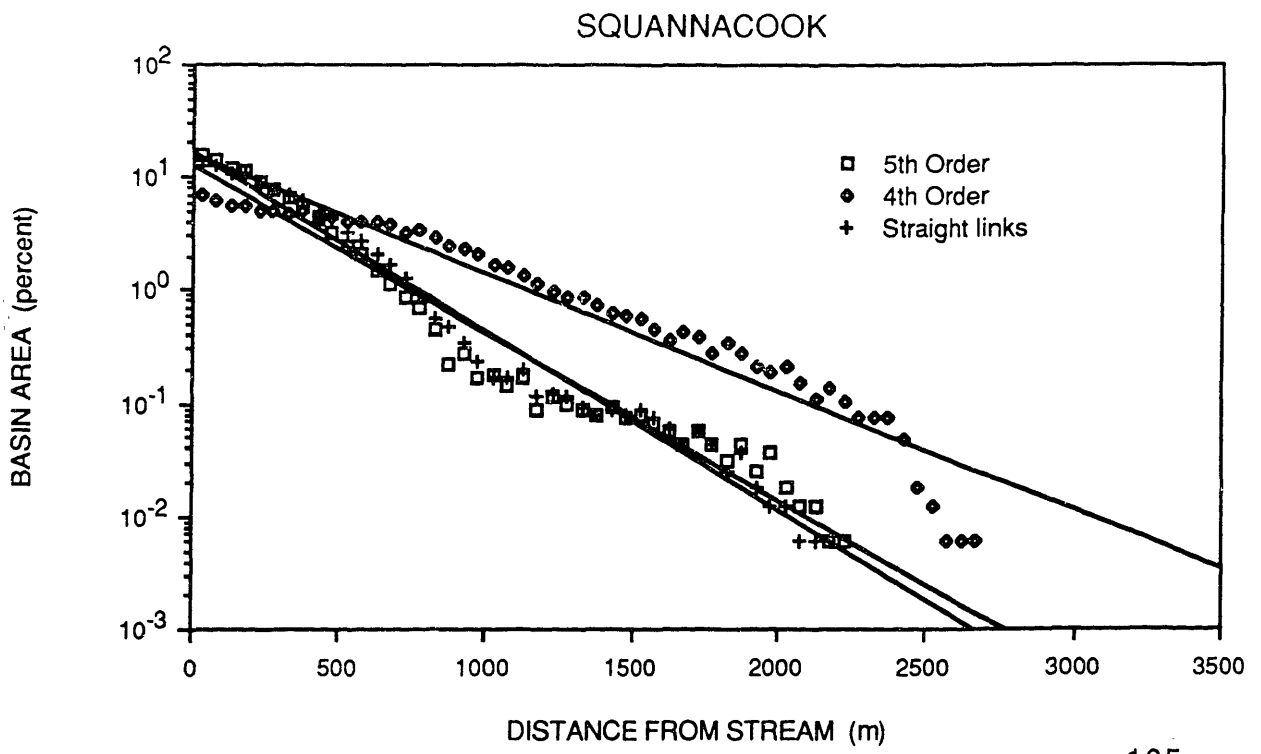

The parameter of the exponential appears to be linked, at least approximately, to the drainage density. Fig. 2-33 shows, in addition to the curves from Fig. 2-31, distribution functions for the other stream networks shown in Figs. 2-32 and 2-33. The networks in Figs. 2-32b and 2-33b result from the omission of all first order streams, a situation which might arise in practice from analyzing a small scale map. This reduction of the drainage density by a factor of two produces an approximate halving of the slope of the distribution curve. Also shown are the same analyses performed with straight links defining the streams (Figs. 2.32c and 2.33c). The small difference between the slopes obtained for the straight link case and that for the complete streams demonstrates that the exponential recession is a property of the basin on the macroscale, and is not a consequence of small scale meandering or other effects.

CHAPTER 3: THE MODEL

This chapter describes the construction and testing of a gridded hydrologic forecast model designed for use with radar rainfall data. Preliminary model results are presented for several storms over the Souhegan and Squannacook basins, and a possible course for future research is suggested on the basis of comparisons between the model results and the streamgauge data.

3.1 MODEL CONCEPTUALIZATION

For the reasons presented in the Introduction, the simplest possible representation of the river basin response was sought. The gridded model, operating at a scale of 100 meters, preserves the resolution and spatial distribution of the radar rainfall data, and the geometry of the stream network, but the processes of runoff generation and streamflow are reduced in the model to the simplest possible linear representations of these mechanisms. The assumption of linearity is central to the design of the model, and is based primarily on the success of other linear models of the basin response. Eagleson (1967) suggested this in writing:

> There is no doubt concerning the essential non-linearity of the idealized processes governing catchment response to input rainfall. . . Equally certain however, is the value of a simple linear model of this phenomenon, particularly for purposes of quick estimation and for studying the effect of parameter variation, but also because thirty years of collective experience with unit hydrograph methods have shown hydrologists that the quantitative effect of non-linearities is often surprisingly small in natural catchments.

For this study, a simple linear model provides a reasonable approximation to the observed hydrograph for the purposes of assessing the accuracy of the radar rainfall measurement. It also allows us to isolate the contribution of the basin geomorphology to the character of the observed hydrograph.

In the kinematic representation of the basin response proposed here, each "parcel" of precipitation available for runoff follows a particular path through the system, from its origin as rainfall, to its measured flow past the stream gauge. Except for the small fraction of the rainfall which lands directly in ponds and streams (less than 5%), this path involves a distance of travel through the soil (or if the soil is saturated, over the soil), and subsequent travel through the stream channels to the basin outlet.

a) Travel times in the streams

If we assume uniform velocities throughout the various streams in each basin, as discussed in the previous chapter, then Fig. 2-27, depicting the distribution of distances to the basin outlet, also represent the distribution of stream travel times, i.e., the unit hydrograph for the basin with an impermeable surface.

The idealization of a constant velocity in all streams of the basin, discussed in Section 2.1b, may be an oversimplification for upland catchments such as those considered in this study, since the hydraulic parameters for the channels could vary substantially between the headwater streams and the main channel of the basin. The effects of systematic variation in the channel velocities were investigated by considering a power law relationship between the discharge (Q) and the velocity (v), $v = Q^x$. Typical values for the parameter x have been suggested in the literature as ranging from 0.1 to 0.3 (c.f., Section 2.1b). Here, the possibility that the discharge in tributary streams may vary according to Strahler order is considered. That is, the discharge in the main stream of order Ω is the sum of discharges from the $N_{\Omega-1}$ streams of order Ω-1 etc.. Values of the velocity in streams of order ω, (V_ω), relative to the velocity in the highest order stream (assumed here to be $1 ms^{-1}$ for the purposes of illustration) are readily calculated from the data in Table 2-3.

Fig 3-1 illustrates the effect of varying the exponent x in the power law expression for the velocity as a function of discharge. Except with extreme variation of the velocity over the basin (x = 0.5, corresponding to a factor of 10 difference between V_1 and V_5), the time to peak of the response function is strongly controlled by the velocity in the highest order stream (c.f. Fig. 2-28 depicting the mean effective length of channels of varying order). For this reason, a constant velocity in all streams, representative of the response of the basin as a whole, was assumed in this study for the sake of simplicity. Of course if suitable measurements of flow velocities were available for individual channels, it would be a straightforward matter to incorporate these velocities into the model.

Comparison of records for the Souhegan and Squannacook gauges reveals that the times to peak (t_p) of the hydrographs are indistinguishable for the two basins. In addition to the data presented in the previous chapter (e.g., Fig. 2-19), this behavior is also evident in the case studies described in

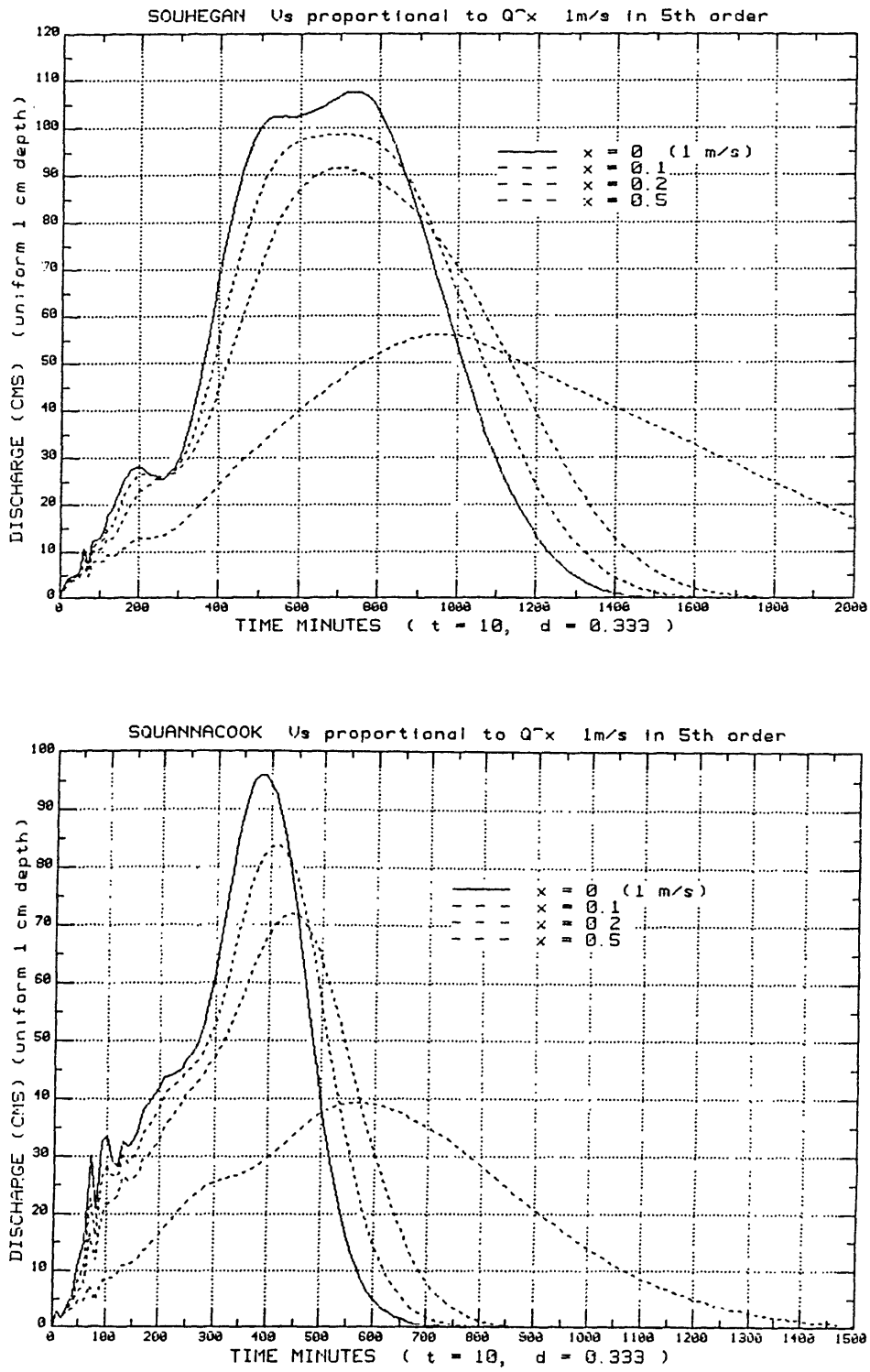

Fig. 3-1. Stream hydrographs with velocities varying as power law of discharge in streams of different Strahler orders, $v = Q^x$. Highest order stream velocity is 1 ms^{-1}; solid curve (x = 0) corresponds to uniform 1 ms^{-1} in all streams. For Souhegan (above), Squannacook (below).

Section 3.3. An objective analysis of the stream gauge records revealed no significant bias in the difference in t_p between the two basins; if anything, the Souhegan was observed to peak slightly earlier, on the average, than the Squannacook. Since the size and mean stream lengths of the two basins differ by more than a factor of two, this is clearly an indication that the characteristic streamflow velocity differs by a similar factor in the two basins.

From the streamgauge data, particularly for the regime of discharges considered in the case studies, representative stream velocities are determined as 0.6 ms^{-1} for the Souhegan, and roughly half that, or 0.3 ms^{-1}, for the Squannacook. Although these velocities correspond to the basin-averaged streamflow response, it is the character of the main channel of each basin that effectively controls the basin lag. The discrepancy between the velocities for the two basins is explained by differences in the hydraulic characteristics of the two rivers; Table 2-8, and Fig. 2-28, show that the slope of the 5th order stream in the Souhegan is nearly twice as steep as the main channel in the Squannacook. Although Souhegan stream velocity records were not available for a direct comparison, rough measurements of flow velocities in the two rivers (Williams, 1987) are in agreement with the values determined for the model.

The streamflow velocities applied in the model correspond to uniform conditions in both space and time. Due to the linearity of the basin response model, it is not possible to incorporate variations of the velocity during the course of the storm, since the rainfall inputs at each time-step are independent of subsequent discharge and velocity conditions. However, despite the relatively strong dependence of the velocity on the discharge reported in Section 2.1b ($v \propto Q^{0.5}$), no significant differences in the time to peak of the basin response were observed to result from such nonlinear effects. The comparatively narrow range of peak discharges considered in this study justifies the selection of a single streamflow velocity for all storm cases. This velocity presumably corresponds to flow rates at or near the peak discharge, as reported by Rodríguez-Iturbe et al. (1979).

b) Travel times to the streams

The time required for runoff to reach the streams depends critically on whether the water infiltrates the soil. Horton (c.f. Chorley, 1978) placed considerable emphasis on this concept in his studies:

> The surface of a permeable soil acts like a diverting dam and head-gate in a stream . . . one part goes via overland flow and stream-channels to the sea as surface runoff; the other goes initially into the soil and thence through the groundwater flow again to the stream or else is returned to the air by evaporative processes.

Where soils are highly permeable and hillslopes covered by vegetation, the mechanism of overland flow generation originally proposed by Horton (rainfall rate exceeding the local infiltration rate) is generally not observed. Water flowing over the surface of the soil is limited to regions of the basin where the soil has reached saturation. Such local saturation of the soil can, and has been observed to occur by a variety of mechanisms, for example, in the work of Dunne and Black (1970), by a rising water table near the streams. Comprehensive reviews of observational and theoretical evidence for the occurrence of saturation overland flow, and discussions of other aspects of the hillslope response can be found in Kirkby (1978 and 1985). Several hydrologic models have considered such mechanisms: Freeze (1972) and Troendle (1985) constructed detailed finite element models of the hillslope response; Beven and Kirkby (1979) present a more computationally realistic representation of the process for larger basins.

The original design of the model described here was also based on this concept of a dynamic, laterally expanding channel network. During initial testing of the model however, it became apparent that such a mechanism could not account for the volume of the runoff associated with the storm hydrographs. Cases in which 50% of the rainfall volume appeared at the stream gauge as runoff could only be accounted for in this model by a saturated zone extending 250 meters to either side of the channels. Furthermore, the recessions of the predicted hydrographs in this model were considerably steeper than those observed. The basin response was more accurately modelled by a much simpler process in which the entire basin contributed runoff flowing at a lesser velocity, through the soil layer to the streams.

Provisions were retained in the model for saturation overland flow near the streams, although this mechanism was supressed in the present study. It is possible that overland flow from saturated areas may in fact represent the dominant runoff generation mechanism during the latter stages of a major flood, when a significant portion of the basin area has reached saturation. Unfortunately, radar data were not available to test this hypothesis. In the model, saturation of a grid element is achieved by exceeding the local saturation deficit (rainfall depth required to reach saturation). Since the response of model grid elements is independent of conditions in neighboring elements, return flow and saturation by flow convergence cannot be modelled explicitly. Instead, the soil moisture deficit is assumed to increase with distance from the stream in such a way that saturation occurs preferentially near the streams. For simplicity, and lacking additional evidence, the moisture deficit increases linearly from a value of zero at the stream. The implementation of this saturation mechanism is described in Section 3.2.

In this study, all of the incident rainfall is assumed to infiltrate the soil and streamflow is generated by subsurface flow. The physical mechanism by which the hillslope generates subsurface storm runoff is the subject of considerable debate. Evidence is available to support two quite different mechanisms. The first mechanism involves flow through the larger soil pores, cracks, and "pipes" remaining from the decay of tree roots. In effect, these provide a subsurface "capillary" network draining to the "venous" network of the surface streams via the adjacent saturated zone. An example of such behavior was observed by Mosely (1979) for a small humid catchment in New Zealand where measurements of "pipe" flows showed velocities to be two to three orders of magnitude larger than percolation rates in the surrounding soil matrix. Subsequent tracer studies conducted by Pierce et. al. (1986), on the same watershed, suggested that virtually all of the streamflow was generated by the displacement of water stored in the soil (translatory flow), and that only 3% of the streamflow actually constituted "new" rainfall. Discussion of subsurface flow mechanisms can be found in Whipkey and Kirkby (1978), and Ward (1984).

The hillslope soils not only generate significant stormflow, but the recession of the flood hydrograph and prolonged base flow can be attributed to drainage of the soil wedge (Hewlett and Hibbert, 1963). Hydrologic forecast models typically represent the soil storage as an exponentially draining reservoir, yet there is little evidence that the hillslope itself drains exponentially; Hewlett and

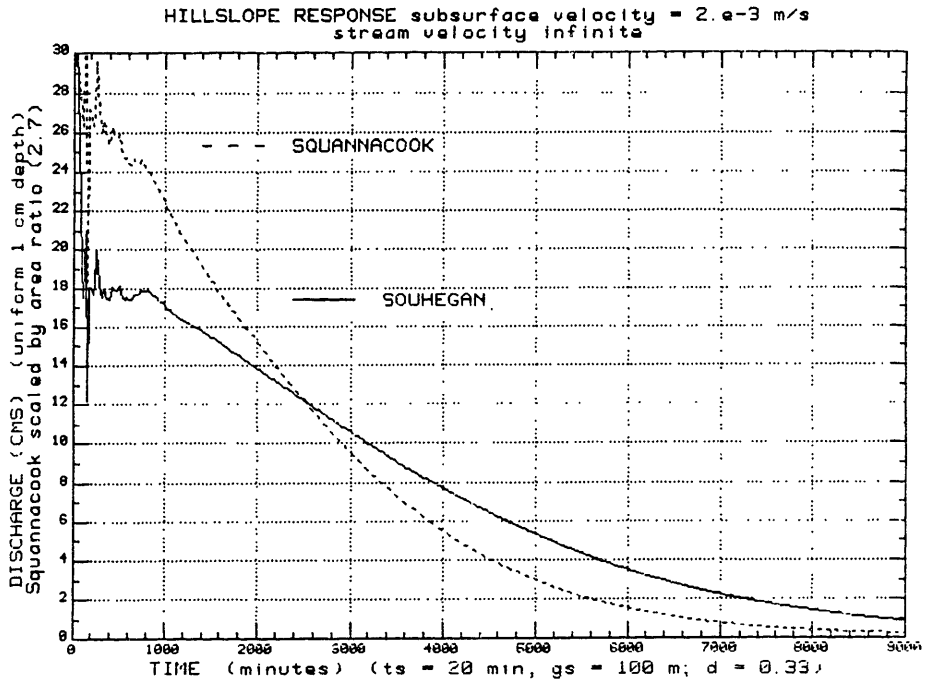

Fig. 3-2. Model hillslope response for the Squannacook (dashed curve), and for the Souhegan (solid curve).

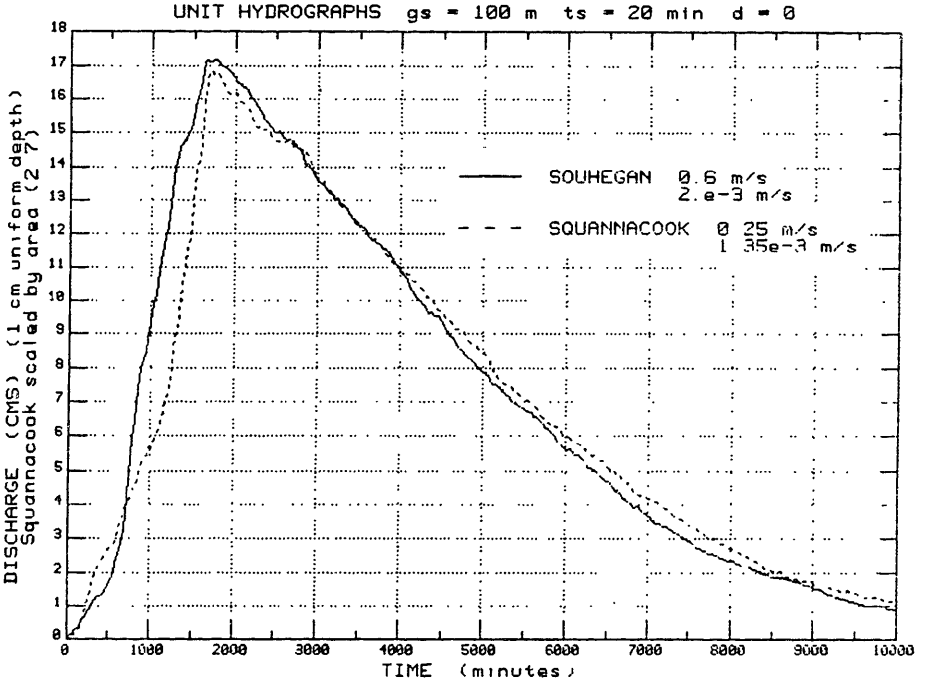

Fig. 3-3. Unit hydrographs generated by the model. Velocity parameters have been adjusted for the Squannacook (dashed curve) to yield a nearly identical response to that produced in the Souhegan model (solid curve).

Hibbert (1963) chose power laws to fit the observed drainage of their sloping soil sample. In the model proposed here, the observed quasi-exponential recession of the flood hydrograph is linked to the nearly exponential distribution of the fraction of basin area from the stream network, as described in the previous Chapter. The time scale of the recession is thus postulated to depend on the geometry of the drainage basin (essentially on the drainage density) as well as on the character of the soil, as represented by the velocity of subsurface flow.

In the model, the complexities of the hillslope response are reduced to the assumption that the transit time for runoff to reach the stream is proportional to the distance of the input from the stream. Moreover, the mean travel time associated with each parcel of water is assumed to be a linear function of the distance from the stream, i.e. the process is parameterized by a single velocity corresponding to the time scale of the hillslope response. This velocity is obtained by considering the observed hydrograph recession curves for the basin under study.

By comparing the slopes of the distributions in Fig. 2-30 with the time scales of the hydrograph recession curves (e.g., Fig. 2-16), the subsurface velocity is calculated to be on the order of 2×10^{-3} ms^{-1}. From Table 2-1 estimates of flow rates through the soils in the basin (vertical percolation, or flow under an imposed pressure gradient of ρg), would be between 10^{-7} and 10^{-4} ms^{-1}. As suggested by Mosely (1979), these percolation velocities are several orders of magnitude smaller than the calculated velocity of 2×10^{-3} ms^{-1} which presumably represents more rapid drainage of the soil through macropores, or as a result of translational flow.

Fig 3-2 depicts the hillslope responses for the two basins. These curves were generated in the model by setting the streamflow velocities to be infinite and the subsurface flow velocities to be 2×10^{-3} ms^{-1} in both basins. It is proposed here that different basin drainage densities will yield different hydrograph recession constants, assuming similar soil characteristics. Although the observed recession time constants for the two basins do not differ significantly, the model produces different responses for the two basins (Fig. 3-2); a subsurface flow velocity of 1.35×10^{-3} ms^{-1} is required in the Squannacook to produce agreement between the two curves. Because of the error introduced in the digitization of the Souhegan basin by using maps of different scales (c.f. Section 2.2a), it is not clear whether the differences

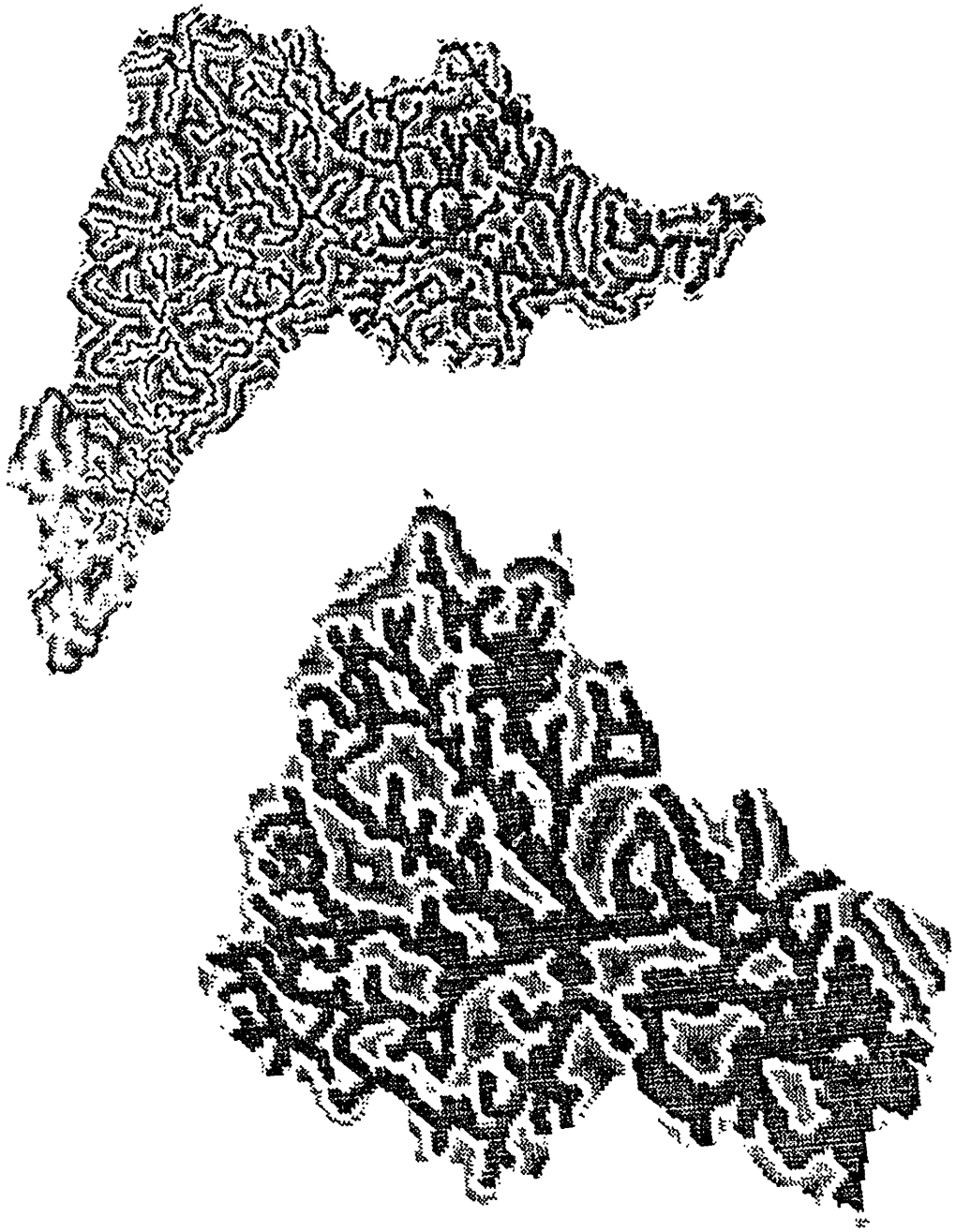

Fig. 3-4. Isochronal maps for the Souhegan (above) and Squannacook (below). Velocity parameters as in Fig. 3-3. Contour interval is one tenth of maximum time to gauge.

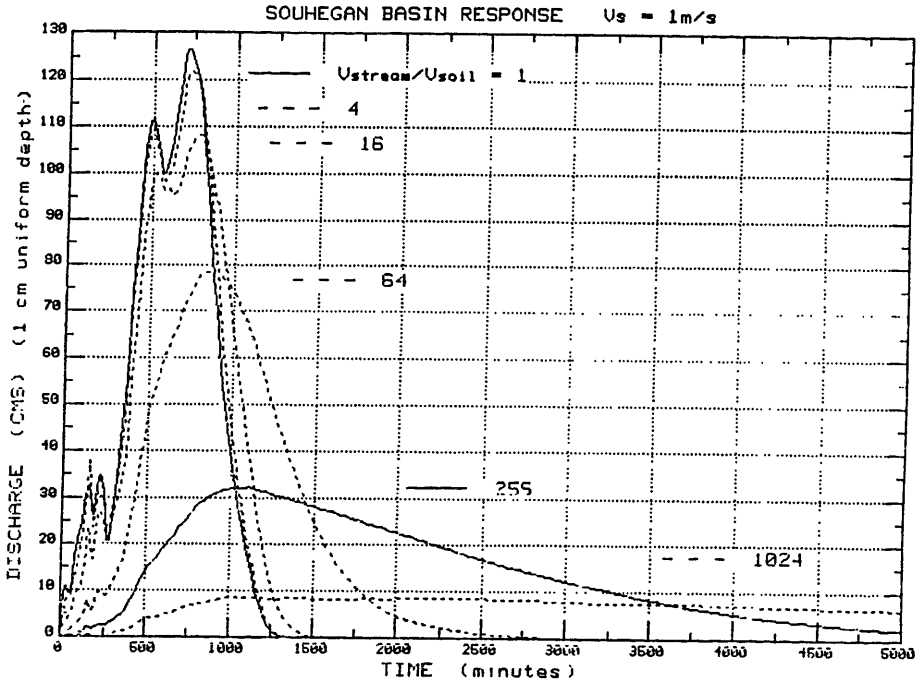

Fig. 3-5. Effects of the variation of the ratio V_{stream}/V_{soil} on hydrograph shape. Ratio is increased successively by a factor of four, from 1 (uniform velocity of 1 ms^{-1}) to 1024.

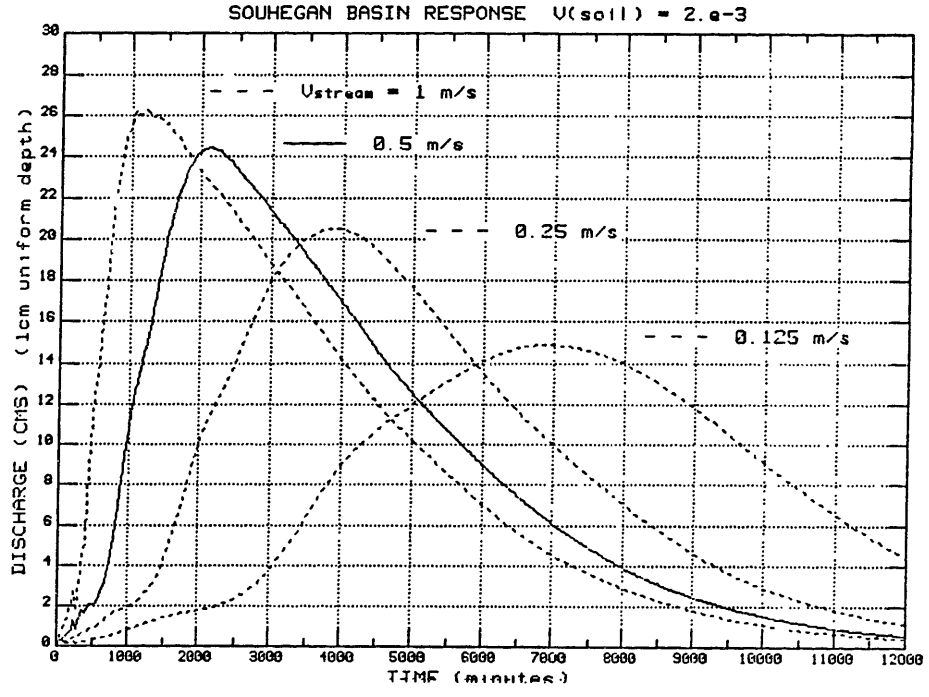

Fig. 3-6. Linear dependence of the hydrograph time to peak on streamflow velocity (V_{stream}). Subsurface flow velocity (V_{soil}) fixed at 2 x 10^{-3} ms^{-1}.

between the drainage densities for the two basins, and hence the model hillslope responses, are as great as Fig. 3-2 would suggest. Further research on several other basins would be desirable in order to determine whether a systematic relation does in fact exist between the drainage density and the slope of the hydrograph recession.

c) Total travel times

Combining the exponential response of the hillslopes with the distribution of travel times to the gauge yields the total basin response to a uniform rainfall input, or unit hydrograph. The unit hydrographs for the two basins shown in Fig. 3-3 represent the sum of the contributions from all grid points in the basin: each travels first through the soil to the nearest stream at velocity V_{soil} (order 10^{-3} ms^{-1}) and subsequently through the stream network to the gauge at velocity V_{stream} (0.1 - 1.0 ms^{-1}). In this plot the velocity parameters for the Squannacook have been adjusted to produce the closest possible agreement between the two response functions in order to compare subtle differences in the hydrograph shapes. These parameters are $V_{soil} = 2 \times 10^{-3}$ ms^{-1} and $V_{stream} = 0.6$ ms^{-1} for the Souhegan, and $V_{soil} = 1.35 \times 10^{-3}$ ms^{-1}, $V_{stream} = 0.25$ ms^{-1} for the Squannacook.

Comparison of the unit hydrographs with actual streamflow data for the two basins (e.g., Fig. 3-17), suggests substantial agreement between the characteristics of the predicted and observed hydrographs. In particular, differences between the shapes of the rising limb of the hydrographs for the two basins are correctly represented: in the Souhegan, the hydrograph rises smoothly, with convex curvature in the upper half of the rise; the rising limb of the Squannacook exhibits more character, with an initial bump, followed by a steep concave rise to the peak.

Apart from these subtleties produced by differences in the spatial arrangement of the stream network, the shape of the hydrograph depends only on the ratio of the stream velocity to the soil velocity. At one extreme, equal velocities in the soil and streams represent a basin with an impermeable surface, i.e. with relatively short overland travel times to the streams; at the other extreme, large velocities in the streams (or small soil velocities) correspond to a situation with very slow soil drainage, but relatively immediate translation of the runoff to the gauge. Isochronal maps of these basin conditions correspond to

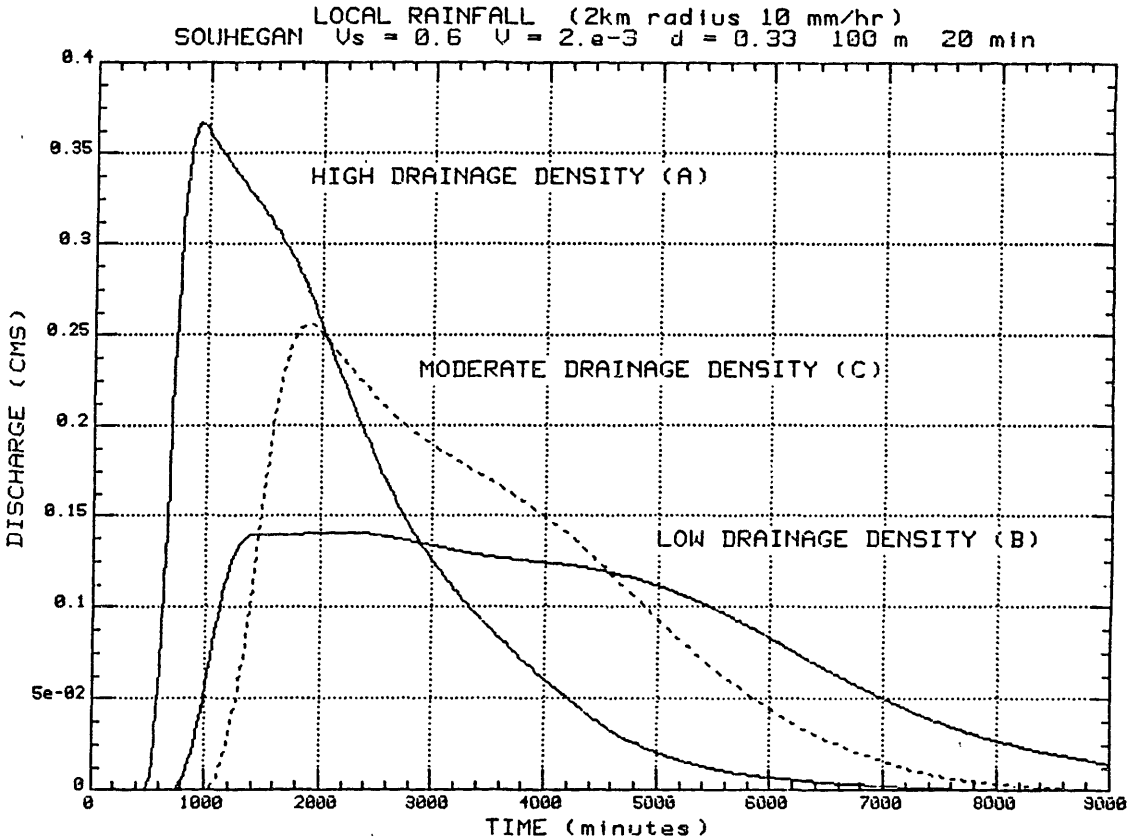

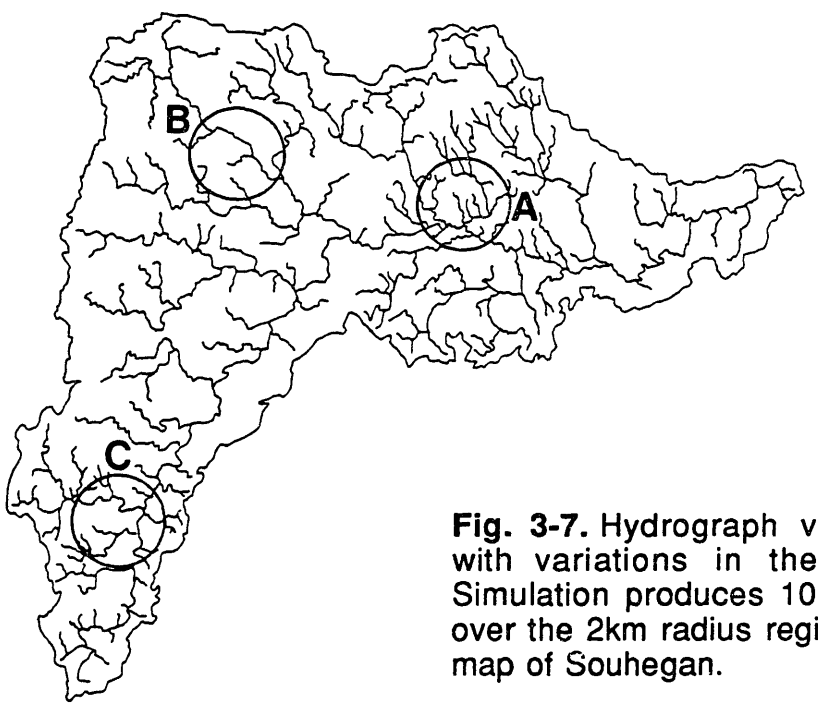

Fig. 3-7. Hydrograph variability associated with variations in the drainage density. Simulation produces 10 mm/hr local rainfall over the 2km radius regions indicated on the map of Souhegan.

Fig 2-23 for the impermeable case, and figures 2-32a and 2-33a for the slow drainage case. The isochronal maps for the actual conditions in the basins, intermediate to these extremes, are depicted in Fig. 3-4.

Fig. 3-5 illustrates the effect on the shape of the hydrograph produced by varying the ratio of the two velocities. In this sequence the stream velocity is fixed at 1 ms^{-1}, while the soil velocity is decreased successively by a factor of 4. The different hydrograph shapes produced are representative of several possible hillslope responses characterized by different flow velocities, e.g. overland flow, subsurface flows, and base flow. In the model, which incorporates only a single representative subsurface flow velocity, V_{stream}/V_{soil} is roughly equal to 256 (solid curve).

Varying each of the two velocity parameters separately produces nearly independent modifications to the unit hydrograph. As above, adjusting the soil velocity modifies the recession time scale, while changing the stream velocity modifies the peak and time to peak of the hydrograph in a linear fashion (Fig. 3-6), without significantly altering the recession portion of the hydrograph.

It is important to emphasize that the exponential behavior of the hydrograph recession is predicted only for the basin as a whole, and may vary considerably for individual hillslopes. As an illustration, Fig. 3-7 depicts a model simulation in which rainfall is generated only over selected regions of the Souhegan. These three areas are characterized by noticeably different drainage densities, and the resulting hydrographs exhibit correspondingly varied shapes which are not representative of the basin as a whole.

d) Dispersion

The previous sections have discussed the distributions of mean travel times to the streams and the travel times in the channels, but have not considered variations about the mean. In reality, contributions to the hydrograph from each grid point do not arrive at the gauge as delta functions in time, but are spread by diffusive effects. In particular, the channel network introduces both a lag and an attenuation of the streamflow peak. Many hydrologic models conceptualize this attenuation as a cascade of linear reservoirs representing the storage properties of the channel reach and other elements of the hydrologic system. Such models have been applied to both lumped and distributed watershed models (c.f. Nash 1957; Laurenson, 1964). Despite the operational value of the

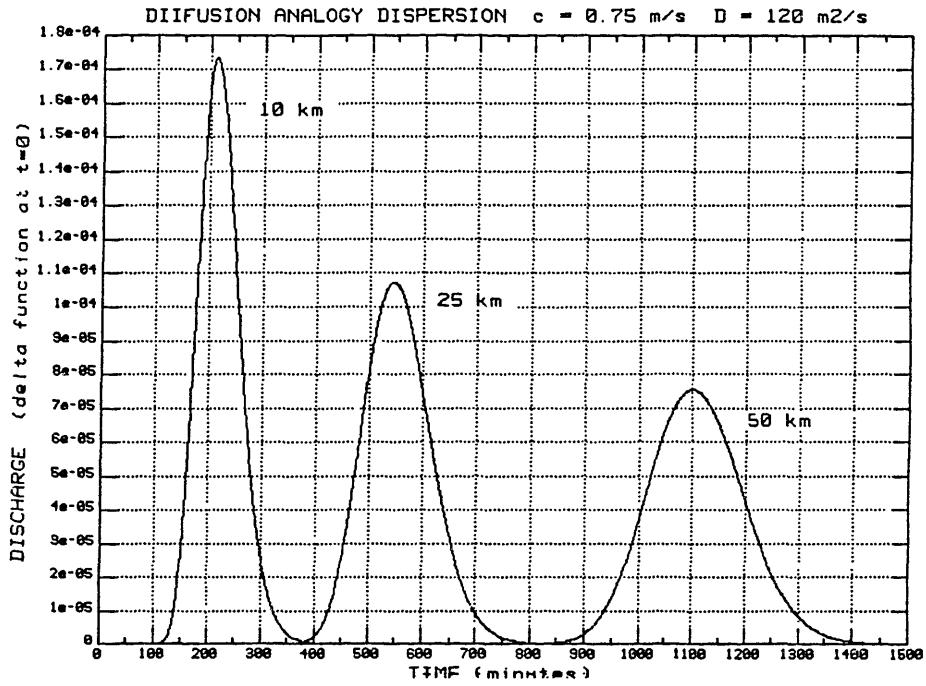

Fig. 3-8. Progression of a delta function flood wave down a uniform channel with hydraulic parameters: velocity = 0.75 ms^{-1}; diffusivity = 120 m^2s^{-1}.

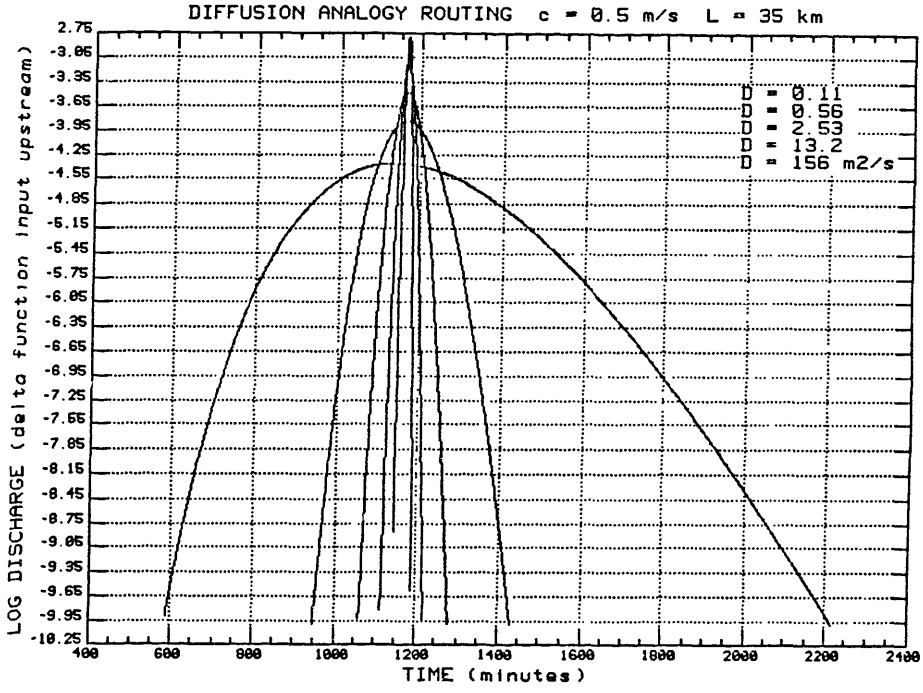

Fig. 3-9. Dependence of the attenuation on the value of the diffusivity (D [m^2s^1]).

linear reservoir models, the nature of the process is obscured in this approach. In keeping with the kinematic representation of the basin response, a diffusion analogue for the dispersion of the flood peak was sought.

Full equations, and tractable approximations, for the flow of water in open channels have of course been formulated, and with suitable boundary conditions can be solved for natural channels of variable slope, width etc. However, even for large rivers, where channel routing is the primary flood forecasting technique, linearizations of the St. Venant equations are generally suitable. In the following, the effects of dispersion on the shape of the flood hydrograph are assessed for the basins considered, by applying a diffusion analogy routing model. On the basis of these experiments, further simplifications to the method are introduced.

Dooge and Harley (1967) examined a suitable linearization of the equations for uniform channel flow with a reference discharge q_o and corresponding values of the depth (y_o), velocity (u_o) and slope (S_o):

$$(gy_o - u_o^2)\frac{\partial^2 q}{\partial x^2} - 2u_o\frac{\partial^2 q}{\partial x \partial t} - \frac{\partial^2 q}{\partial t^2} = 3gS_o\frac{\partial q}{\partial x} + \frac{2gS_o}{u_o}\frac{\partial q}{\partial t}$$

An alternative linearization of the full equations, due to Hyami (c.f., Eagleson, 1970), yields an equation of the form

$$\frac{\partial q}{\partial t} + c\frac{\partial q}{\partial x} = D\frac{\partial^2 q}{\partial x}$$

which is recognizable as the equation for the diffusion of a conservative quantity. For the case of a uniform channel, the velocity c is given by

$$c = \frac{3}{2}u_o$$

and the "diffusivity", D, is a function of the channel width (w_o), discharge (q_o), slope (S_o), and a reference Froude number (F_o), (Troutman and Karlinger, 1985):

$$D = \frac{1}{2S_o w_o} q_o (1 - F_o^2) \; ; \; F_o = \frac{u_o}{\sqrt{gy_o}}$$

Dooge and Harley also derive the variance of the channel response function about the mean:

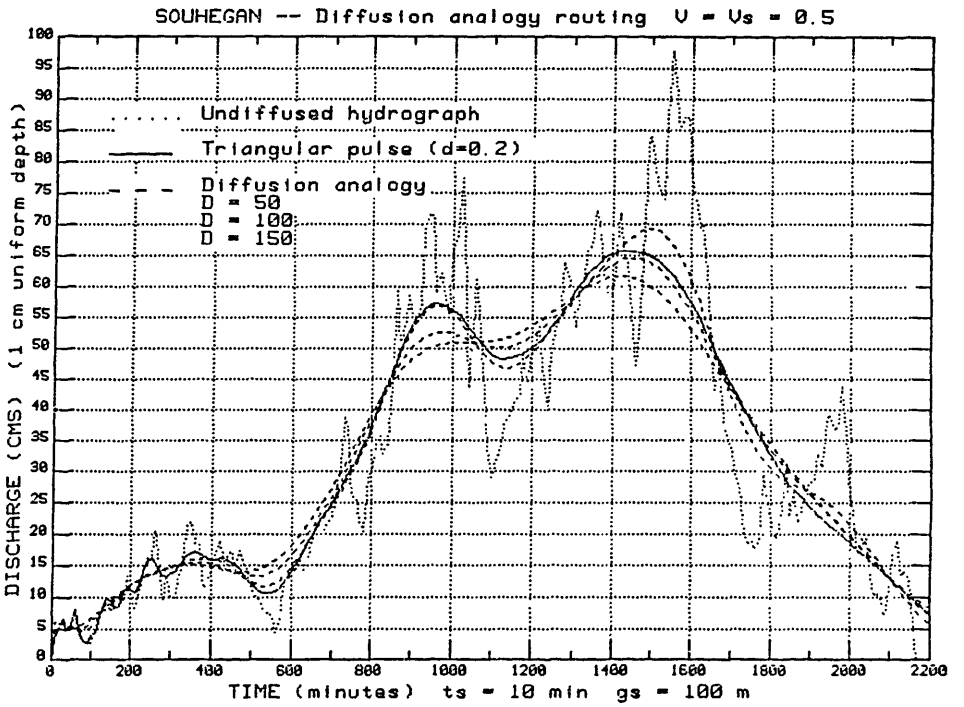

Fig. 3-10. Effects of attenuation on the impermeable basin hydrograph. Model hydrograph (dotted) is smoothed by triangular pulses dispersion (solid) which offers a reasonable approximation to the full diffusion analogy routing solutions (dashed).

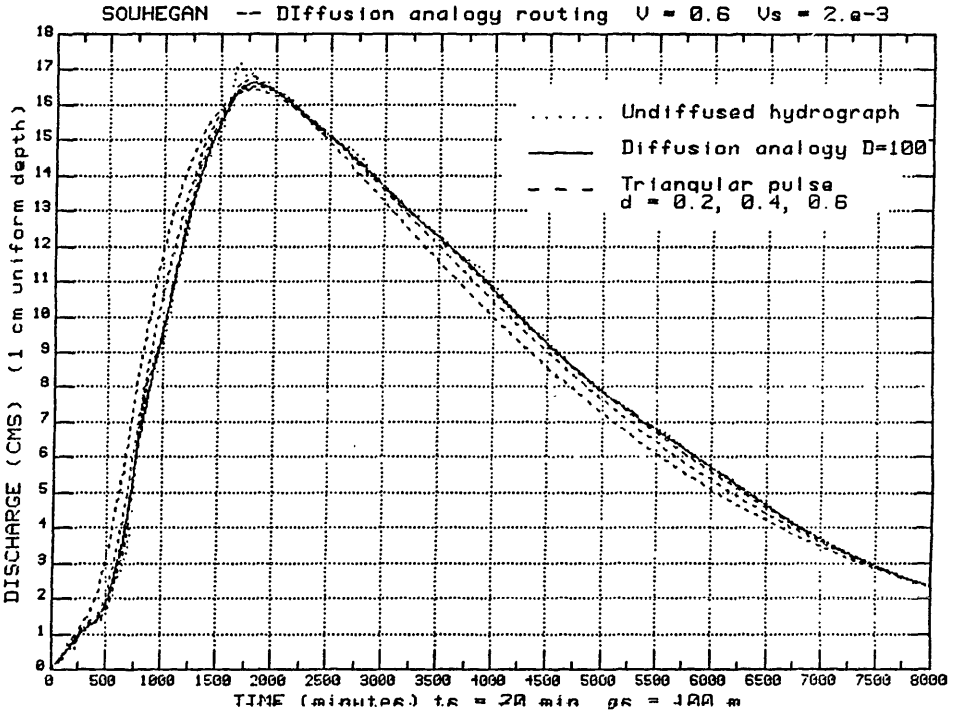

Fig. 3-11. Effects of attenuation on unit hydrograph. Both the triangular pulse (dashed), and the diffusion analogy methods (solid), show negligible differences from the undiffused hydrograph (dotted).

$$\sigma^2 = \frac{2}{3}\left(1 - \frac{F_o^2}{4}\right)\left(\frac{y_o}{S_o x}\right)\left(\frac{x}{1.5u_o}\right)^2 .$$

Defining $k = \frac{2}{3}\left(1 - \frac{F_o^2}{4}\right)^{\frac{1}{2}}\left(\frac{y_o}{S_o u_o}\right)^{\frac{1}{2}}$, $(\sigma = k\sqrt{t})$, the standard deviation of the dispersion is expressed in terms of the square root of the time of travel $(\sqrt{x/u_o})$, in accord with the diffusion equation solutions, and as depicted in Fig. 3.8 which shows the progressive attenuation of a delta function input moving along a uniform channel with parameters typical of the lower reaches of the Souhegan and Squannacook rivers ($c = 0.75\ ms^{-1}$, $D = 120\ m^2s^{-1}$). Introducing the power law relations valid at the Squannacook gauge ($u_o = 0.243Q^{0.473}$; $y_o = 0.623Q^{0.275}$):

$$k = 1.067\left(1 - 2.4x10^{-3}Q^{0.671}\right)^{0.5} Q^{-0.099}\, S_o^{-0.5} .$$

For meaningful values of Q (between 1 and 100 m^3s^{-1}), k is nearly independent of the discharge, and depends only on the slope of the channel (S_o). The greatest attenuation thus occurs in the higher order streams with small channel slopes. Fig. 3-9 depicts the effect of attenuation on a delta function translating through a uniform channel of length 35 km ($c = 0.5\ ms^{-1}$), for a variety of values of the diffusivity (D). These values are calculated from the mean properties of Squannacook channels of various orders (Section 2.2). The mean diffusivity varies by three orders of magnitude from 0.11 m^2s^{-1} in the first order streams, to 156 m^2s^{-1} in the fifth order channel.

Because the above routing schemes could not be used for real-time model calculations (routing the runoff contribution from each grid element in this fashion is computationally inefficient), two further simplifications were made to the diffusion analogy routing. In the model, the Gaussian dispersion is approximated by a unit triangular pulse whose base width varies linearly with the time of travel. Linear smoothing was adopted because it is more easily implemented in the model than the square root of time dependence predicted by the diffusion analogy routing theory.

Figs. 3-10 and 3-11 provide an appreciation of the limited effects of dispersion on the hydrograph and justify the application of the above scheme. The smoothing by triangular pulses is compared to actual routing calculations performed applying the diffusion analogy equations, for various values of the

diffusivity. In the model results presented here and in subsequent sections, the value of "d" refers to the half width of the triangular pulse (i.e. a delta function arriving at the gauge at time t is spread over a triangle whose time base is given by $t \pm (t \times d)$. In Fig. 3.10, for an impermeable basin, the effects of the diffusion analogy routing (for a variety of values of D) are well approximated by the triangular pulse method with d (the half width) assuming values near 0.2. In Fig 3-11, for the Souhegan unit hydrograph, the results of the diffusion analogy routing (D=100) and the triangular pulse method (d = 0.2) are virtually indistinguishable. Moreover, even extremely large values of the dispersion parameter (d = 0.6) yield less than 10% differences between the attenuated and unattenuated hydrographs.

It is important to emphasize that the dispersion is applied at each time step of the hydrograph, rather than for each grid element independently. The amount of diffusion applied thus depends simply on the travel time to the gauge, regardless of whether the water travels through the soil for a large portion of this time (i.e. the diffusion in the soil is the same as the diffusion in the streams). While this may not be valid physically, in practice, as shown above, the net effect on the shape of the hydrograph will be small. The reason for this lies in the very small flow velocities characteristic of the soil response. At $V_{soil} = 2 \times 10^{-3}$ ms^{-1}, the contribution from a 100m x 100m grid square will arrive at the gauge at time $t \pm 400$ minutes. As will be described in the following section, the model already represents the "delta function" contribution from this grid element as a rectangular pulse on the time series, with a time base of approximately 14 hours in this case.

Various values of the parameter d (the triangular pulse half-width) are applied in the model runs (never greater than 0.33). Some of the earlier figures of this chapter (e.g., Figs. 3-1 and 3-2) already included some dispersion for the sake of clarity.

3.2 MODEL IMPLEMENTATION

Development of the model was constrained by several factors, notably available computer memory, and the speed of operation. For real-time applications, the model was designed to operate during the interval between radar scans (typically five minutes), on the same computer that controls the radar. The computer system used, (Charles River Data Systems), has four megabytes of run-time memory. The model was designed to operate within these limits to avoid inefficient data transfers to and from disk storage. For a typical model configuration, this restricts the size of the model grids to about 160,000 elements (100 m resolution over the Souhegan for example), since several grids are required simultaneously for the operation of the model.

The grid resolution is the ultimate factor controlling the speed of the model calculations. Depending on the grid spacing and time step used in the model, the time to process a single scan varies from about 10 seconds to 150 seconds. The run times also vary with the velocity parameters (longer for smaller flow velocities), and are shorter when only a fraction of the basin is covered by rain.

The code for the model was written in the language C, to allow direct interface with the radar controller for eventual real-time applications. Although the code for the actual model is in fact very simple, the inclusion of provisions for various secondary calculations, interactive control, and system dependent graphic displays makes the complete program rather cumbersome, and it is not reproduced here. Instead, a description of the principal features of the model are provided in this section, with particular attention to technical difficulties encountered in the implementation of the model.

The model uses for input the radar data converted to a Cartesian coordinate system by the method described in Section 1.3b. The radar maps are stored as individual files on disk accompanied by an inventory file containing the sequence and times of the scans. The primary output of the model is a color graphics display that is updated as the model progresses. Fig. 3-12 shows a black and white printout of a typical display. The display can be customized to show a variety of model properties: maps of the radar reflectivity pattern, total storm depth, basin saturated zones, and isochronal maps; and time series of the rainfall rate over the basin and at specified locations; the basin response to each rainfall input; and the cumulative forecast of the discharge at the streamgauge.

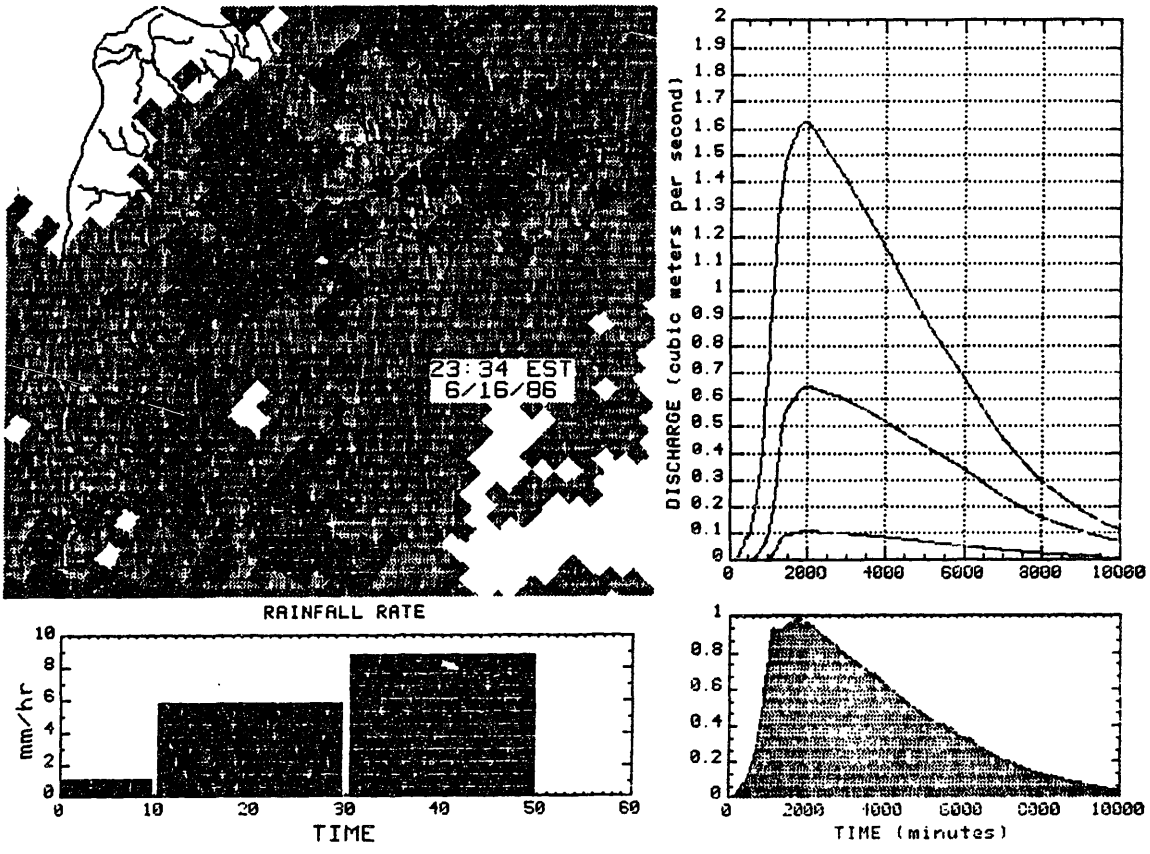

Fig. 3-12. Example of model real-time display. Upper left quadrant shows radar rainfall pattern over the Souhegan as a squall line moves across the basin. Basin average rainfall rates for the previous hour are depicted below. Lower right shows the instantaneous basin discharge resulting from the current scan; upper right is the cumulative discharge forecast. Translation of the storm towards the gauge is evident in the cumulative hydrograph display.

As many calculations as possible are performed prior to the model run. A separate program is used to generate the isochronal maps for the specified grid scale, using the data previously generated at 25 meter resolution. The time of travel in the streams is stored (with the possibility for different velocities in streams of various orders), and three separate grids are stored for the distances to the nearest stream (mean, minimum and maximum distances for each grid element). These are used to generate the operational grids at the time of model initialization.

Integral to the model development process was the desire to create a model that could be operated for variable grid sizes and time steps. Clearly, if the gridded model concept were to be applied to a larger basin, the model could not be used operationally at 100 meter and 5 minute resolution. A method for "averaging" the model in space and time was devised; the radar data input is averaged in accordance with the model. This method is described here.

In practice, even at 100 meter resolution, certain aspects of the model require parameterization. The model must, in essence, be operated in the time domain, rather than from the spatial grid alone. With streamflow velocities differing from subsurface velocities by two orders of magnitude, the subsurface flow contribution from a grid element must be spread over a time base on the hydrograph correspondent with the dimensions of the grid element in the time domain, i.e. the first arrival and the last arrival of the water at the gauge. The manner in which this is performed differs for those grid elements containing streams, and those without. The "stream elements" are modelled with greater care than the "hillslope elements" because they, under certain conditions, might include saturated zones near the stream (narrower than the grid size even at 100 meters), and also because, in the limit of large grid spacing, the basin is composed only of stream elements.

Fig. 3-13 illustrates the model representation for a stream element. Each stream element is reduced to this form, where the length of the stream (x) and the width of the hillslope (y) depend on the arrangement of streams within the element. In fact, for reasons to be described below, the stream channel is assumed to flow diagonally across the grid element, but the rectangular arrangement (originally used) is simpler to discuss. The length of the stream (x) is the difference between the farthest stream point from the gauge and the closest. The width of the hillslope (y) is calculated as twice the mean

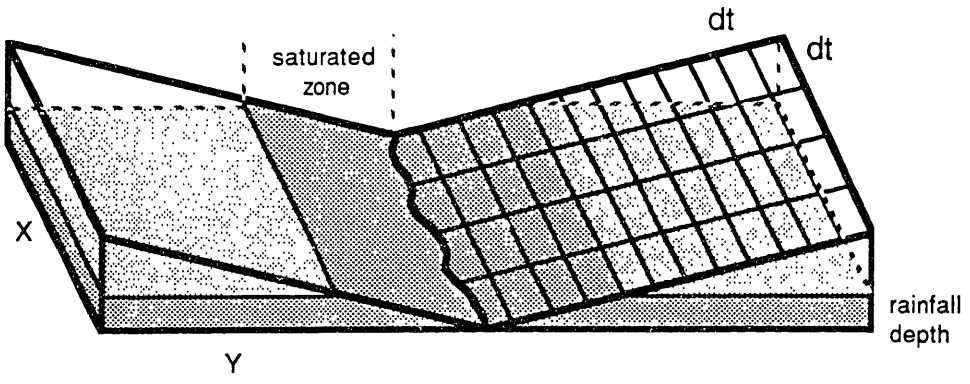

Fig. 3-13. Schematic of model stream element representation.

distance to the stream. Thus, even for a grid spacing of 5 km, the hillslope width will be on the order of a few hundred meters, while the length of the stream will be on the order of the grid spacing. In the model, these distances are expressed in time steps (dt). The response of each stream element is in this case trapezoidal.

The width of the saturated zone is determined for each grid element by considering the ratio of the rainfall depth to the saturation deficit (shown schematically by the height of the wedge). As mentioned in the previous section, the saturation deficit is assumed to increase linearly with distance from the stream, and the stream element provides the sub-gridscale representation of this. Knowing the fraction of the element that is saturated, the rainfall is partitioned into overland and subsurface flows. For the model results presented in the next section, the entire basin was forced to be subsaturated throughout the storm.

Hillslope elements are modelled in a similar fashion, although the x dimension is not considered; all runoff from the element has the same stream travel time. The hydrograph response for each grid square is a rectangle with a time base given by the difference between the closest and farthest points to the stream. The rectangular pulse is centered on the mean travel time to the gauge. Saturation occurs when the soil moisture deficit is exceeded by the rainfall depth.

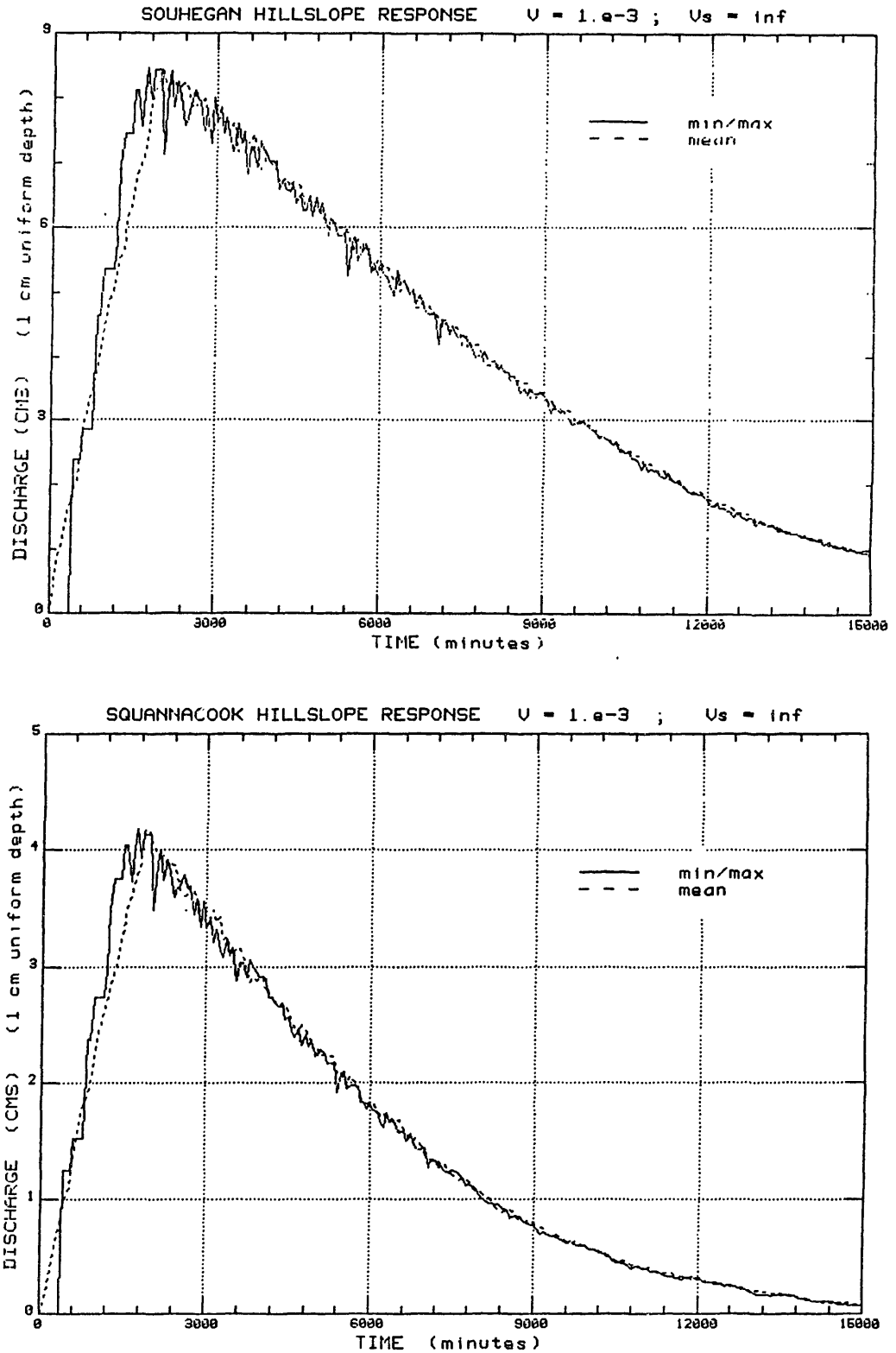

Fig. 3-14. Response of model hillslope elements to uniform rainfall depth. Model stream elements have been suppressed. Grid spacing is 100 meters; time step 10 minutes.

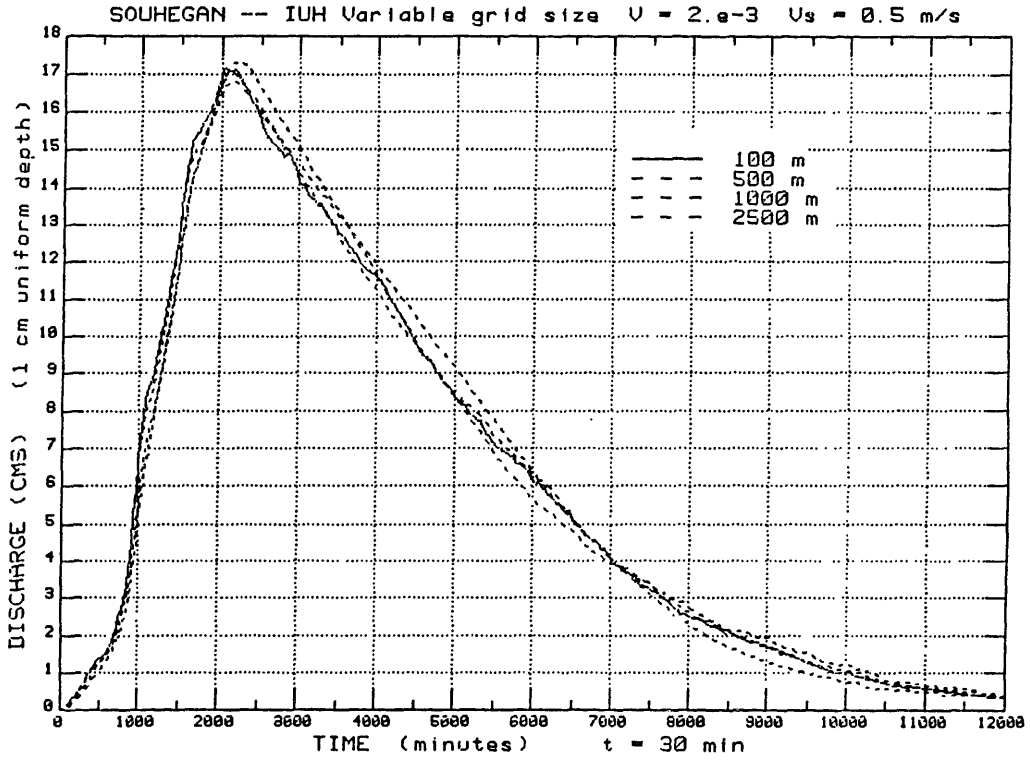

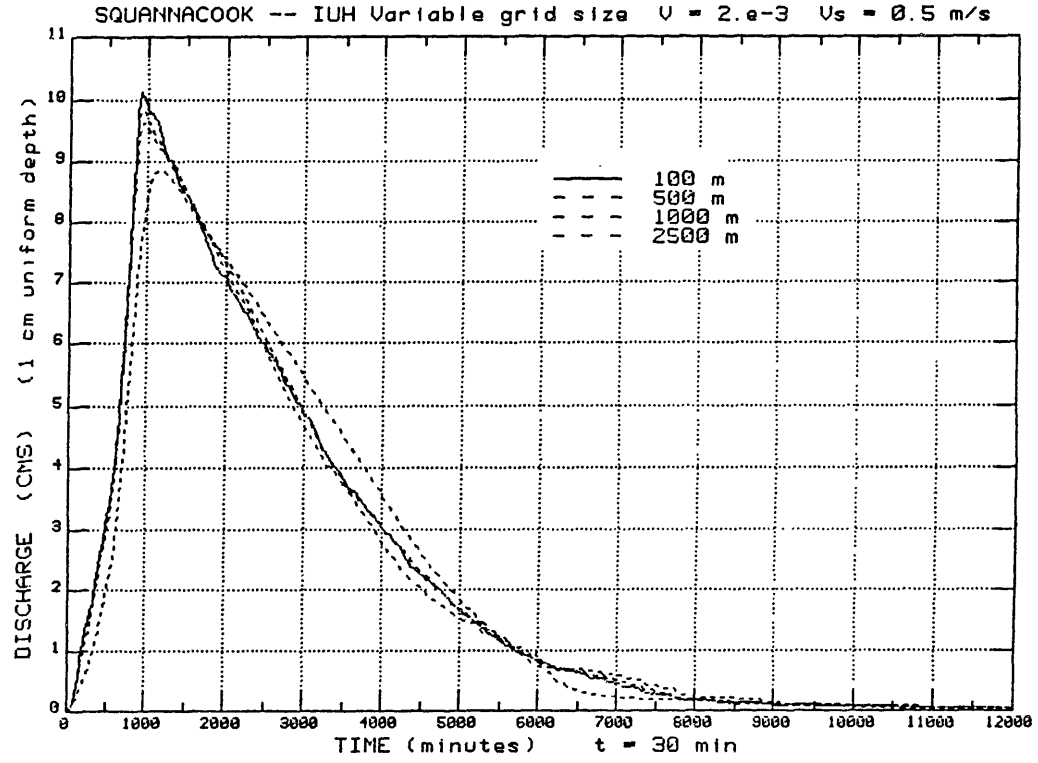

Fig. 3-15. Variable model grid spacing (100 - 2500 meters) for Souhegan (above), and Squannacook (below).

Difficulties arise in ensuring a smooth transition between the stream elements and the hillslope elements. If sufficient care is not taken in this regard, the basin hillslope response will not increase smoothly to zero (as required by the analysis in Section 2.2h). The maximum in the function will result in a spurious hydrograph peak with a lag corresponding to the grid spacing. Fig. 3-14 shows the basin response for the hillslope elements only (runoff from the stream elements having been suppressed). Two curves are shown: the solid curve considers the dimension of each hillslope element to be variable, with the width given by the difference between the maximum and minimum distances to the stream (calculated from the 25 meter grid); the dashed curve assumes a constant width, determined as the mean for all hillslope elements in the basin. The latter result was selected, as it exhibits smaller numerical fluctuations. With an infinite streamflow velocity, these figures represent the hillslope response, and we anticipate that the function should be continued smoothly to the y axis when the response of the stream elements is added.

As mentioned above, the most satisfactory means of doing so involves the assumption that the response of each stream element is triangular rather than rectangular. This corresponds to depicting the hypothetical stream as traversing the stream element diagonally. There is, in reality, a greater probability for this configuration than for the rectangular representation; if there is more than one stream within the stream element, this will almost certainly be the case. Fig. 3.2 has already illustrated the resulting response function when the triangular stream element contributions are included. The transition between the stream elements and hillslope elements is sufficiently smooth for the model operation. It is assisted by allowing the addition of a random fraction of 25 meters to the width of the triangle (to account for the 25 meter grid used in calculating this distance). The fluctuations that remain disappear when the streamflow lag is introduced with moderate smoothing by dispersion.

The triangular representation of the stream elements retains consistency even for extremely large grid spacing. With a single stream element covering the entire basin, a triangular hydrograph results: the time to peak is given correctly as the mean travel time to the gauge, while the base of the hydrograph corresponds to the time of concentration of the basin, in this case, twice the mean travel time to the stream plus the longest travel time in the stream.

Fig. 3-15 depicts the total basin response for typical values of the stream and subsurface velocities (0.5 ms^{-1} and 2 x 10^{-3} ms^{-1} respectively). The

success of the variable grid algorithm is clearly evident. Even with a grid spacing of 2500 meters (only 30 elements over the Squannacook) the resulting hydrograph differs by less than 10% from the result generated by the most detailed version of the model operating at 100 meters. Fig. 3-27 provides an example of a model run with varying model grid spacing and time steps.

Model operation is straightforward, with separate grids generated for stream transit times and subsurface travel times (and for the widths of grid elements in time steps), the rainfall field and for soil moisture. Each grid element with measurable rainfall within the basin (grid elements on the edge of the basin are scaled by the fraction of area internal to the basin) is considered in turn. Separate algorithms are used to sum each contribution to the hydrograph according to the nature of the grid element (stream or hillslope), and whether or not the grid element is saturated (stream elements may contribute overland flow from saturated zones as well as subsurface flow, if this feature is operating).

After the entire rainfall grid has been processed, the time series is smoothed by the dispersion algorithm. The value at each time step is spread by a unit triangular pulse whose width varies linearly with time (c.f., Section 3.1d). For efficiency, the triangular pulse representation is stored as a lookup table, which is also used for the triangular stream element representation. The resulting instantaneous hydrograph is added, with a lag of one time step, to the cumulative forecast hydrograph. The time series is stored as a floating point vector, since the computer is equipped with a floating point co-processor, and floating point numbers are the same length as integers. Truncation errors are thus kept to a minimum; differences between the input rainfall volume and the volume of the output hydrograph amount to only a fraction of a percent.

3.3 MODEL RESULTS

Preliminary model results are presented here in the form of case studies for several storms over the Souhegan and Squannacook basins. The primary intention of this section is to demonstrate the value of the radar data for hydrologic applications. No attempt has been made to "fine tune" the model to fit all of the observed features of the flood hydrographs. Instead, the simplest version of the model is used, employing only two controlling parameters (the subsurface and stream velocities), and the volume of the runoff associated with the hydrograph is scaled linearly. Storm hydrographs are separated from the streamflow record by the method described in section 2.1c: an exponential curve with an e–folding of 3 days (c.f. Fig. 2-16) is fit to the immediately preceding hydrograph recession and subtracted from the streamflow peak of interest; an example of this is shown in Fig. 3-29. Errors associated with this separation method are estimated to be less than 5% in the rising limb, and less than 10% in the recession of the separated hydrograph (to 100 hours). In graphs comparing the model results to the streamgauge data, the observed time series is plotted (dashed line) so as to include the rise resulting from the next rainfall event (not modelled).

Different features of the model response are discussed in each of the case studies for the purposes of illustration, as a lack of data of all kinds for all cases prevents a more systematic comparison of each aspect of the modelling study. For example, for some storms a comparison between the response of the two basins is not possible, as the streamgauge data for one of the rivers were not available. The cases include all of the storms considered thus far, and are not simply a subset presented in support of the model. Despite an archive of several years of radar data, discouragingly few cases were available with complete coverage of the storm over the basins at intervals of 10 minutes or better; the MIT radar is operated for research purposes, and does not scan 24 hours a day, as it would in an operational context.

The majority of cases correspond to summer storms (1987 in particular), for which adequate radar coverage and improved resolution streamgauge data for the Souhegan were available. Comparisons for a few events from other seasons are also included. Unfortunately, data were not available to test the model under extreme flood conditions, and the cases considered here correspond to streamflow peaks of only moderate amplitude.

a) Case Studies: i) June 27, 1987

During the summer of 1987, several cases of widespread frontal and pre-frontal rain with associated convection produced significant hydrograph peaks. The period of record from June through August is depicted in Fig. 3-16 which shows the Souhegan and Squannacook gauge records, as well as a comparison of the two (Squannacook scaled by the ratio of basin areas). Referring to the annual records in Fig. 2-15, it is obvious that these streamflow peaks are an order of magnitude smaller than the spring flood of the same year, yet their characteristics are typical of streamflow rises produced by isolated rainfall events. Radar data are available for the period from the end of June to the beginning of July. We shall examine here the two latter peaks of the set of three hydrograph rises depicted in Fig. 3-17.

Figure 3.18 shows a PPI scan typical of those recorded during the storm, with peak reflectivities near 35 dBZ. The bold curves in Fig. 3-19 depict the average rainfall rates over the two basins as determined by the radar ($Z = 230R^{1.4}$) for the 12 hour period beginning at 1:05 EST on June 27th (c.f. Fig. 1-15). The time series exhibits three peaks in the rainfall: the first is associated with an isolated thunderstorm moving rapidly northward (15 ms^{-1})

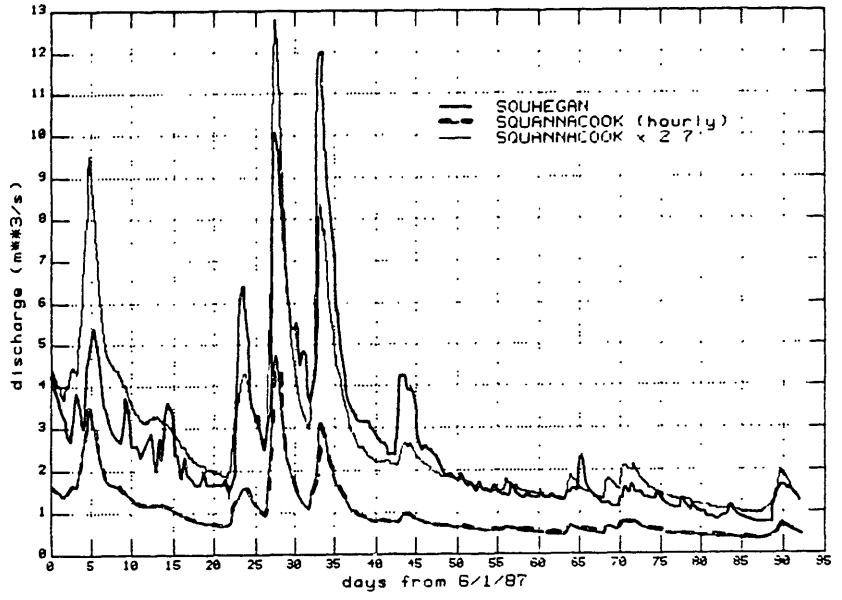

Fig. 3-16. Streamgauge records (summer 1987). Time series of discharge measurements at Souhegan and Squannacook gauges over the period June 1 through August 31 1987. Souhegan data shown as heavy line, Squannacook data as heavy dashed. Squannacook data scaled by the ratio of the basin areas (2.7) for comparison with the Souhegan is plotted as a light line.

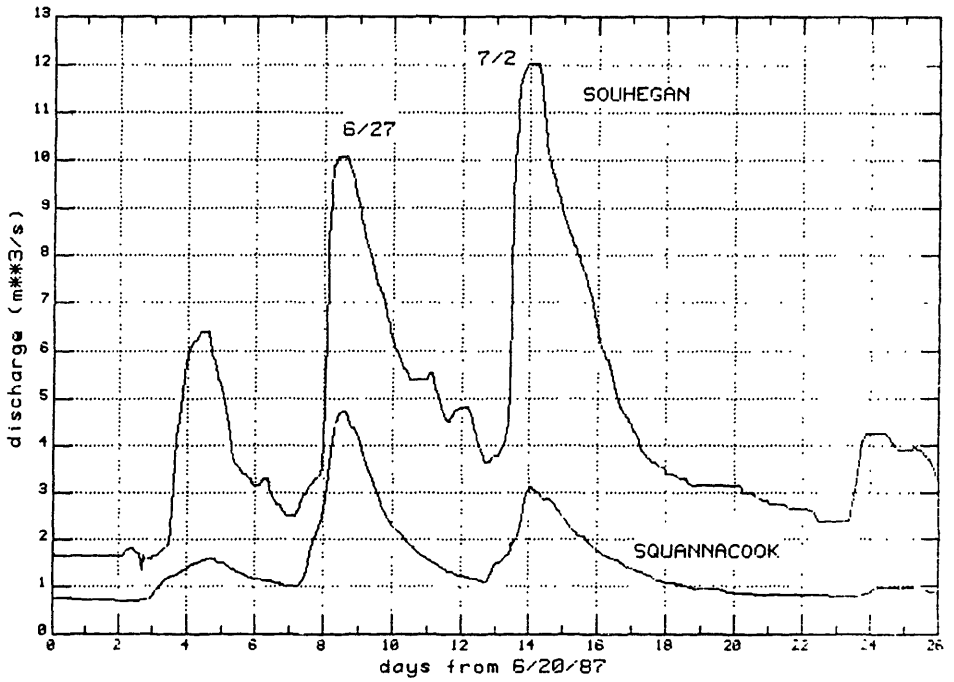

Fig. 3-17. Hydrographs 20 June through 5 July, 1987. Souhegan and Squannacook discharge records plotted in cubic meters per second.

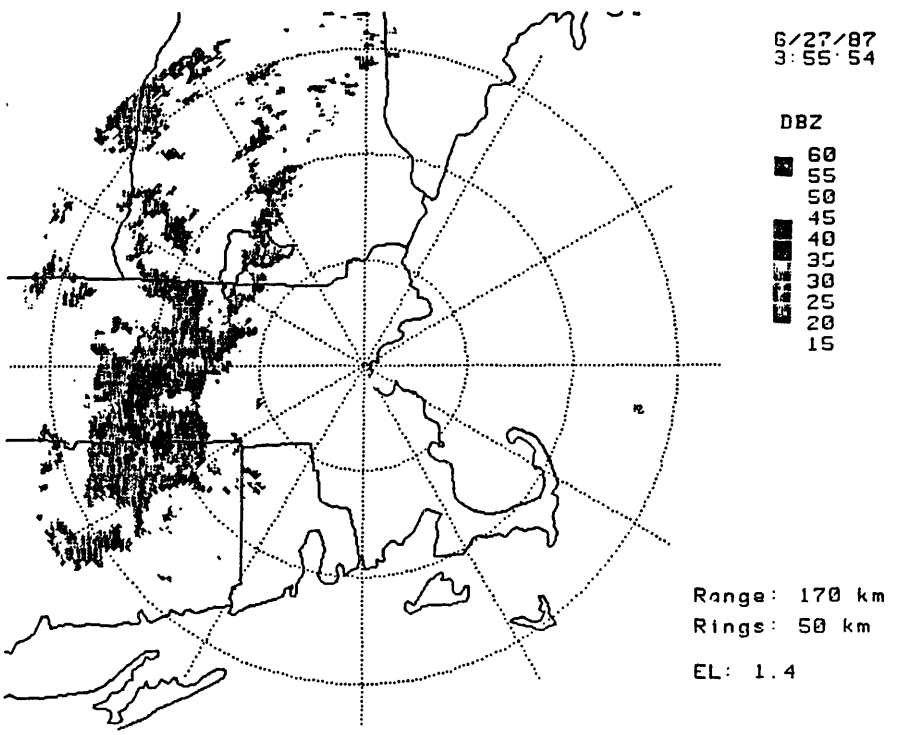

Fig. 3-18. PPI radar scan June 27, 1987 3:55 EST depicting typical rainfall pattern.

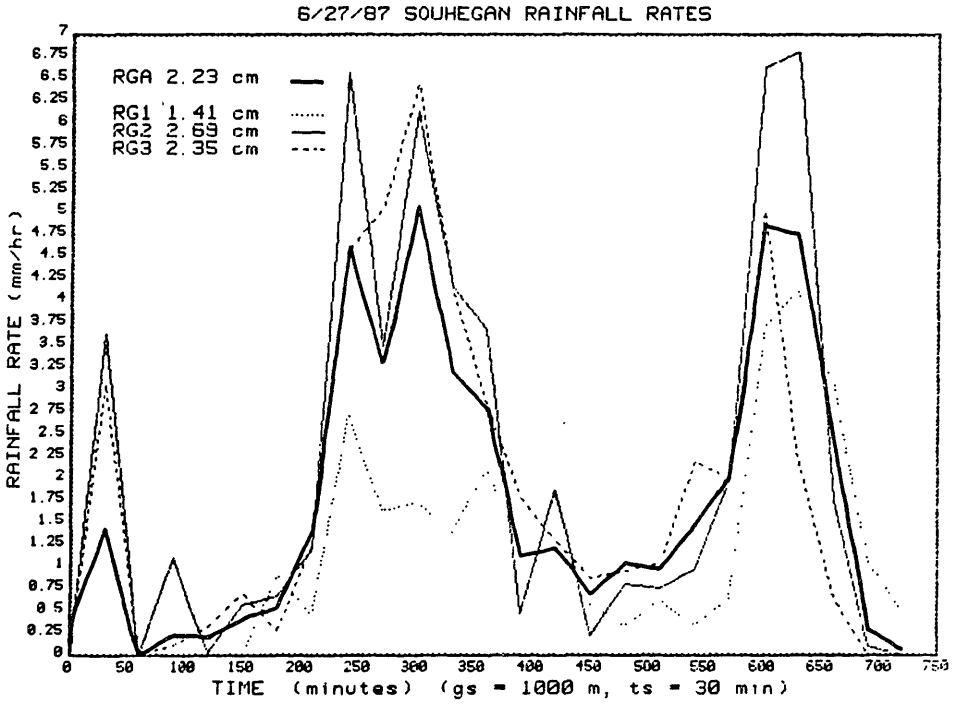

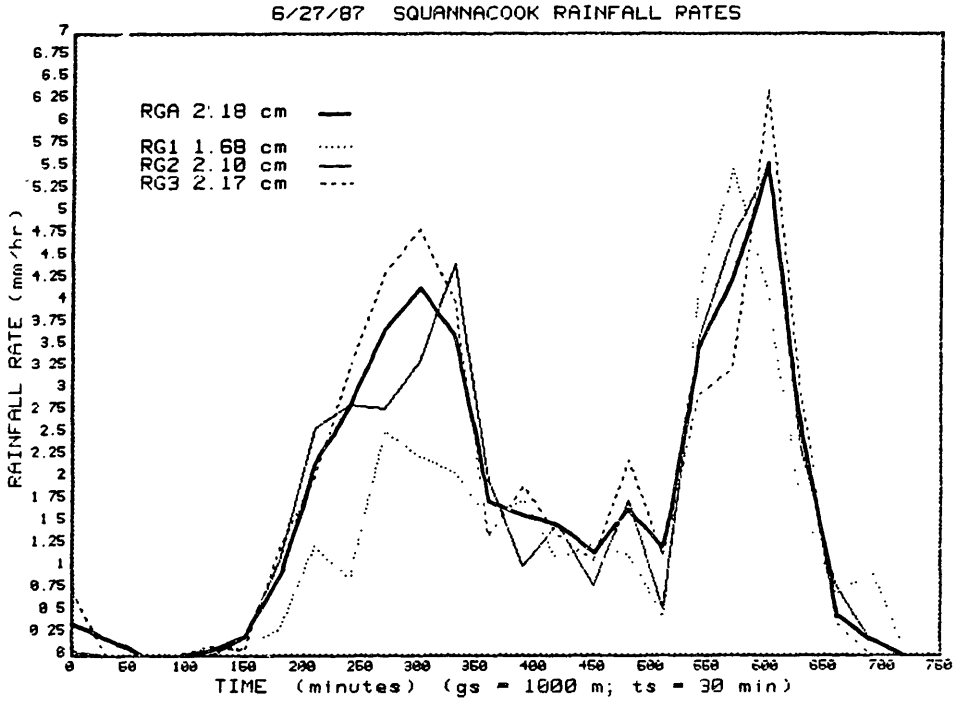

Fig. 3-19. Rainfall rates June 27, 1987. Bold lines (RGA) represent areal average rainfall rates over the Souhegan (a) and Squannacook (b) as determined by the radar. Total rainfall depth is indicated in the legend. The other three curves correspond to the rainfall rate measured by the radar at selected sites in each basin (c.f., Fig. 3-20).

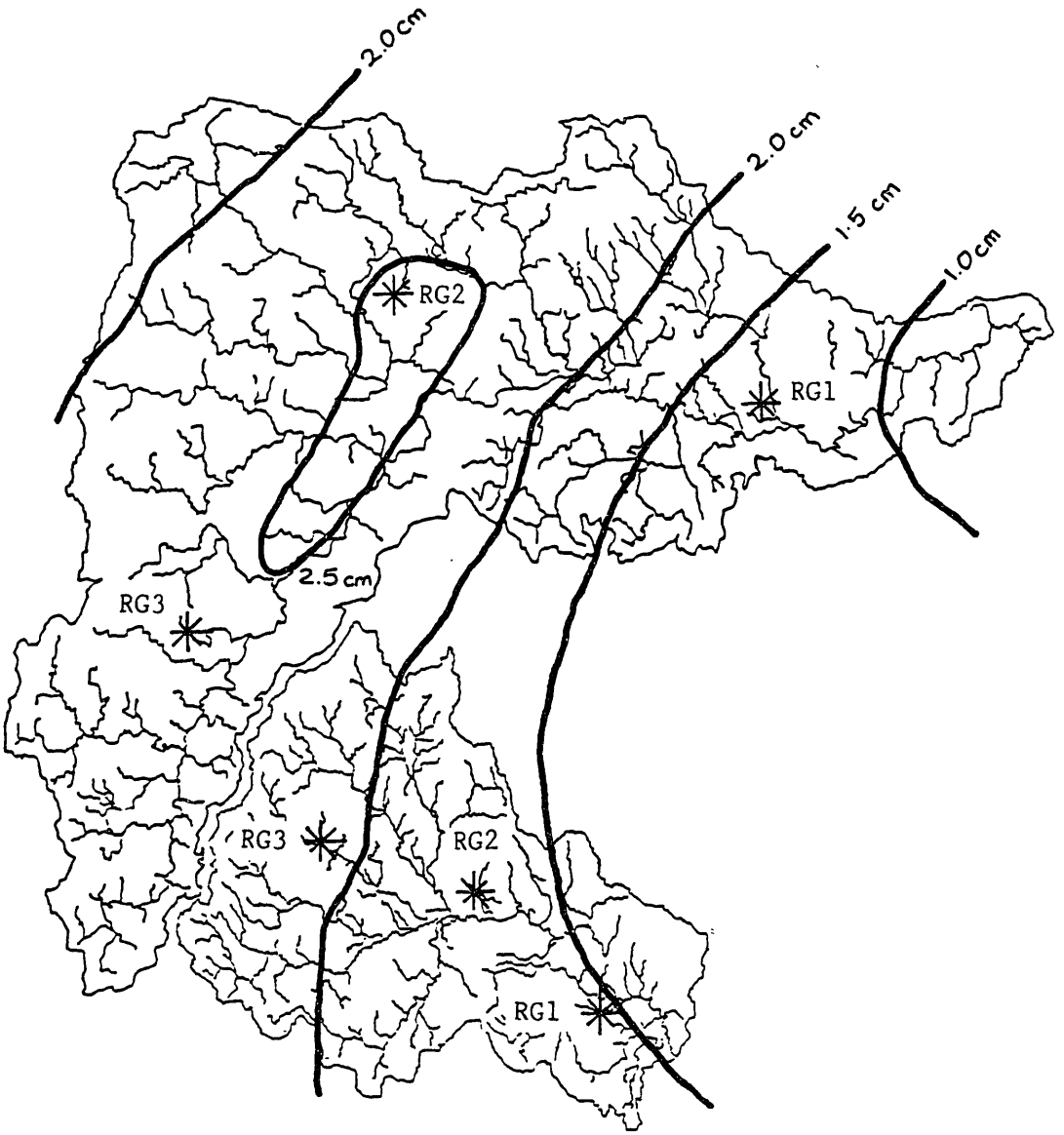

Fig. 3-20. Isohyetal map June 27, 1987. Contours of equal rainfall depth (cm), as determined by radar. Locations of "raingauge" sites in each basin (RG1, 2, and 3) indicated by asterisks.

over the western half of the Souhegan; the latter two peaks correspond to nearly complete coverage of the basin by rain of moderate intensity. Despite the strong reflectivities associated with the thunderstorm, the overall contribution to the total rainfall depth is small, due to the limited fraction of the basin area involved (roughly one fourth), and due to the rapid translational velocity of the storm. In this, as in most of the cases observed, significant streamflow generally results only from significant areal coverage of the basin by rainfall.

The thunderstorm did not affect the Squannacook, yet the total rainfall depths observed over the two basins are nearly equal: 2.23 cm (3.6×10^6 m^3 over the Squannacook) versus 2.18 cm (9.7×10^6 m^3 over the Souhegan). There is however, a considerable gradient in the storm isohyets of more than a factor of two from east to west across the basins, as depicted in Fig 3-20.

In addition to the areal average rainfall rates, Fig. 3-19 also shows the radar rainfall rate at three selected locations in each basin. Lacking time resolved data from real raingauges, comparisons between the areal average of the radar rainfall rates and rates recorded at these points will provide some indication of sampling differences between radar and raingauge measurements. The locations of these "raingauges" are indicated in Fig. 3-20. In the Souhegan, the three sites are spaced at 13 km intervals; in the Squannacook, at 6 km intervals. The rainfall time series were accumulated over half hour intervals using a 1 km grid.

Total storm depths at the raingauge sites are noted in Fig. 3-19. In both basins, significant differences are observed between the areal average storm depth and the depths measured at individual gauges, particularly at the easternmost sites. Two comparisons are possible with the areal mean values: the average of the three sites, and the single gauge located near the center of the basin. For the Souhegan, the total depth at the single site (RG2, 2.69 cm) differs by more than 20% from the areal mean, while the average of the three sites (2.15 cm) is within 5%. For the Souhegan, by chance, the average of the three sites (1.98 cm, within 10% of the areal mean) is actually not as close to the areal average as the single gauge located in the center of the basin (RG2), which measured 2.10 cm.

Model forecasts for the streamflow are plotted against the observed hydrographs for the two basins in Fig. 3-21. The parameters used are the same

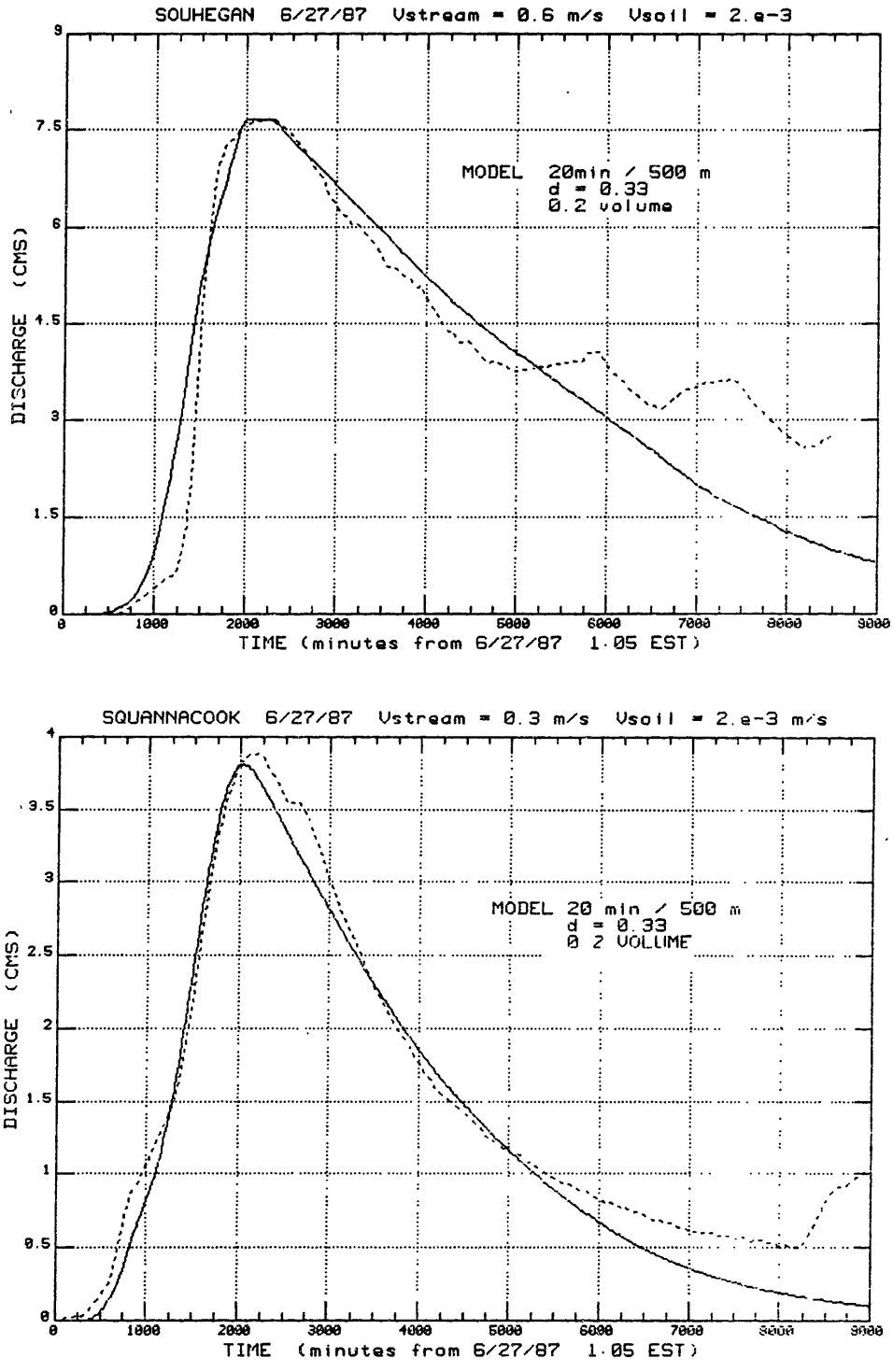

Fig. 3-21. Model results June 27, 1987. Comparison of model results and discharge data for the Souhegan (a) and for the Squannacook (b). In this and subsequent plots the model output is drawn as a solid line, and the gauge data is drawn as a dashed line. V_{stream} and V_{soil} identify the stream and subsurface flow velocities (ms^{-1}) used in the model, and the value of the dispersion parameter (d) is noted. Also indicated are the model time step (minutes) and grid spacing (meters) employed in the model run. The volume scale factor is written as a decimal fraction.

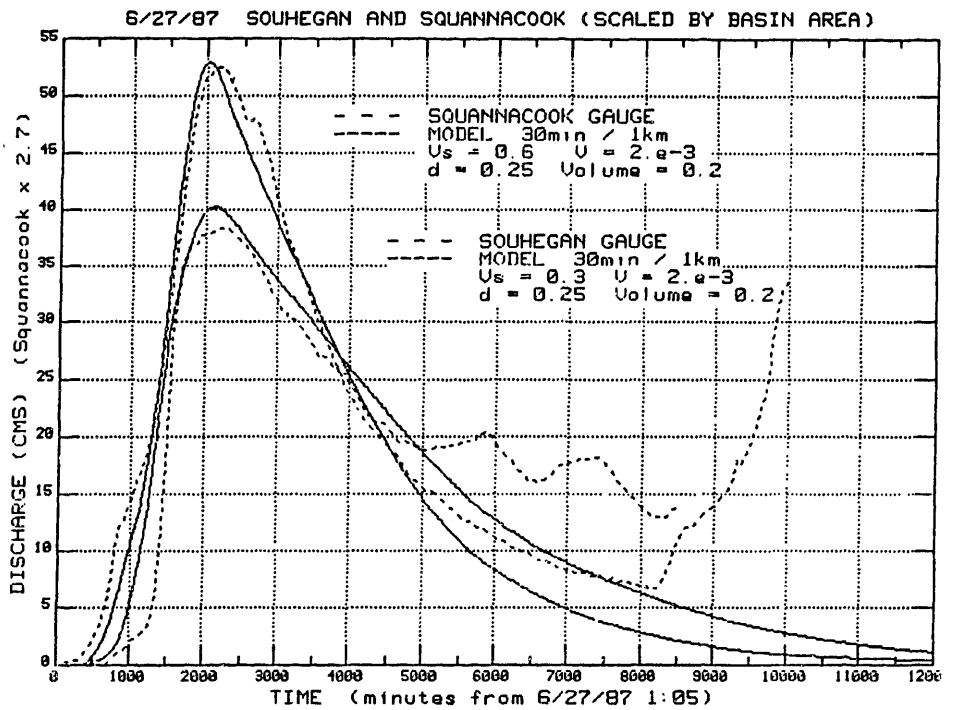

Fig. 3-22. Model results June 27, 1987. As in Fig. 3-21, with Squannacook results and data scaled by the ratio of the basin areas (2.7), for comparison.

for the two basins, with the exception of the streamflow velocity (0.6 ms^{-1} in the Souhegan; 0.3 ms^{-1} for the Squannacook). The discharge volumes associated with the forecast hydrographs for both basins are scaled by a factor of 0.2, i.e. 20% of the rainfall contributes to storm runoff. Consulting Fig. 2-14, it is clear that this fraction (reflecting storage in the soil and subsequent evapotranspiration or percolation to the groundwater) is entirely consistent with typical rainfall-runoff ratios for the summer months (e.g. 18% for the July climatological mean). Figure 3.22 presents, for comparison, the same model results for the two basins (with somewhat coarser spatial and temporal resolution of the model).

Clearly there are shortcomings in the accurate modelling of the basin response, but the basic character of the hydrographs is accounted for by the simple model. By incorporating the geometry of the stream network, the model, with two parameters, is capable of explaining most of the variance of a function which would require at least three parameters to describe by fitting the moments of the distribution.

ii) July 2, 1987

This streamflow peak (c.f. Fig. 3-17) resulted from widespread rain (peak: 35 dBZ) on the afternoon of the 2nd of July (Fig. 3-23). Movement of cells was from the west, with a north/south gradient in the precipitation pattern. Total rainfall depth over the Souhegan was measured as 2.0 cm; 1.6 cm over the Squannacook ($Z = 230R^{1.4}$), as plotted in Fig. 3-24. Model results for the Souhegan are presented in Fig. 3-25. Using the same parameters as in the previous storm, the model shows excellent agreement with the data. The volume scale factor (28 %) is somewhat greater than in the previous case (20%). This result was anticipated, as the July 2 hydrograph begins from a higher initial discharge on the recession of the previous peak, a possible indicator of more moist soil conditions in the basin.

Applying the same model parameters to the Squannacook, however, yields a considerable overestimate of the peak discharge (Fig. 3-26a). For reasons that are not understood at this time, the recession of the model hydrograph appears much too rapid.

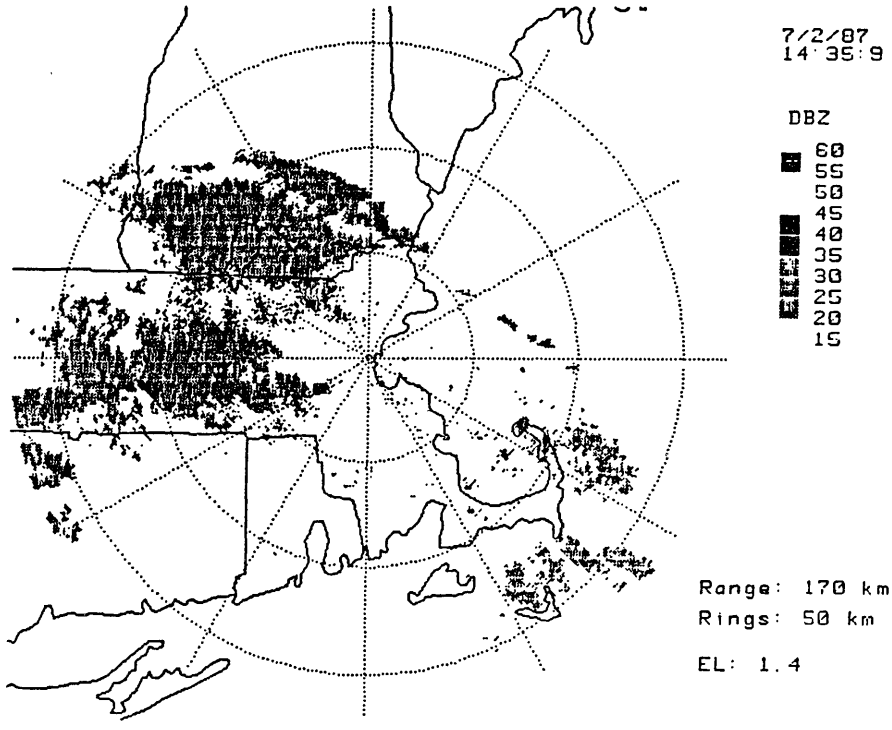

Fig. 3-23. Radar scan depicting typical rainfall pattern for the July 2, 1987 storm.

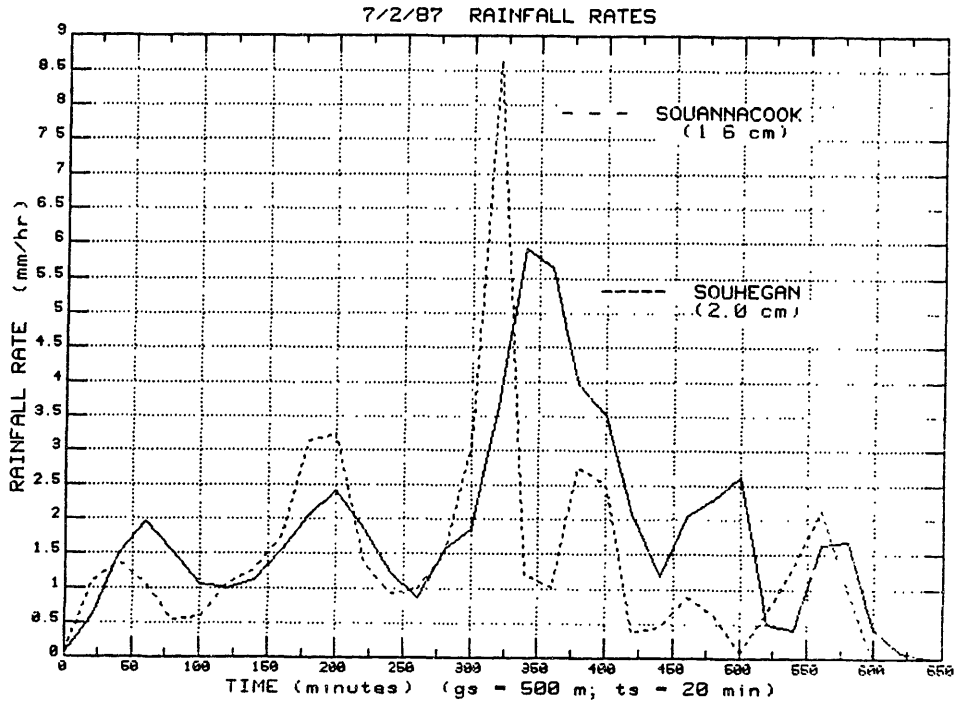

Fig. 3-24 Basin average rainfall rates for the Souhegan and Squannacook during the course of the storm (10 hours beginning at 13:24 EST 7/2/87). Total storm depths are indicated in parentheses.

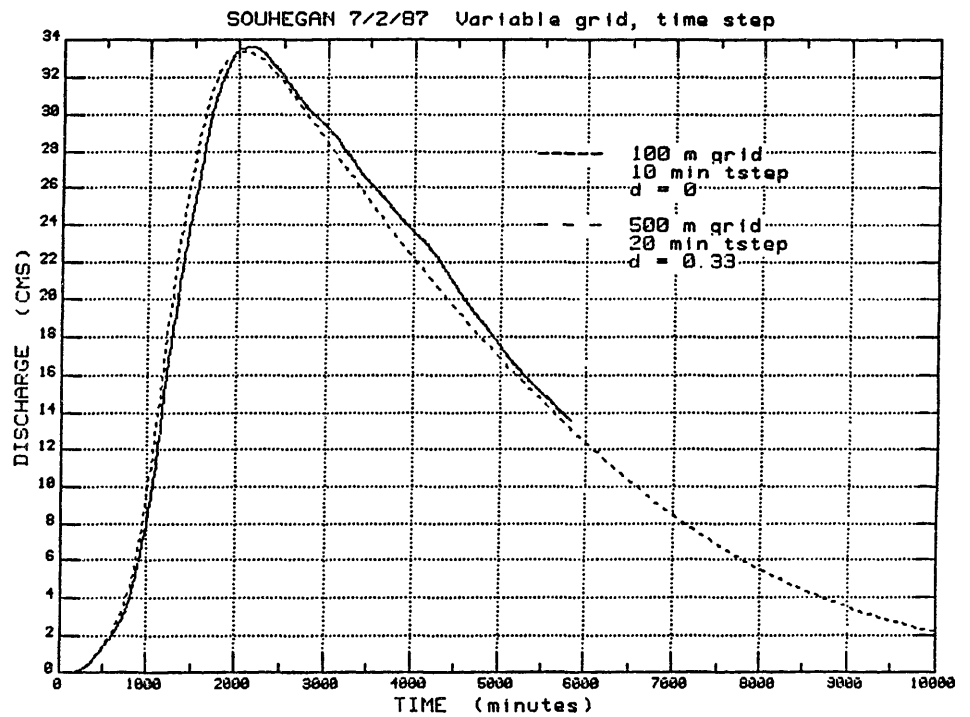

Fig. 3-25. Souhegan model result July 2, 1987.

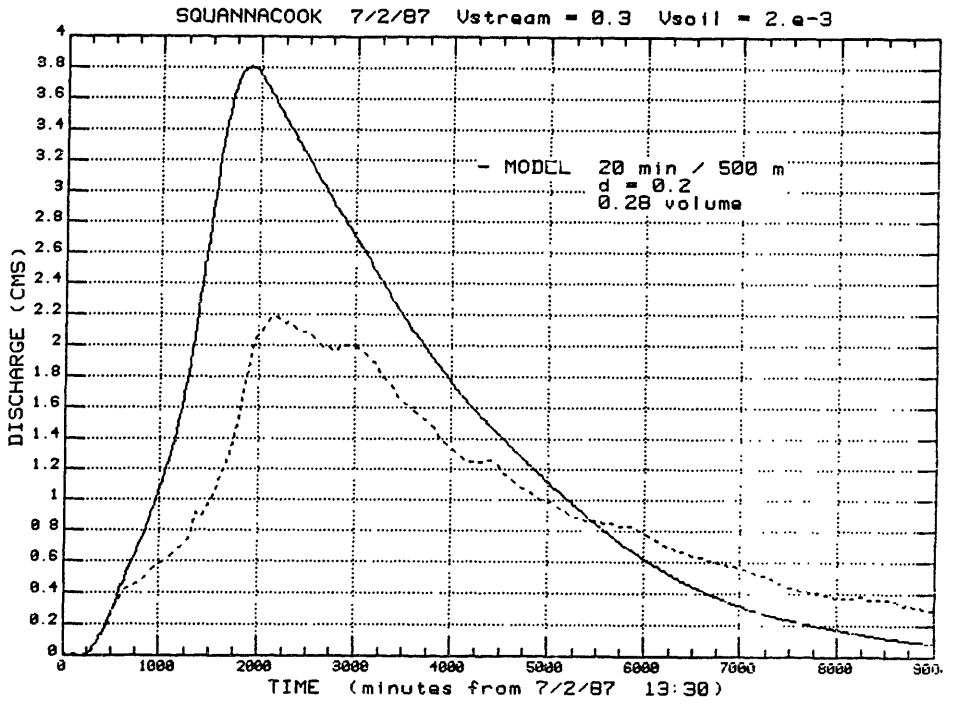

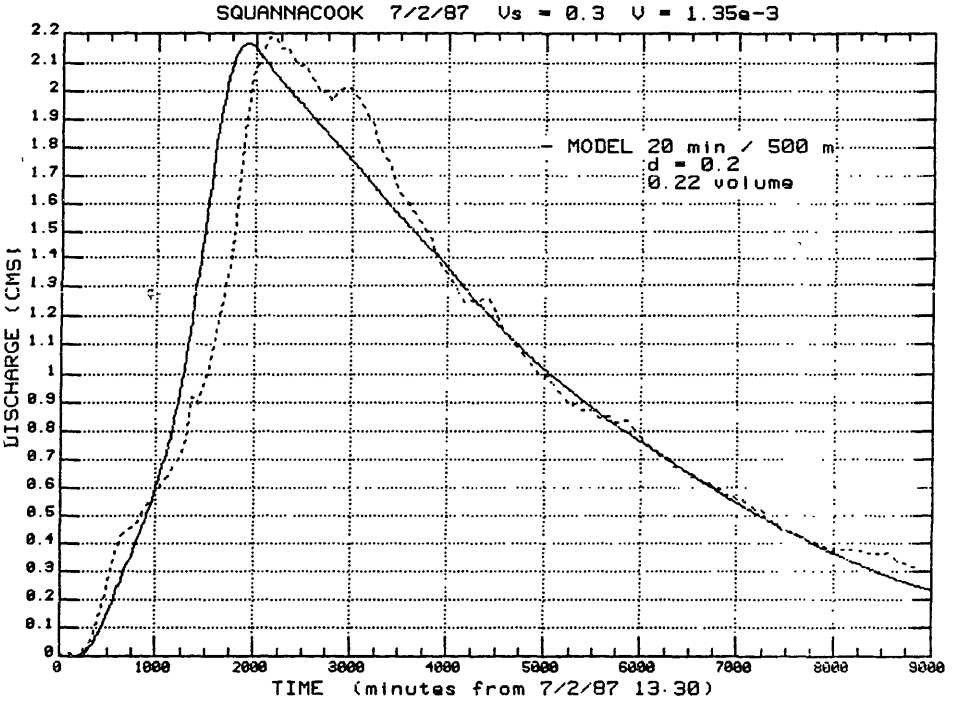

Fig. 3-26. Squannacook model result July 2, 1987.
a) $V_{soil} = 2 \times 10^{-3}$ ms^{-1}; volume scale factor 28 %.
b) $V_{soil} = 1.35 \times 10^{-3}$ ms^{-1}; volume scale factor 22 %.

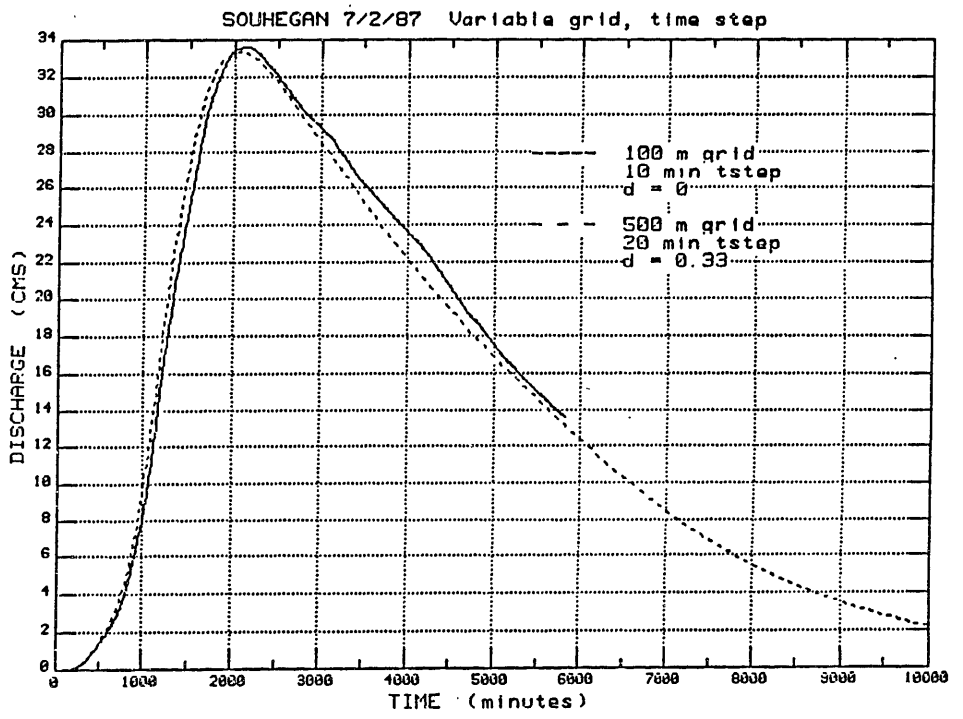

Fig. 3-27. Variable grid and time steps. Model results for the Souhegan July 2, 1987 case with different model grid spacings, time steps and dispersion parameters.

In order to compare the volumes of the hydrographs, the parameter V_{soil} was set to 1.35 x 10^{-3} ms^{-1}, (instead of 2 x 10^{-3} ms^{-1}), which produced a much closer fit to the observed data (Fig. 3-26b). In this case the volume scale factor is 22%. Again, this result is consistent with more moist conditions over the Squannacook during the second storm. For this and the previous case for the Squannacook, using a streamflow velocity of 0.25 ms^{-1}, (instead of 0.3 ms^{-1}), would yield an even more accurate representation of the hydrograph peaks.

For the sake of interest, Fig. 3-27 shows a comparison of model results for the Souhegan using different model configurations. This figure demonstrates the success of the variable grid spacing and time step scheme (with the grid spacing varying from 100 to 500 meters, and the time step varying from 10 to 20 minutes), as well as the insensitivity of the model results to the smoothing (for no dispersion and for d = 0.33). The run using the10 minute time step is truncated at 100 hours because of limitations to the length of the model time series. Because of this, most of the model results are presented for 20 minute time steps in order to include the full hydrograph recession.

iii) June 16, 1986

The PPI display in Fig. 3-28 depicts an intense squall line system over New England, with peak reflectivities above 50 dBZ. The system crossed the Souhegan basin from northwest to southeast in little over one hour. Despite heavy rain, rapid translation of the system limited the total rainfall depth to 0.52 cm, producing only a small rise in the streamflow (indicated by the arrow in Fig. 3-29). The Z-R relation used was $Z = 400R^{1.3}$, suitable for thunderstorms, (c.f. Section 1.2; Austin, 1987). Fig. 3-29 also shows (heavy dashed line), the exponential recession used for hydrograph separation. The separated stream-flow peak is presented in Fig. 3-30 (dashed), along with the model forecast. The volume scale factor, which yields reasonable agreement between the model and data, is 23 %, i.e. within the standard deviation of the climatological mean for June (53 %, σ = 35% ; Fig. 2-14).

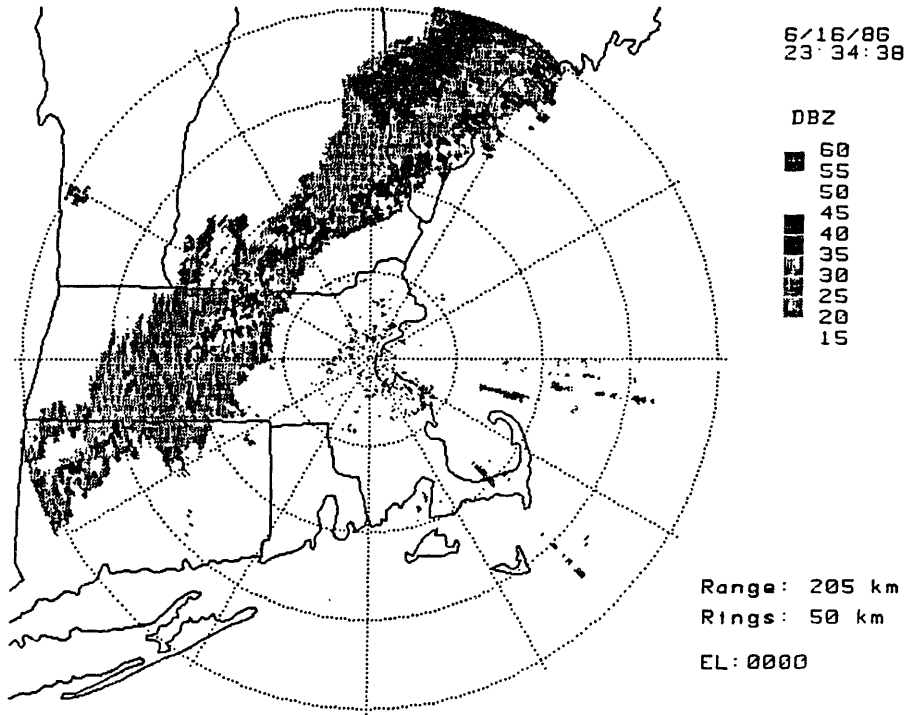

Fig. 3-28. PPI radar scan June 16, 1986 23:34 EST.for squall line over New England.

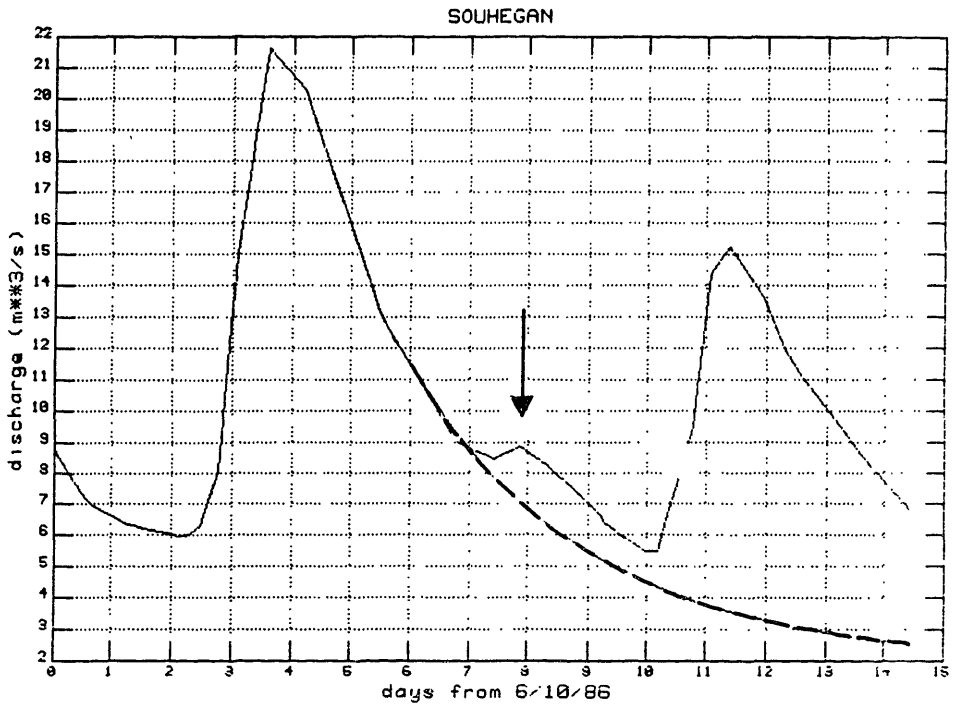

Fig. 3-29. Souhegan streamflow record. Hydrographs for the period June 10 to June 25 1986. Arrow indicates peak for June 16 squall line case. Exponential recession (3 day e-fold) used for hydrograph separation is shown as heavy dashed line.

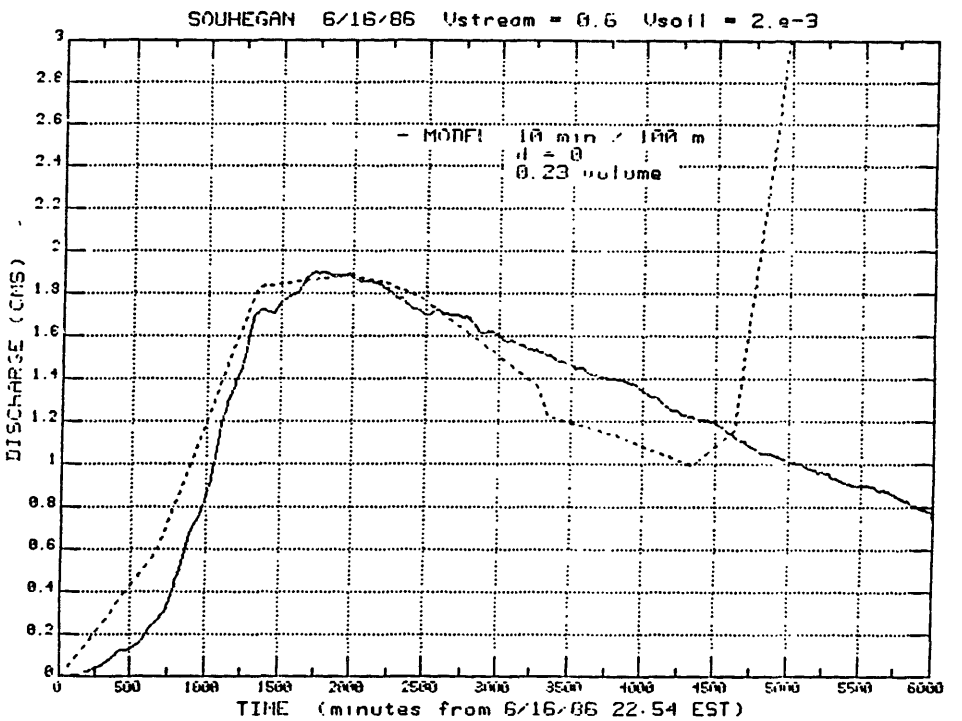

Fig. 3-30. Souhegan model result June 16, 1986.

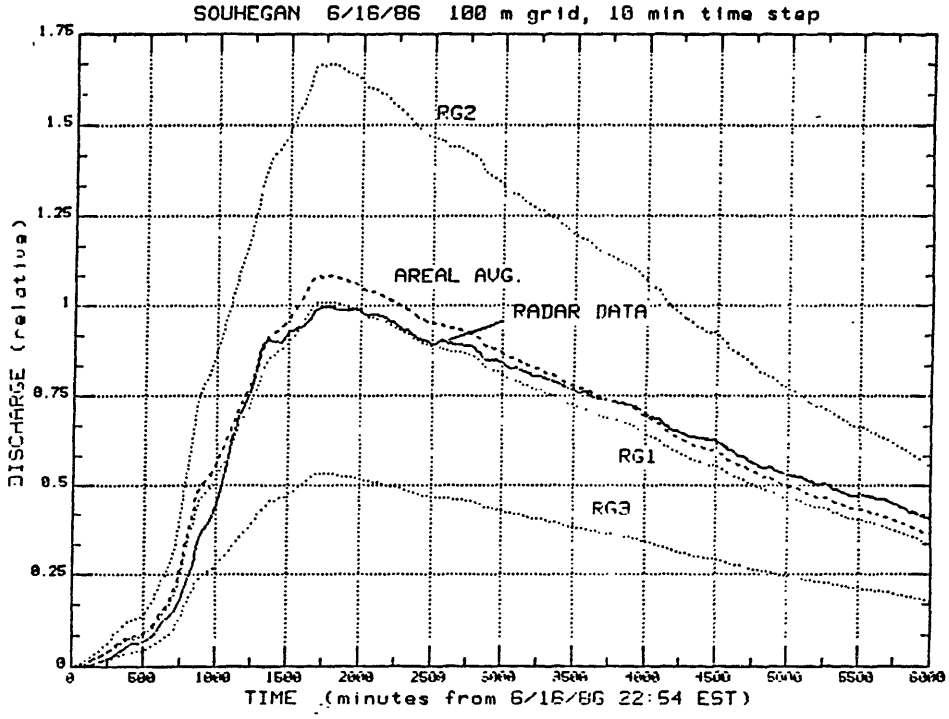

Fig. 3-31. Distributed radar data versus areal average radar data. Solid curve labelled "radar data" is the model result of Fig. 3-30. Dashed curve ("areal avg.") corresponds to model run with uniform rainfall inputs given by the basin average rainfall rate. Dotted curves result from uniform rainfall inputs determined from radar rainfall rates at sites in Fig. 3-20. Vertical scale is discharge relative to peak of "radar data" curve.

Fig. 3-31 considers the effects on the model hydrograph when radar data averaged over the basin are used instead of the spatially distributed data. The curve labelled "RADAR DATA" is the model hydrograph in Fig. 3-30. The uniform rainfall case (labelled "AREAL AVG" in Fig. 3-31) is shown to be in close agreement with the distributed model result. The model operating with uniform radar data corresponds to the unit hydrograph method of forecasting. Clearly, even for this squall line case which exhibits large spatial gradients in the rainfall rate (c.f., Fig. 3-12), the basin response is relatively insensitive to the motion of the storm and the tracks of individual cells. This is a consequence of the control which the subsurface flow exerts on the basin response. The curves labelled RG1, 2 and 3 represent the basin response to uniform rainfall inputs given by the rainrates measured at the "raingauge" sites shown in Fig. 3.20. Peak flow rates vary by more than 50 % for the three curves, with site RG1 fortuitously in agreement with the hydrograph for the distributed rainfall data.

iv) September 30, 1987

All of the previous cases considered storms occurring during the summer months. In order to assess the performance of the radar relative to the known seasonal variations in the rainfall-runoff ratio (Fig. 2-14), cases from other months of the year must be examined.

Fig. 3-32 shows the PPI display at 13:21 on September 30th, 1987 (peak reflectivity: 40 dBZ). A series of convective elements embedded in more widespread precipitation moved northeastward over the basin during a six hour period. A total rainfall depth of 1.2 cm was recorded over the Souhegan ($Z = 230R^{1.4}$), nearly uniformly distributed over the basin. However, when the stream gauge record for the Souhegan was examined a few days later, the extremely small amplitude of the hydrograph peak was astounding (Fig. 3-33). Fig. 3-34 shows the model result, using the previously successful parameters, compared with the observed hydrograph. No simple scaling of the amplitude will produce a resemblance to the observed hydrograph. The model determination of the time to peak is too early, and the recession is too shallow. A volume scale factor of 3% is required to equate the rainfall volume to the observed runoff.

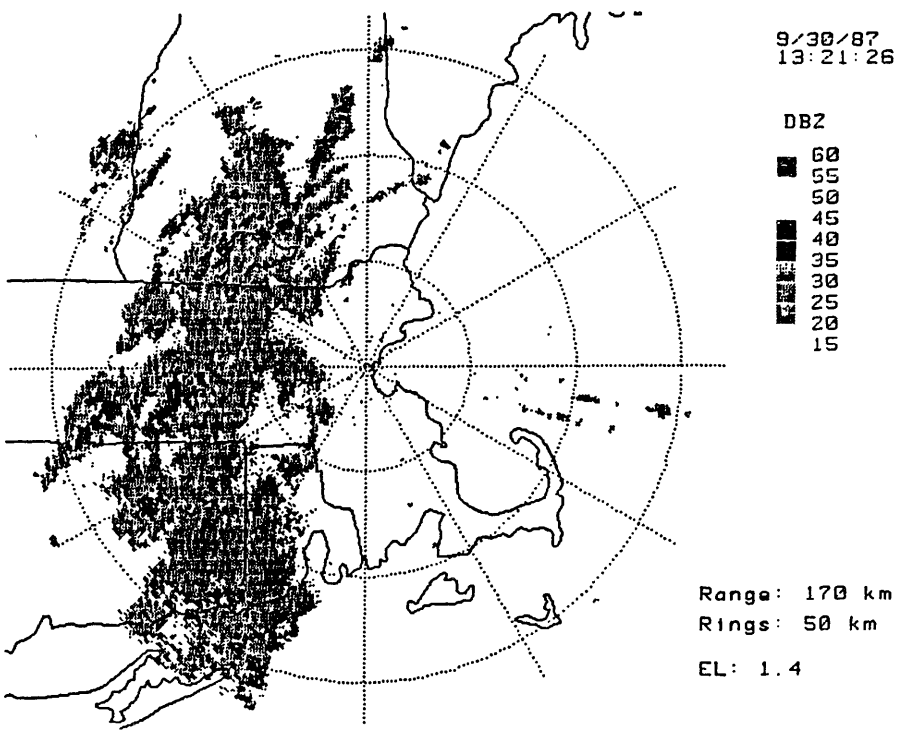

Fig. 3-32. PPI radar scan September 30, 1987 13:21 EST.

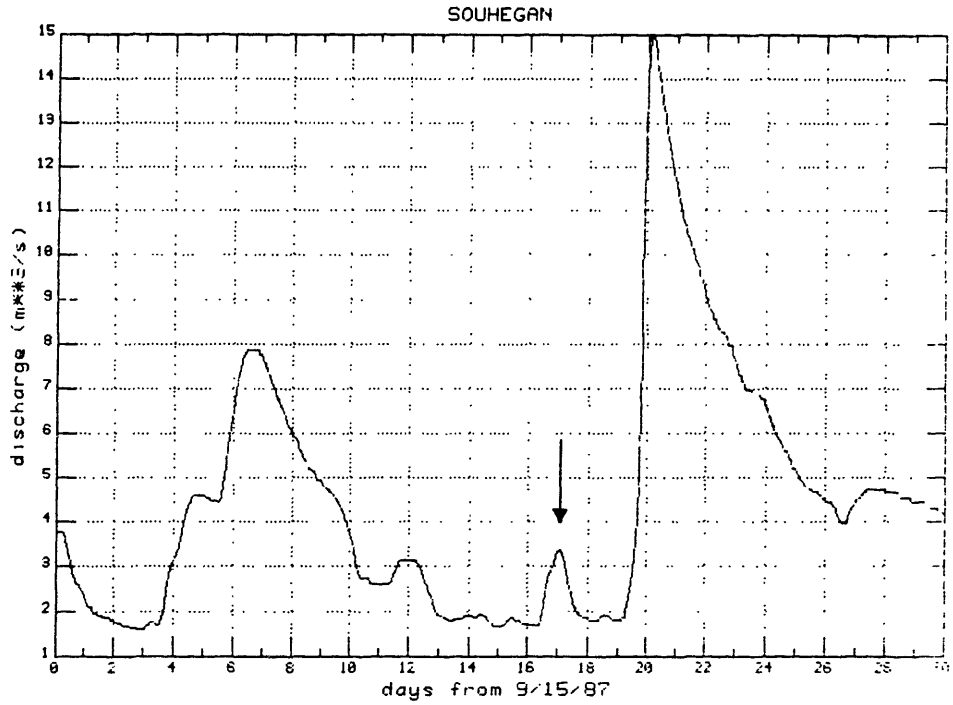

Fig. 3-33. Streamgauge record for the Souhegan, September 1987. Hydrograph for 9/30/87 case is indicated by arrow.

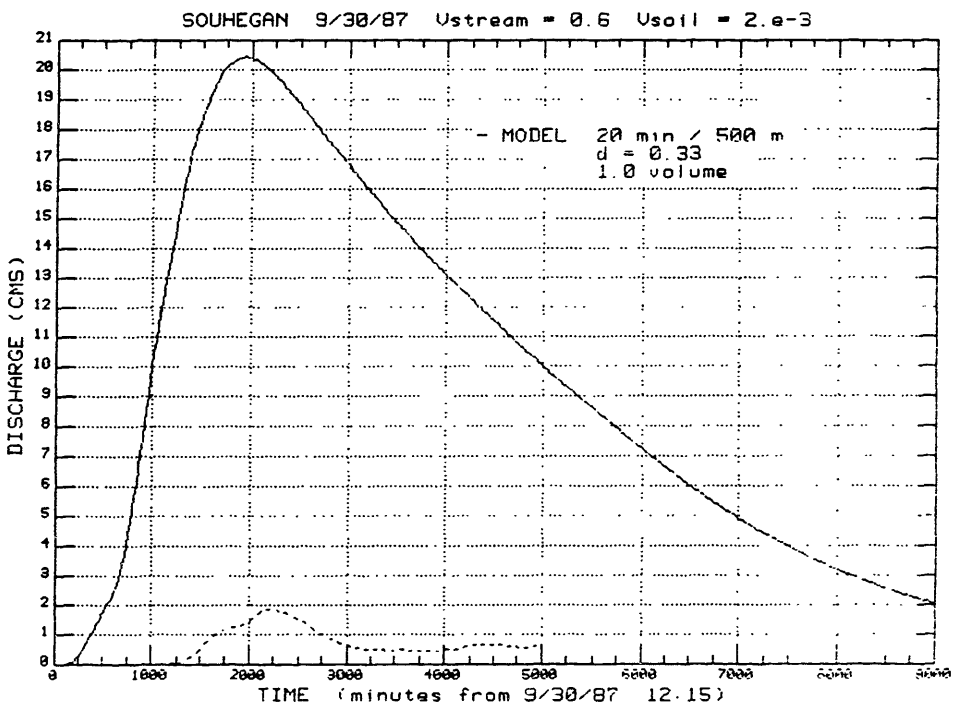

Fig. 3-34. Souhegan model result. September 30, 1987. Observed hydrograph plotted as dashed line. Volume of model hydrograph has not been scaled.

The rainfall-runoff ratio appears so small as to cast doubt on the accuracy of the radar rainfall measurement. However, despite the late date in the season, there is no evidence for bright band contamination or other bias in the radar data. Moreover, the raingauge at the Souhegan gauge site recorded a total depth of 1.7 cm for the storm (of which it appears that a fraction may even have resulted from rain that occurred prior to the first radar scans recorded). If there is, in reality, no error in the rainfall or streamgauge record, then we must conclude that during this storm all but 3% of the rainfall volume was retained in the soil. The only portion of the rainfall contributing to streamflow must then have been from precipitation very near, or directly, on the channels. However, this explanation is not altogether satisfactory as, despite the relatively dry summer and the low streamflows at the beginning of the month, rain fell for several days during the week previous to the storm in question (c.f., Fig. 3-33).

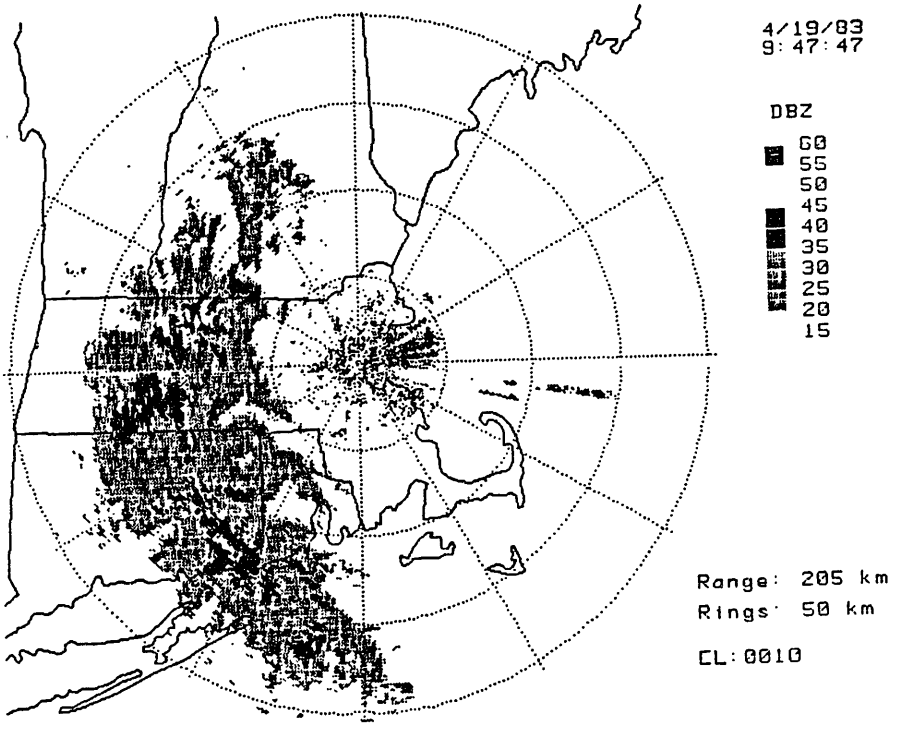

Fig. 3-35. Radar rainfall pattern April 19, 1983.

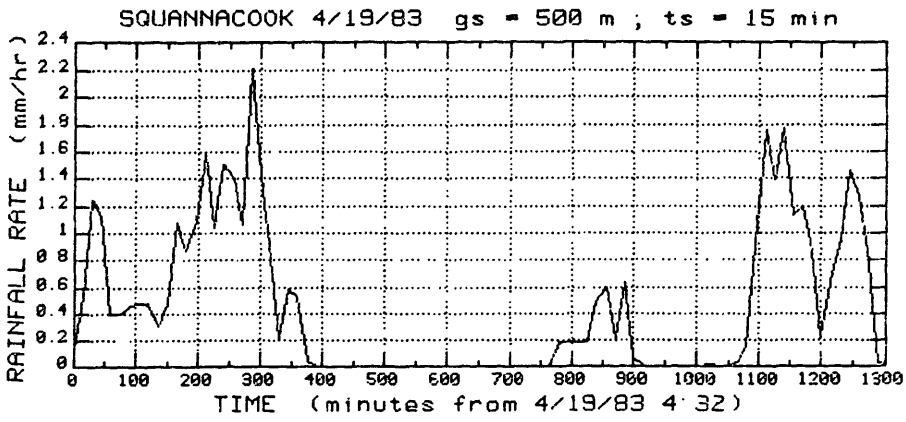

Fig. 3-36. Basin average rainfall rates over the Squannacook exhibiting two distinct rainfall peaks (22 hours beginning April 19, 1983, 4:32 EST).

v) April 19, 1983

This final test of the model to be presented here was conducted for an early springtime case on the Squannacook. The rainfall pattern and time series are depicted in Fig. 3-35. A band of moderate to heavy precipitation (40 dBZ), quasi-stationary, traversed the basin twice, producing two independent rainfall peaks, approximately 1 day apart. This model run was conducted "blind": the volume scale factor was selected in advance by considering the climatological mean data in Fig. 2-14; the model was run; and the resulting hydrograph was compared to the data. A volume scale factor of 100% was selected on the basis of the climatological mean for April (123%) and the mean for April 1983 (87%). This equality between rainfall and runoff does not necessarily imply that the soils in the basin are saturated, but only that an equal volume of runoff was produced for the volume of rainfall input.

Fig. 3-37 depicts the forecast hydrograph. The model hydrograph shows remarkable agreement with the observed data, apart from an overestimate of the runoff due to the first rainfall peak. The assumption of a constant volume scale factor throughout the storm is probably the cause of this discrepancy; we might logically anticipate that the loss factor should in fact decrease during the course of the rainfall event. Nonetheless, the use of constant values for both the volume scale factor and the velocity parameters throughout the storm provides an operationally useful forecast of the observed hydrograph.

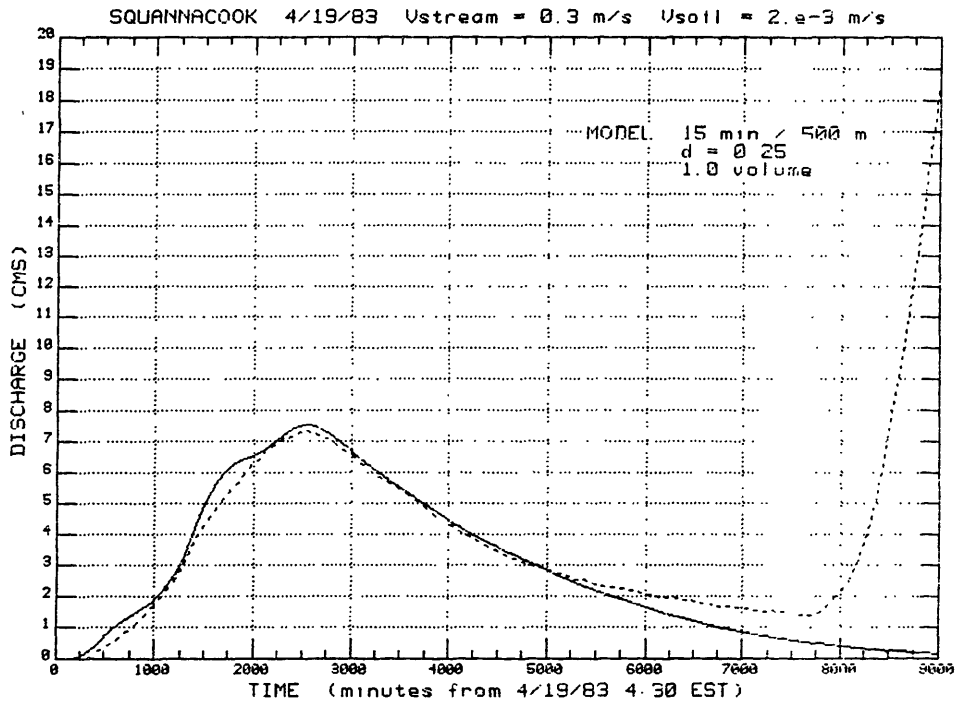

Fig. 3-37. Squannacook model result, April 19, 1983.

b) Conclusions and further research

The above results, summarized in Table 3-1, have demonstrated, at least in a qualitative manner, the value of radar for hydrologic applications. Even for basins of moderate size such as those considered here, spatial gradients in the rainfall often result in differences of a factor of two in the total rainfall depth from one side of the basin to the other. While such gradients appear to have only limited effects on the response of the basins considered, the potential for significant bias in isolated raingauge measurements is evident.

Although only a few storms have been analyzed, the cases presented here span the observed seasonal variation in the rainfall-runoff ratio. In most of the summertime cases considered, the runoff volume was correctly forecast from the radar data by accounting, in a very simple manner, for the loss due to storage in the soil and subsequent evaporanspiration. In the springtime case considered, with all of the rainfall volume appearing as runoff, the model also reproduced the observed hydrograph. Between the summer and springtime cases the climatological mean rainfall-runoff factor varies from 20% to 100%,

Table 3.1. Summary of model parameters and results. "n.a." indicates data not available.

Storm date		4/19/83	6/16/86	6/27/87	7/2/87	9/30/87
Total depth	SOU	n.a.	0.5 cm	2.2 cm	2.0 cm	1.2 cm
	SQUAN	1.0 cm	n.a.	2.2 cm	1.6 cm	n.a
Duration		6 / 8 hrs	1 hr	12 hrs	10 hrs	6 hrs
Peak Intensity		40 dBZ	50 dBZ	35 dBZ	35 dBZ	40 dBZ
Z-R relation		$230R^{1.4}$	$400R^{1.3}$	$230R^{1.4}$	$230R^{1.4}$	$230R^{1.4}$
V_{stream} (m/s)	SOU	n.a	0.6	0.6	0.6	?
	SQUAN	0.3	n.a	0.3	0.3	n.a
V_{soil} (m/s)	SOU	n.a	2×10^{-3}	2×10^{-3}	2×10^{-3}	?
	SQUAN	2×10^{-3}	n.a	2×10^{-3}	1.35×10^{-3}	n.a
Initial flow	SOU	n.a	8.5 cms	2.5 cms	3.7 cms	1.7 cms
	SQUAN	7.6 cms	n.a	1.0 cms	1.1 cms	n.a
Peak flow	SOU	n.a	8.9 cms	10.1 cms	12.0 cms	3.4 cms
	SQUAN	13.5 cms	n.a	4.7 cms	3.1 cms	n.a
Runoff volume	SOU	n.a	23 %	20 %	28 %	3 %
	SQUAN	100 %	n.a	20 %	22 %	n.a

i.e. by a factor of 5. Although it is not possible at this stage to quantify any bias due to errors in the radar rainfall measurement over the basin, it appears that the radar is capable of significantly better accuracy for hydrologic applications than the factor of two error commonly ascribed. In many situations, any bias in the radar rainfall measurement will be substantially less than the error in the determination of the fraction of the rainfall contributing to runoff. To substantiate these initial observations quantitatively, will require continuous radar coverage during the course of a year, with simultaneous evapotranspiration and stream-gauge measurements to obtain an accurate estimate of the water budget over the basin.

One of the goals of this research was to consider the simplest possible conceptual, but physically based, hydrologic model. The kinematic representation of the basin response provides this framework. The true framework of the model is in fact the geometry of the stream network. With only two parameters, describing the velocity at which water traverses the basin, the

model reproduces the observed hydrograph response. For the conditions considered in this study, the two model velocities do not vary appreciably from storm to storm, and in the linear model, do not vary during a storm. Also, the model parameters are consistent with the observed similarities and differences between the two basins studied: differences in the streamflow velocities in the two basins are attributed to differences in the physical properties of the river channels; while the volume scale factor (which depends on the climate), and the subsurface flow velocity (which depends on the topography and soil charactersistics), are virtually the same in the two basins.

The model's simplicity allows us to isolate the contribution of the basin geometry to the shape of the hydrograph. For subsurface flow, the model has predicted the dependence of the hydrograph recession on the basin drainage density, a hypothesis that can be readily tested by analyzing the recession characteristics of a variety of watersheds. However, the distributed model and the radar remain untested for the storm cases to which they are potentially best suited; localized rain in watersheds where the response of the basin is sensitive to the spatial distribution of the rainfall.

It would be desireable to implement the model and radar on a different river basin with more sensitive runoff characteristics. An impermeable (presumably mountainous) basin would be ideal. The catchment would then perform as a giant raingauge, allowing an accurate comparison of the radar determined rainfall and the runoff. An even more exacting test would be to apply the model to a region where the dominant runoff generation mechanism is true Hortonian overland flow. Under these conditions runoff generation at each grid element would be linked directly to the radar determined instantaneous rainfall rate, and the rapid response of the basin would justify the use of the gridded kinematic streamflow model.

REFERENCES

Ackerman, B., (1967): The nature of the meteorological fluctuations in clouds. *J. Appl. Meteor.*, **6**, 61-71.

Ahnert, P. R., M. D. Hudlow, E. R. Johnson, D. R. Greene, and M. P. Rosa Dias, (1983): Proposed "on-site" precipitation processing for NEXRAD. *Preprints 21st Conf. Radar Meteor.*, AMS, 378-385.

Atlas, D. and R. Tatehira, (1968): Precipitation-induced mesoscale wind perturbations in the melting layer. *Preprints 13th Conf. Radar Meteor.*, AMS, 166-175.

Austin, G. L., (1980): Radar and satellite measurements of rain. *Proc. Canadian Hydrology Symposium.* National Research Council Canada. 14-17.

Austin, P. M., (1971): Some statistics of the small-scale distribution of precipitation. Final report contract NASA/ERC 0420, Goddard Space Flight Center, Maryland.

-------- (1981): On deducing rainfall from radar reflectivity measurements. *Preprints 20th Conf. Radar Meteor.*, AMS. 200-207.

-------- (1987): Relation between radar reflectivity and surface rainfall. *Mon. Wea. Rev.*, **115**, 1053-1070.

Battan, L. J., (1973): *Radar observation of the atmosphere.* University of Chicago Press, 324 p.

Bell, T., (1987): A space-time stochastic model of rainfall for satellite remote sensing studies. *J. Geophys. Res.*, **92**, 9631-9643.

Bellon, A. and G. L. Austin, (1978): The evaluation of two years of real-time operation of a short-term precipitation forecasting procedure (SHARP). *J. Appl. Meteor.*, **17**, 1778-1787.

-------- (1984): The accuracy of short-term radar rainfall forecasts. *J. Hydrol.*, **70**, 35-49.

Beven, K. J., and M. J. Kirkby, (1979): A physically based, variable contributing area model of basin hydrology. *Hydrol. Sci. Bull.*, **24**, 43-69.

Brandes, E. A., (1975): Optimizing rainfall estimates with the aid of radar. *J. Appl. Meteor.*, **14**, 1339-1345.

Bras, R. L., D. Grossman, and D. Schafer, (1985): The effects of hydrometeorology on the GOES random data collection system. *Hydrol. Sci.*, **30**, 1-22.

Calheiros, R. V., and I. Zawadzki, (1987): Reflectivity-rain rate relationship for radar hydrology in Brazil. *J. Appl. Meteor.*, **26**, 118-132.

Carlston, C. W., (1969): Downstream variations in the hydraulic geometry of streams: special emphasis on mean velocity. *Amer. J. Sci.*, **267**, 499-509.

Cavanaugh, R. W., (1985): *A dynamic rain attenuation model.* Master's Thesis, Dartmouth.

Chandrasekar, V., and V. N. Bringi, (1986): Problems in intercomparing radar measurements of rainfall with raindrop sampling devices. *Preprints 23rd Conf. Radar Meteor.*, AMS, 112-115.

Chorley, R. J., (1969): The drainage basin as the fundamental geomorphic unit. Chap. 2, *Water, Earth and Man.* ed. R. J. Chorley. Methuen, London. pp 77-99.

Chorley, R. J., (1978): The hillslope hydrological cycle. in *Hillslope Hydrology*, M. J. Kirkby ed., Wiley-Interscience, New York. Chap. 1, pp 1-42.

Coffin, G. W., (1950): Yield of the Boston Meteropolitan District Waterworks. *J. Amer. Water Works Assoc.*, **42**.

Collier, C. G., (1986): Accuracy of rainfall estimates by radar, part I: Calibration by telemetering raingauges., *J. Hydol.*, **83**, 207-223.

Collier, C. G., and J. M. Knowles, (1986): Accuracy of rainfall measurements by radar, part II: Applications for short term flood forecasting. *J. Hydrol.*, **83**, 237-249.

Crane, R. K., (1985): Evaluation of global and CCIR models for estimation of rain rate statistics. *Radio Sci.*, **20**, 865-879.

Crane, R. K., (1986): Horizontal small scale structure of precipitation. *Preprints 23rd Conf. Radar Meteor.*, AMS, 181-184.

Curry, R. G., R. A. Clark, and R. C. Runnels, (1970): Hydrograph synthesis from digitized radar data for streamflow routing. *Preprints 14th Conf. Radar Meteor.*, AMS, 249-252.

Dalezios, N. R., (1982): *Real-time radar rainfall measurements for hydrologic modeling.* PhD thesis. Univerisity of Waterloo, Ontario.

Dooge, J. C. I., and B. M. Harley (1967): Linear routing in uniform open channels. *Preprints Intl. Hydrol. Symp.* Colorado State Univ., Ft. Collins, Colo., vol 1, 57-63.

Douglas, M., A. Jones, and A. L. Sims, (1970): Climatology of instataneous rainfall. *J. Appl. Meteor.*, **17**, 1135-1140.

Doviak, R. J., (1983): A survey of radar measurement techniques. *J. Climate Appl. Meteor.*, **22**, 832-849.

Drufuca, G., and I. I. Zawadzki, (1975): Statistics of raingage data. *J. Appl. Meteor.*, **14**, 1419-1429.

Dunne, T., and R. D. Black, (1970): An experimental investigation of runoff on permeable soils, *and* Partial area contributions to storm runoff in a small New England watershed. *Water Resour. Res.*, **6**, 478-490 and 1296-1311.

Eagleson, P. S., (1967): A distributed linear model for peak catchment discharge. *Proc. Intl. Hydrol. Symp.* Colorado State Univ., Ft. Collins, Colo., vol 1, 2-17.

-------- (1970): *Dynamic Hydrology.* McGraw-Hill, New York. 462 pp.

Fortin, J. P., H. Proulx, and A. Bellon, (1987): Utilisation des données d'un radar météorologique pour la simulation des écoulements en rivière à l'aide d'un modèle hydrologique matriciel. *J. Hydrol.*, **90**, 327-350.

Freeze, R. A., (1972): Role of subsurface flow in generating surface runoff. *Water Resour. Res.*, **8**, 609-623, 1272-1283.

Frenny, A. E., and J. D. Gabbe, (1969): A statistical description of intense rainfall. *Bell Sys. Tech. J.*, **48**, 1789-1851.

Gage, K. S., (1979): Evidence for a $k^{-5/3}$ law inertial range in mesoscale two–dimensional turbulence. *J. Atmos. Sci.*, **36**, 1950-1954.

Georgakakos, K. P., and R. L. Bras, (1984): A hydrologically useful station precipitation model. *Water Resour. Res.*, **20**, 1585-1610.

Gupta, V. K., E. Waymire, and C. T. Wang, (1980): A representation of an instantaneous unit hydrograph from geomorphology. *Water Resour. Res.*, **16**, 855-862.

Hewlett, J. D., and A. R. Hibbert, (1963): Moisture and energy conditions within a sloping soil mass during drainage. *J. Geophys. Res.*, **68**, 1081-1087.

Holtz, C. D., (1983): Radar precipitation climatology program. *Preprints 21st Conf. Radar Meteor.*, AMS, 390-393.

Hosking, J. D., and C. D. Stow, (1987): The arrival of raindrops at the ground. *J. Appl. Meteor.*, **26**, 433-442.

Hudlow, M. D., (1972): Use of radar data from D/RADEX for operational hydrology. *Preprints 15th Radar Meteor. Conf.* , AMS, 117-123.

Huebner, G. L., (1985): Use of radar for precipitation measurements. in *Hydrologic forecasting.* M. G. Anderson and T. P. Burt eds. Wiley-Interscience, New York.

Jones, D. M. A., and A. L. Sims, (1978): Climatology of instantaneous rainfall. *J. Appl. Meteor.*, **17**, 1135-1140.

Joss, J., and A. Waldvogel, (1970): A method to improve the accuracy of radar measured amounts of precipitation. *Preprints 14th Conf. Radar Meteor.*, 237-238.

Kessler, E., and K. E. Wilk, (1968): *Radar measurements of precipitation for hydrological purposes.* Report No. 5 International Hydro. Decade. WMO, Geneva.

Kirkby, M. J., (1978): *Hillslope Hydrology*, ed., Wiley-Interscience, New York. pp 389.

-------- (1985): Hillslope Hydrology. in *Hydrologic Forecasting*, M. G. Anderson and T. P. Burt eds., John Wiley, New York. Chap. 3, pp 37-75.

Klatt, P., and G. A. Schultz, (1983): Flood forecasting on the basis of radar rainfall measurement and rainfall forecasting. Hydrol. Applic. of Remote Sensing and Remote Data Transmission, *Proc. Hamburg Symp.*, Aug. 1983. IAHS Publ. No. 145.

Kraichnan, R. H., (1967): Inertial ranges in two-dimensional turbulence. *Phys. Fluids*, **10**, 1417-1423.

Krajewski, W. F., and P. R. Ahnert, (1986): Near real-time tests of a multivariate analysis system. *Preprints 23rd Conf. Radar Meteor.*, AMS, JP66-69.

Kundzewicz, Z. W., (1986): The hydrology of tomorrow.*Hydrol. Sci.*, **31**, 223-235.

Laurenson, E. M., (1964): A catchment storage model for runoff routing. *J. Hydrol.*, **2**, 141-163.

Leopold, L. B., (1953): Downstream change of velocity in rivers. *Amer. J. Sci.*, **251**, 606-624.

Lilly, D. K. (1983): Stratified turbulence and the mesoscale variability of the atmosphere. *J. Amos. Sci.*, **40**, 749-761.

Lin, S. H., H. J. Bergmann, and M. V. Pursley, (1980): Rain attenuation on earth-satellite paths -- Summary of 10 year experiments and studies. *Bell Sys. Tech. J.*, **59**, 183-228.

Lovejoy, S. and B. B. Mandelbrot, (1985): Fractal properties of rain, and a fractal model. *Tellus*, **37A**, 209-232.

Lumley, J. L., and H. A. Panofsky, (1964): *The structure of atmospheric turbulence.* Wiley-Interscience, New York. 239 pp.

MacCready, P.B., (1962): Turbulence measurements by sailplane *and* The inertial subrange of atmospheric turbulence. *J. Geophys. Res.*, **67**, 1041-1050, 1051-1059.

Marshall, J. S., and W. M. K. Palmer, (1948): The distribution of raindrops with size. *J. Meteor.*, **5**, 161-166.

Mollo-Christensen, E., (1962): The distribution of raindrops and gusts in showers and squalls. *J. Atmos. Sci.*, **10**, 181-182.

Mosley, M. P., (1979): Streamflow generation in a forested watershed, New Zealand. *Water Resour. Res.*, **15**, 795-806.

Nash, J. E., (1957): The form of the instantaneous unit hydrograph. *Intl. Assoc. Sci. Hydrol.*, **45**, 114-121.

NOAA, (1986): *Climatological data annual summary.* National Climatic Data Center, Asheville, N. Carolina. 1975 - 1986.

Pierce, A. J., M. K. Stewart, and M. G. Sklash, (1986): Storm runoff generation in humid headwater catchments. *Water Resour. Res.*, **22**, 1263-1282.

Pilgrim, D. H., (1977): Isochrones of travel time and distribution of flood storage from a tracer study on a small watershed. *Water Resour. Res.*, **13**, 587-595.

Rodríguez-Iturbe, I., and J. B. Valdés (1979): The geomorphologic structure of the hydrologic response. *Water Resour. Res.*, **15**, 1409-1420.

Rodríguez-Iturbe, I., G. Devoto, and J. B. Valdés (1979): Discharge response analysis and hydrologic similarity: The interrelation between the geomorphologic IUH and the stream characteristics. *Water Resour. Res.*, **15**, 1435-1444.

Rodríguez-Iturbe, I., M. González-Sanabria, and R. L. Bras, (1982). A geomorphoclimatic theory of the instantaneous unit hydrograph. *Water Resour. Res.*, **18**, 877-886.

Rosso, R., (1984): Nash model relation to Horton order ratios. *Water Resour. Res.*, **20**, 914-920.

Schertzer, D. and S. Lovejoy (1987): Physical modeling and analysis of rain and clouds by anisotropic scaling multiplicative processes. *J. Geophys. Res.*, **92**, 9693-9714.

Shreve, R. L., (1966): Statistical law of stream numbers. *J. Geol.*, **74**, 17-37.

-------- (1967): Infinite topologically random channel networks. *J. Geol.*, **75**, 178-186.

-------- (1969): Stream lengths and basin areas in topologically random channel networks. *J. Geol.*, **77**, 397-414.

Smart, J. S., (1973): The random model in fluvial geomorphology. Chap. 2, *Fluvial Geomorphology*. ed. M Morisawa. George and Allen, London. pp 27-49.

-------- (1978): The analysis of drainage network composition. *Earth Surf. Proc.*, **3**, 129-170.

Smart, J. S., and C. Werner (1976): Applications of the random model of drainage basin composition. *Earth Surf. Proc.*, **1**, 219-233.

Srivastava, R. C., and D. Atlas, (1974): Effect of finite radar pulse volume on turbulence measurements. *J. Appl. Meteor.*, **13**, 472-480.

Strahler, A. N. (1950): Equilibrium theory of erosional slopes approached by frequency distribution analysis. *Amer. J. Sci.*, **248**, 673-696, 800-814.

Strahler, A. N. (1952): Hypsometric (area-altitude) analysis of erosional topography. *Bull. Geol. Soc. Amer.*, **63**, 1117-1142.

Sychra, J., (1972): Inverse problem in the theory of turbulence filtering by the radar pulse volume. *Preprints 15th Conf. Radar Meteor.*, AMS, 286-291.

Takasao, T., and M. Shiiba, (1984): Development of techniques for on-line forecasting of rainfall and flood runoff. *Natural Disaster Sci.*, **6**, 83-112.

Taylor, G. I., (1938): The spectrum of turbulence. *Preprints Roy. Soc. London,* **A164**, 476-490.

Tennekes, H., and V. L. Lumley, (1972): *A first course in turbulence*. MIT Press. Cambridge, Mass. 300 pp.

Torlaschi, E. and R. Humphries, (1983): Statistics of reflectivity gradients. *Preprints 21st Conf. Radar Meteor.*, AMS, 173-175.

Troendle, C. A., (1985): Variable source area models. in *Hydrologic Forecasting*, M. G. Anderson and T. P. Burt eds., Wiley-Interscience, New York. Chap. 12, 347-403.

Troutman, B. M., and M. R. Karlinger, (1985): Unit hydrograph approximations assuming linear flow through topologically random channel networks. *Water Resour. Res.*, **21**, 743-745.

Tsonis, A. A., and G. L. Austin, (1981): An evaluation of extrapolation techniques for the short-term prediction of rain amounts. *Atmosphere-Ocean*, **19**, 54-65.

U. S. Dept. of Agriculture, Soil Conservation Service, (1981): *Soil Survey of Hillsborough County N.H., Eastern Part.*.

U. S. Dept. of Agriculture, Soil Conservation Service, (1985): *Soil Survey of Hillsborough County N.H., Western Part.*.

U. S. Geol. Survey (1968): *Ground-water resources of the lower Merrimack river valley, south-central New Hampshire.* Hydrologic Invetigations Atlas HA-277. by J. M. Weigle.

U. S. Geol. Survey (1977): *Water resources of the Nashua and Souhegan river basins, Massachusetts.* Hydrologic Investigations Atlas HA-275. by R. A. Brackley, and B. P. Hansen.

U. S. Geol. Survey, (1984): *Gazatteer of hydrologic characteristics of streams in Massachusetts – Merrimack River basin.* Water-Resources Investigations Rept. 84–4284. Boston, Mass.. pp 54.

Valdés, J. B., Y. Fiallo, and I. Rodríguez-Iturbe, (1979): A rainfall-runoff analysis of the geomorphologic IUH. *Water Resour. Res.*, **15**, 1421-1434.

Walton, M. L., E. R. Johnson, P. R. Ahnert, and M. D. Hudlow, (1985): Proposed on-site flash-flood potential system for NEXRAD. *6th Conf. Hydromet.*, 122-129.

Ward, R. C., (1984): On the response to precipitation of headwater streams in humid areas. *J. Hydrol.*, **74**, 171-189.

Whipkey, R. Z., and M. J. Kirkby, (1978): Flow in the soil. in *Hillslope Hydrology*, M. J. Kirkby ed., Wiley-Interscience, New York. Chap. 4.

Wiggert, V., and S. Ostlund, (1975): Computerized rain assesment and tracking of south Florida weather radar echoes. *Bull. Amer. Meteor. Soc.*, **56**, 17-26.

Williams, E. R., (1987): Personal communication.

Wilson, J. W., (1970): Integration of radar and raingage data for improved rainfall measurement. *J. Appl. Meteor.*, **9**, 489-497.

Wilson, J. W., and E. A. Brandes, (1979): Radar measurement of rainfall -- a summary. *Bull. Amer. Meteor. Soc.*, **60**, 1048-1058.

Zawadzki, I. I., (1973): Statistical properties of precipitation patterns. *J. Appl. Meteor.*, **12**, 459-472.

Zawadzki, I. I., (1975): On radar-raingage comparison. *J. Appl. Meteor.*, **14**, 1430-1436.

-------- (1984): Factors affecting the precision of radar measurements of rain. *Preprints 22nd Conf. Radar Meteor.*, AMS, 251-256.

-------- (1987): Fractal structure and exponential decorrelation in rain. *J. Geophys. Res.*, **92**, 9586-9590.

Zawadzki, I., C. Desrochers, E. Torlaschi, and A. Bellon, (1986): A radar-raingage comparison. *Preprints 23rd Conf. Radar Meteor.*, AMS, 121-124.

Zoch, R. T., (1934): On the relation between rainfall and streamflow. *Mon. Wea.Rev.*, **62**, 315-322.